

https://dspace.org/

Adjoint-based optimization for optimal control problems governed by nonlinear hyperbolic conservation laws

Yohana, Elimboto

2012-09-05
http://hdl.handle.net/10539/11894

Downloaded from a DSpace repository. https://dspace.org/

Adjoint-based optimization for optimal control problems governed by nonlinear hyperbolic conservation laws

Elimboto Yohana



A dissertation submitted for the degree of a
master of science

School of Computational and Applied Mathematics,
University of the Witwatersrand,
Johannesburg, South Africa.

May 20, 2012

Abstract

Research considered investigates the optimal control problem which is constrained by a hyperbolic conservation law (HCL). We carried out a comparative study of the solutions of the optimal control problem subject to each one of the two different types of hyperbolic relaxation systems [64, 92]. The objective was to employ the adjoint-based optimization to minimize the cost functional of a matching type between the optimal solution and the target solution. Numerical tests were then carried out and promising results obtained. Finally, an extension was made to the adjoint-based optimization approach to apply second-order schemes for the optimal control problem in which also good numerical results were observed.

Declaration

I, the undersigned, hereby declare that this dissertation is my own, unaided work, and that any work done by others has been acknowledged and referenced accordingly. It is being submitted for the Degree of Master of Science at the University of the Witwatersrand, Johannesburg. It has not been submitted before for any degree or examination to any other university.

Elimboto Yohana, May 20, 2012

Acknowledgements

I would like to thank all those who assisted me hand in hand to accomplish this project. My grateful thanks are conveyed to Professor Mapundi Banda, being my supervisor and a close friend, for helping me to secure funding for this research project and for his outstanding contribution in terms of ideas, skills, proper direction, recommendations and motivation during the whole period of research. I also want to thank the University of the Witwatersrand and the African Institute for Mathematical sciences (AIMS) staff who also secured funding for my studies. Many thanks especially, to the AIMS Director, Professor Barry Green, the former Head of the School of Computational and Applied Mathematics (CAM), professor David Sherwell, the current Head of School, Professor Ebrahim Momoniat and to all lecturers and researchers in the School of CAM: Block, Charis, Conraaed, David, Joel, Montazi, Robert, just to name a few.

I would also like to extend my sincere thanks to the CAM staff members working in different ways to sustain a facilitative and supportive living and learning environment. My special gratitudes go to Barbie, Dorina, Keba and Wendy for their care and skillful management.

I would also like to thank my employer, the Dar Es Salaam University College of Education, a constituent college of the university of Dar Es salaam for granting me permission to pursue this study.

Many thanks to my friend Said Sima who worked closely with me during the whole period of research, his advice and willingness to assist, will always make me remember him. I thank all CAM PGD students, namely, Naval, Morgan, Gideon, Guo-Dong, Terry, Tanya, Dario, Viren, Franklin, Obakeng, Asha, Tumelo, Charles Fodya and Innocent, for their outstanding academic and social contribution which have made CAM school an excellent place and enchanting center for researchers.

I highly recognize the contribution given by my family: my parents, brothers and sisters in terms of advice, encouragement, and prayers. Since when I joined the education system, unquestionably, any success in my academic advancement has their hands.

I do not want to leave behind various friends, at Johannesburg, Dar Es salaam, Cape Town and elsewhere for their prayers, spiritual support and social advice. Special thanks goes to Rugare, Ogana, Armstrong, Ruth, Emmanuel, Anne, Wilbert, Gerald, Davids, Greg, Mackllen, John, Navin, Andrew, Leonard, Lois and Richard. Thanks to my friend Bwasiri for his encouragement and valuable social advice during my stay at Wits.

All these contributions, collectively amounted to a lenient conducting of my research.

Lastly, I convey my gratitude to Almighty God for giving me strength and healthy during the whole period of my stay at Wits.

Contents

Abstract i

List of Tables v

List of Figures vi

1 Introduction 1

1.1 Objectives of the Study . . . 1

1.2 Solutions of nonlinear hyperbolic conservation laws . . . 2

1.3 Relaxation system . . . 5

1.4 Adjoint-based optimal control . . . 5

1.4.1 Organization of the work . . . 6

2 Mathematical Framework 8

2.1 Governing System of Conservation Laws . . . 8

2.2 General Hyperbolic Systems . . . 10

2.2.1 Linear hyperbolic systems . . . 10

2.2.2 Nonlinear hyperbolic systems . . . 11

2.2.3 Diagonalization of hyperbolic systems . . . 11

2.2.4 Transform to characteristic variables . . . 11

2.3 Weak Solutions . . . 12

2.4 Relaxation Approaches . . . 14

2.5 JIN XIN Relaxation Approximation Methods . . . 14

2.5.1 Chapman-Enskog analysis for JIN XIN relaxation system . . . 15

2.5.2 Diagonalization of JIN XIN relaxation system . . . 16

2.5.3 Characteristic variables for JIN XIN relaxation system . . . 17

2.6 A BGK Model . . . 18

2.7 Problem Formulation and Adjoint Approach to Optimization . . . 19

2.7.1 Derivation of the optimality system from JIN XIN relaxation system . . . 20

2.7.2 Derivation of the adjoint system for the discrete kinetic model . . . 22

3 Discretizations of the Relaxation Systems **25**

3.1 Construction of the First-order JIN XIN Relaxing Scheme 25

3.1.1 Spatial discretization 25

3.1.2 TVD Runge-Kutta time discretization 27

3.2 First-order Discretization of the Adjoint System 28

3.2.1 Spatial discretization 28

3.2.2 TVD Runge-Kutta time discretization for the adjoint system 29

3.3 MUSCL, TVD High Resolution Schemes: JIN XIN Relaxation Scheme 30

3.3.1 Construction of MUSCL, TVD second-order in space schemes 30

3.3.2 TVD, Runge-Kutta second-order in time discretization 32

3.4 Discretization of the Adjoint Equation, Second-order in Time and Space 33

3.4.1 Spatial discretization 33

3.4.2 Time discretizations 35

3.5 Relaxing Scheme for the Discrete Kinetic Relaxation system 37

3.5.1 Discretization of the discrete kinetic model, first-order in time and space . 37

3.5.2 Spatial discretization for the discrete kinetic model, second-order in space 38

3.5.3 Second-order Runge-Kutta time discretizations for the discrete kinetic model 38

3.5.4 Time and space adjoint discretizations of discrete kinetic model, second-order 40

3.6 Boundary conditions 42

3.6.1 Periodic boundary conditions 42

3.6.2 Transparent boundary conditions 43

3.6.3 Algorithm for gradient computing 43

4 Numerical Results **45**

4.1 Numerical Discretizations of Spatial and Temporal Domains 45

4.2 General Descriptions 45

4.3 Numerical Experiments for Scalar HCLs 46

4.3.1 Numerical experiments for scalar linear HCLs 46

4.3.2 Numerical experiments for scalar nonlinear HCLs 47

4.4 Numerical Solutions for Systems of HCLs 50

4.5 Numerical Solutions for Nonlinear Systems of HCLs 53

4.5.1 Sod Shock Tube Problem 55
4.5.2 First and second order numerical tests 55
4.6 Adjoint-Optimization Tests 61
4.6.1 Optimization tests for scalar nonlinear HCLs 64
4.6.2 Optimization tests for systems of nonlinear HCLs 64
4.7 Functional Convergence 71
4.8 Comparison of Computation time 71

5 Conclusions **77**

List of Tables

4.1 Computational time for first-order JIN XIN and discrete kinetic schemes 76
4.2 Computational time for second-order JIN XIN and discrete kinetic schemes . . . 76

List of Figures

2.1 Initial solution and final solution at time = 0.5 for the linear advection equation 9

2.2 Initial and final solution of the Inviscid Burgers' equation at time t = 0.5 10

4.1 Solution of the linear advection equation (4.3.1) for JIN XIN scheme (black solid line with squares at data points), kinetic scheme (green asterisk), and a reference solution (red solid line) for $a = 1$, $M = 400$ and $\epsilon = 10^{-8}$. The x-axis represents the space variable x and the y-axis represents the advected quantity, u. 48

4.2 Solution of the Burgers' Equation using JIN XIN scheme (black solid line with squares at data points), kinetic scheme (green asterisk), and a reference solution (red solid line) for $a = 1.3$, $M = 400$ and $\epsilon = 10^{-8}$. The x-axis represents the space variable x and the y-axis represents the conserved quantity, u. 49

4.3 First and second-order numerical solutions for JIN XIN and discrete kinetic relaxing schemes. The x-axis represents the space variable x and the y-axis represents the velocity field, u. 51

4.4 Solution of the wave equation (4.4.5), JIN XIN scheme (black solid line with squares at data points), kinetic scheme (green asterisk), and exact solution (red solid line); $T = \frac{\pi}{2}$, $M = 400$, $\epsilon = 10^{-8}$, $a = 1$. The x-axis represents the space variable x and the y-axis represents the wave profile, u. 53

4.5 Sketch of the initial configuration of the shock tube at time $t = 0$. P_L, T_L, V_L and P_R, T_R, V_R are, respectively pressure, temperature and velocity; on the left and right part of the tube. 56

4.6 Sketch of the shock tube showing waves interaction after the membrane breakdown, $t > 0$. 57

4.7 First and second order numerical solutions for density, velocity and pressure profiles with JIN XIN and discrete kinetic schemes, for 1D Euler Equations at time, $T = 0.17$, $u_L = (1.25,\ 0.0,\ 1.2)$, $u_R = (0.25,\ 0.0,\ 0.25)$, for $a_1 = 1.0$, $a_2 = 2.5$, $a_3 = 5.2$, $M = 400$ and $\epsilon = 10^{-8}$. The x-axis represents the space variable x and the y-axis represents density (top), velocity (middle) and pressure (bottom). 58

4.8 First and second order numerical solutions for density, velocity and pressure profiles with JIN XIN and discrete kinetic schemes, for 1D Euler Equations at time, $T = 0.17$, $u_L = (1.45,\ 0.0,\ 1.5)$, $u_R = (0.45,\ 0.0,\ 0.5)$; $a_1 = 2.2$, $a_2 = 2.5$, $a_3 = 5.0$, $M = 400$ and $\epsilon = 10^{-8}$. The x-axis represents the space variable x and the y-axis represents density (top), velocity (middle) and pressure (bottom). 59

4.9 First and second order numerical solutions for density, velocity and pressure profiles with JIN XIN and discrete kinetic schemes, for 1D Euler Equations at time, $T = 0.17$, $u_L = (2.5,\ 0.0,\ 2.0)$, $u_R = (0.5,\ 0.0,\ 0.6)$; $a_1 = 3.5,\ a_2 = 4.5,\ a_3 = 5.5$, $M = 400$ and $\epsilon = 10^{-8}$. The x-axis represents the space variable x and the y-axis represents density (top), velocity (middle) and pressure (bottom). 60

4.10 Comparing first-order and second-order solutions for different grids with JIN XIN scheme; $T = 0.17$, $u_L = (2.5,\ 0.0,\ 2.0)$, $u_R = (0.5,\ 0.0,\ 0.6)$; $a_1 = 2.0,\ a_2 = 3.5,\ a_3 = 5.5$, $\epsilon = 10^{-8}$. The x-axis represents the space variable x and the y-axis represents density (top), velocity (middle) and pressure (bottom). 62

4.11 Comparing first-order and second-order solutions for different grids with discrete kinetic scheme. Same parameters as in Figure 4.10. The x-axis represents the space variable x and the y-axis represents density (top), velocity (middle) and pressure (bottom). 63

4.12 First-order adjoint-based optimization of scalar nonlinear HCL results for JIN XIN and kinetic schemes, $M = 400$ and $\epsilon = 10^{-8}$. The x-axis represents the space variable x and the y-axis represents the conserved quantity, u. 65

4.13 Same parameters as in Figure 4.12 but second-order tests. The x-axis represents the space variable x and the y-axis represents the conserved quantity, u. 66

4.14 First-order (Left) and second-order (Right) 1D Euler Equations optimal control results. The optimal solution is shown by the red solid line and target by black solid line with squares at data points, $T = 0.17$, $u_L = (1.2,\ 0.078,\ 1.2)$, $u_R = (0.325,\ 0.285,\ 0.295)$, $a_1 = 2.183,\ a_2 = 3.004,\ a_3 = 4.286$, $M = 400$ and $\epsilon = 10^{-8}$. The x-axis represents the space variable x and the y-axis represents density (top), velocity (middle) and pressure (bottom). 67

4.15 First-order (Left) and second-order (Right) 1D Euler Equations optimal control results obtained with discrete kinetic scheme. Optimal solution is depicted by the red solid line and target by black solid line with squares at data points, same parameters as used for Figure 4.14. The x-axis represents the space variable x and the y-axis represents density (top), velocity (middle) and pressure (bottom). 68

4.16 First-order (Left) and second-order (Right) 1D Euler Equations optimal control results. Optimal (red solid line) and target (black solid line with squares at data points) solutions, for density, velocity and pressure profiles with JIN XIN scheme at time, $T = 0.17$, $u_L = (1.2,\ 0.2,\ 1.25)$, $u_R = (0.32,\ 0.73,\ 0.32)$, $a_1 = 2.47,\ a_2 = 3.5,\ a_3 = 4.36$, $M = 400$ and $\epsilon = 10^{-8}$. The x-axis represents the space variable x and the y-axis represents density (top), velocity (middle) and pressure (bottom). 69

4.17 First-order (Left) and second-order (Right) 1D Euler Equations optimal control results. Optimal (red solid line) and target (black solid line with squares at data points) solutions, for density, velocity and pressure profiles with discrete kinetic scheme. Same parameters as in Figure 4.16. The x-axis represents the space variable x and the y-axis represents density (top), velocity (middle) and pressure (bottom). 70

4.18 First-order (Left) and second-order (Right) 1D Euler Equations optimal control results. Optimal (red solid line) and target (black solid line with squares at data points) solutions, for density, velocity and pressure profiles with JIN XIN scheme at time; $T = 0.17$, $u_L = (1.24,\ 0.1852,\ 1.25)$, $u_R = (0.366,\ 0.629,\ 0.33)$, $a_1 = 1.96,\ a_2 = 2.9,\ a_3 = 4.33$, $M = 400$ and $\epsilon = 10^{-8}$. The x-axis represents the space variable x and the y-axis represents density (top), velocity (middle) and pressure (bottom). 72

4.19 First-order (Left) and second-order (Right) 1D Euler Equations optimal control results. Optimal (red solid line) and target (black solid line with squares at data points) solutions, for density, velocity and pressure profiles obtained with the discrete kinetic scheme. Same parameters as in Figure 4.18. The x-axis represents the space variable x and the y-axis represents density (top), velocity (middle) and pressure (bottom). 73

4.20 First-order (Left) and second-order (Right) 1D Euler Equations optimal control results. Optimal (red solid line) and target (black solid line with squares at data points) solutions, for density, velocity and pressure profiles with JIN XIN scheme at time, $T = 0.17$, $u_L = (1.0,\ 0.0,\ 1.0)$, $u_R = (0.1,\ 0.0,\ 0.125)$ for optimal; and $u_L = (1.1,\ 0.0,\ 1.1)$, $u_R = (0.2,\ 0.0,\ 0.2)$ for target. $a_1 = 1.96,\ a_2 = 2.9,\ a_3 = 4.33$, $M = 400$ and $\epsilon = 10^{-8}$. The x-axis represents the space variable x and the y-axis represents density (top), velocity (middle) and pressure (bottom). 74

4.21 First-order (Left) and second-order (Right) 1D Euler Equations optimal control results. Optimal (red solid line) and target (black solid line with squares at data points) solutions, for density, velocity and pressure profiles with discrete kinetic scheme at time, $T = 0.17$. Same parameters as in Figure 4.20. The x-axis represents the space variable x and the y-axis represents density (top), velocity (middle) and pressure (bottom). 75

4.22 Convergence history for the solution of the optimization problem computed with the first order (left) and second-order (right) relaxing schemes for both JIN XIN and discrete kinetic schemes. The x-axis represents the number of iterations and the y-axis represents the cost functional value. 76

1. Introduction

Hyperbolic conservation laws (HCLs) is an active research field with rapidly increasing applications in areas such as fluid mechanics, aircraft designs, traffic flows, elasticity and relativity. This work is devoted to discuss the mathematical framework and numerical solutions for the adjoint-based optimization of the optimal control problem subject to one-dimensional relaxation systems of HCLs. We are interested in the numerical solutions of optimization problems governed by a system of hyperbolic conservation laws (HCLs). The approach under consideration is called adjoint, and in this case, it requires solutions of two systems of equations in each optimization cycle, as it is explained in the later sections.

Since 1970s, there has been intensive research in the field of HCLs. This research has accelerated the applications of HCLs in fields such as Computational Fluid Dynamics (CFD) [89]. HCLs are very important in our daily life because they model different sorts of physical processes. Several studies conducted led to successful application of HCLs in science [27, 82], technology of combustion, detonation, aerodynamic designs and gas dynamics [49, 125], to name only a few. Today, there is a lot of research which aims to apply HCLs in solving challenging problems in engineering and science (reactive flows, multi-component flows, groundwater flows, semiconductors and meteorology), economical and industrial platforms. There are typical applications of HCLs, such as Buckley Leverett [126] in modeling flows in oil and gas reservoirs, the shallow water equations in meteorology and oceanography, equations of magnetohydrodynamics (MHD) in studying supernovas in astrophysics, also applied in plasma physics, solid mechanics; and Euler Equations in aircraft designs and traffic flow models [4, 79, 126]. Some other references on successful applications of HCLs are found in [63].

Apart from numerous existing literature on the relaxation approach to solutions of HCLs, to our knowledge, few reports are available on the optimal control problems subject to relaxation systems. In this study, we investigated two relaxation approaches as constraints to the optimization problem (to be defined later), namely: the JIN XIN relaxation approach [64], and the discrete velocity model approach in [5, 92]. Contrary to the existing results in [10, 94, 128], we have extended the adjoint method to second-order relaxing schemes for numerical optimization of the problem governed by nonlinear scalar and systems of HCLs. Effective relaxation approaches have been developed and their performances compared in connection to adjoint-based optimization. The aim is to minimize the cost functional that matches the optimal solution and the target, subject to this set of relaxation systems.

1.1 Objectives of the Study

Objectives for this study are as follows:

- to derive optimality systems for the two variants of the relaxation system: the JIN XIN relaxation approach, [64] and the discrete kinetic model [92]. The optimality system is comprised of the systems of equations, namely: state equations, the co-state equations and the optimality condition, which are then discretized in the numerical implementation;
- to derive first-order relaxing schemes and test them by solving different systems of HCLs, including the real world examples and apply these solution procedures to the problem of optimal control. The interest has been to realize the more computationally effective approach, challenging them, pointing out drawbacks and giving suggestions whenever necessary. We have comparatively checked the validity of the two approaches and drawn conclusions based on their numerical results;
- Investigation of the application of second-order relaxing schemes for the solutions of HCLs and for the optimal control problem as well.

Successful optimization in this sense, depends on suitable approach used to approximate solutions of HCLs. HCLs exhibit unique behavior and require special treatment, (see [18, 33, 67, 69, 75, 78, 126]) for their solutions. Generally, numerical schemes for hyperbolic conservation laws available in the literature are numerous. In this regard, it is not possible to explore all of them under this limited space, but in the following section, we discussed some common and frequently used numerical methods for solutions of HCLs.

1.2 Solutions of nonlinear hyperbolic conservation laws

In the past decades, numerous numerical methods have been developed to solve nonlinear hyperbolic conservation laws. The most challenging feature of the nonlinear hyperbolic conservation laws is the development of singularities as their solution evolves with time. These singularities which are jumps are also called shock waves. In general, the property of nonlinear hyperbolic conservation law is that, even if the solution at a given time is smooth, it may in general develop discontinuities at a later time.

Different methods have been used to solve HCLs, with some attempts to generalize solution approaches to high orders of accuracy. For many years, traditional numerical schemes have been used to solve partial differential equations (PDEs). Most of these schemes are not suitable for solving PDEs especially when the function is discontinuous as their solutions, often result into over-smeared representation of shocks or oscillations near discontinuities [121]. Under nonlinear conservation laws (CLs) for example, some schemes fail to capture the correct direction of information propagation yielding incorrect or oscillatory solutions. There are well known methods under this category, namely, Lax-Wendroff second-order method [108], upwind method [109], Godunov's method [47], methods of Hyman [61], MacCormack method [85], Rusanov method

[111], method of Boris and Book [16], method of Harten and Zwas [54], Glimm's method [32] and the random choice method [33]. These methods rely on approximation of derivatives appearing in the differential equations by finite difference method (FDM) [130, 131], finite volume method (FVM) [29, 123] or finite element method (FEM) [30, 31, 66] to obtain discrete forms of PDEs. Detailed discussion on these methods with applications in some cases is found in [106], and basics for the conservation laws-based ideas were discussed in [76].

It is preferred and it has been found valuable to use finite volume methods [77] in the setting of nonlinear hyperbolic conservation laws. The Godunov's method that was introduced in [47] for the purpose of solving the Euler Equations of gas dynamics in the presence of discontinuities for example, is probably the most appealing finite volume approach. Although the derivation of both finite difference and finite volume methods may be quite different, the resulting representation formulae may be identical, but normally, each method is interpreted differently. Finite volume methods involve solutions of Riemann problems. There are well known and frequently used approximate Riemann solvers [125] in finite volume or high-resolution methods reported in various papers and books: The all-shock solver [32], Osher Solver [100], which is an extension of the Engquist-Osher method [39, 40, 41] derived for scalar conservation laws, the HLLE solver [57] and its improvement in [36], and the Roe solver scheme [110]. Riemann problems are usually computationally costly, and one would therefore like to devise a method that avoids solution of the Riemann problem.

Finite volume methods like Godunov's method are at most first-order accurate on smooth regions of solution and in general, these methods perform poorly near or at shock waves or other discontinuities giving very smeared approximations. An improvement is made by developing a method which can be interpreted as a correction phase to the solution of the Riemann problem and through reconstruction of the finite volume fluxes to obtain high-resolution versions of the finite volume methods. High-resolution methods resolve discontinuities more sharply and produce at-least second-order accurate solutions in smooth regions of the flow at the same time trying to remain faithful to the physics of the problem by avoiding nonphysical oscillations near discontinuities. Most high-resolution methods for capturing shocks are based on solutions of Riemann problems between states in neighboring grid cells. Numerous literature rich in history and development of these methods is presented in various books [1, 46, 65, 76, 107, 120, 125]. Second-order methods include for example, Monotone upstream-centred Scheme (MUSCL) [71, 72, 73] and flux-corrected transport (FCT) algorithms by Boris and Book [16] for nonlinear conservation laws.

The class of high-resolution methods also includes high-order accurate finite difference essentially non-oscillatory (ENO) [53, 55, 58, 133, 134] and its extension, weighted ENO [26, 43, 83, 101, 116] schemes designed for problems with piecewise smooth solutions containing discontinuities [119]. ENO and WENO schemes use nonlinear adaptive procedure to automatically choose the locally

smoothest stencils in order to avoid interpolating across discontinuities. The class of these schemes has been successful applied to problems containing shocks as well for smooth solutions with complex structures. ENO and WENO methods are among of the more recent classes which efficiently solve hyperbolic conservation laws. Stable spatial discretization for hyperbolic conservation laws with high-resolution schemes such as ENO [133, 134] and WENO [26, 43, 101] are usually applied in combination with strong stability-preserving (SSP) time discretizations methods discussed below.

Most of these numerical approaches to PDEs, especially HCLs uses semi-discrete methods. These approaches first discretize the PDE in space to obtain a system of ordinary differential equations (ODEs) while retaining continuous time. The ODE is then discretized in time by an appropriate ODE method, typically TVD [48, 54, 56, 98, 99, 117, 118, 124] or SSP [49, 50, 117, 119] Runge-Kutta methods [50, 52, 112, 113, 119]. For Runge-Kutta schemes, one may decide to use multi-level [62, 90] or one-step methods. Multi-level schemes, such as TVD high-order Runge-Kutta time discretizations are rarely used in practice because they are not self starting in the sense that they may need other methods at initial levels to get started. However, these methods may also require large storage during computations. As a result, usually one-step Runge-Kutta TVD methods are preferable because they need low storage and are self starting. Low storage Runge-Kutta methods are discussed in [25, 132]. The advantage of semi-discrete method is that high-order accuracy in space and time can be achieved through a decoupled process, making them much simpler than the fully discrete ones. Due to this reason, high-order schemes, such as Runge-Kutta type time discretizations can easily be applied in combination with different spatial discretizations.

TVD Semi-discrete schemes in combination with Runge-Kutta methods have been a success story in many numerical applications. It has been shown in [48], even if linearly stable, non-TVD Runge-Kutta methods may develop oscillations. It is, therefore, recommended to always maintain TVD property in both time and spatial discretizations for high-order schemes. SSP methods have been widely applied in many areas, some of them include compressible flow [130], incompressible flow [105], viscous flow [123], atmospheric transport [29]. For a complete list of references on applications of SSP methods, an interested reader may consult [49].

There is another numerical approach analogous to Godunov's method based on flux-vector splitting which evaluates fluxes at the cell average discussed in [78]. Mathematical discussion based on this approach is found in various literature referenced in [78]. Equivalent flux-vector splitting approaches have since then been developed, they include Steger-Warming [122], Beam scheme [115], the Marquina flux [35, 86], and the one introduced in [74], followed by a number of other variants and improvements reported in [80, 81].

1.3 Relaxation system

We considered relaxation approximation to HCLs as was first discussed in [64]. Since the first introduction in [64], numerous discussion on relaxation schemes have been emerging [13, 10, 17, 94, 116]. Analysis on the existence and uniqueness of the solution for the relaxation approach described in [64] was given in [129].

A different relaxation framework has been introduced in [6, 5]. This relaxation system basically takes the form of the discrete BGK [14] model approximation. Under this relaxation setting, estimates on the discrete schemes as well as convergence analysis for first-order and second-order spatial dimensions have been studied [6]. Further study is found in [88, 91, 92, 93].

Relaxation methods are based on the replacement of the nonlinear systems of HCLs on a continuous level (before any kind of discretization) by a semilinear system with a stiff relaxation source term. This system reverts to the original conservation law as the relaxation parameter tends to zero. Convergence analysis for scalar hyperbolic conservation law has been fully realized. The case of systems is an ongoing research problem. In numerical computation, our focus is on relaxing schemes which are the limits for small positive relaxation parameter.

We have chosen the relaxation method due to its promising features of simplicity which can lead to generalization to both higher orders and high dimensional systems of HCLs without further modification. However, relaxation approximation preserves the hyperbolic nature of the system on the expense of additional source terms and additional equations. The semilinearity structure of the relaxation system allows for Riemann-solvers free treatment and avoids the computation of Jacobians. All these features make this method incredibly advantageous especially in situations where Jacobians and Riemann problems are difficult to solve [64].

1.4 Adjoint-based optimal control

There is a lot of theoretical and numerical discussion of hyperbolic conservation laws in the optimal control setting. It is well known that a flow generated by hyperbolic conservation laws is not differentiable with respect to the linear structure of L^1 even for scalar $1D$ case [10, 21]. A generalized notion of differential structure for maps taking values within a class of piecewise Lipschitz functions was studied in [22], and the flow generated by a HCL was proven to be differentiable in this generalized sense. The list of papers [15, 19, 20] discuss the notion of shift differentiability of the flow generated by a system of conservation law. The latter two papers also introduce a new differential structure on the BV space of integrable functions having bounded variation. It is also shown in [19], that the flow generated by a scalar conservation law is generally differentiable with respect to this new introduced structure. Adjoint and sensitivity calculus based on shift differentiability in the optimal control of entropy solutions of scalar conservation

laws with source term is discussed in [127]. First-order necessary optimality conditions for systems of conservation laws are given in [23]. This discussion on differentiability of conservation laws is motivated by its applications in the optimal control problems.

HCLs are highly applied in the optimal control problems [15, 20, 22, 84, 127] - finding some geometry that optimizes performance subject to a set of constraints [44]. Applications of conservation laws in optimization are becoming more prominent in traffic flow, turbulent flow, gas dynamics, trajectory planning and in aircraft designs. Discussion on adjoint-based optimization of problems governed by partial differential equations (PDEs) is presented in [45, 51]. Many adjoint-based softwares for CFD have been developed by different pioneers. These include: adjoint-based optimal designs with an application to designing business jets [44], adjoint approach to aerodynamic designs [37, 38], adjoint approach to shape and airfoil designs [2, 24] and continuous adjoint formulation [3, 95]. For trade-off between continuous and discrete adjoint approach to automatic aerodynamic optimization, consult [89].

Several authors including [60] have employed the nonsmooth optimization in combination with the adjoint methods for subgradient computation. They studied the optimal control of flows with discontinuities and tested the approach using one dimension (1D) Riemann problem of Euler Equations. In the cases where gradient-based methods were employed, either discontinuities were ignored or means to circumvent their effects were employed. In many situations shocks were smoothed using numerical dissipation. It has been shown that smoothing is sometimes equivalent to modifying the cost function [87].

In realistic situations one has to deal with nonlinear systems. The nonlinearity in systems of HCLs poses both analytical and numerical difficulties to their solutions due to discontinuities that may arise. Since it is generally known that the semi-group generated by a HCL is not differentiable in L^1 even in the scalar, 1D case [10]; and the solution of HCL is needed in the optimization cycle, it is therefore important to pay close attention to its solution.

The adjoint approach is robust in the sense that all sensitivities are calculated only once via the adjoint equation in each iteration cycle regardless of the number of control parameters [51]. In combination with the adjoint approach, the relaxation method becomes more appealing. However, the adjoint approach avoids unnecessary repetition which we would encounter if we would have opted to use sensitivity-based optimization, hence may reduce CPU time and memory required for storage.

1.4.1 Organization of the work

To this point, the scope, and plan of the work are outlined as follows: The next Chapter is devoted to discuss useful mathematical and physical notions that are important for this study. It is very important to clearly understand the physics of the problem since this serves as a

fundamental tool to successfully solve numerically an optimization problem. This is particularly true because numerical solutions of the optimization problem and that of HCLs are a coupled process, in the sense that, the optimization cannot be achieved independently of the solution of HCL. It is known that discontinuities may arise in the solution of HCL; thus both mathematical and physical analysis must be carried out correctly prior to numerically solving HCLs. We therefore discussed general physical and mathematical behavior underlying the HCLs. It is in this Chapter, where we introduced and discussed the concept of adjoint-based optimization. Next, we presented a brief mathematical explanation of relaxation systems, for both relaxation approximation and the discrete kinetic model. Finally, we discussed and applied the Lagrangian approach to derive optimality systems based on relaxation approaches for the two variants of the relaxations: the JIN XIN [64] and the discrete kinetic model [92]. The derived optimality systems then help in determining the gradients of the cost functional during the numerical optimization process. Optimality system is comprised of the flow equations, the adjoint system and the optimality conditions. In Chapter three, we centered our discussion on derivation of relaxing schemes. Under this Chapter, relaxing schemes from the two relaxation approaches mentioned previously were constructed. For iterative optimization process, we had to discretize equations that comprise the optimality systems. Thus discretization is done under this Chapter, where we use the method of lines (MOL) to discretize the systems of flow and adjoint equations. With the MOL, we proceeded by discretizing the spatial domain while retaining the relaxation HCL continuous in time, to form systems of ODEs, and then we suitably discretized in time by appropriately applying Runge-Kutta methods. For time discretization, we used TVD Runge-Kutta methods, where as for first-order spatial discretization, a simple upwind method is applied. Total variation diminishing (TVD) monotone upstream-centered schemes (MUSCL) scheme was constructed for second-order spatial discretizations by using minmod slope-limiter. In Chapter four, we presented and discussed numerical results for both solutions of HCLs and the optimal control problem. Optimal control results obtained by applications of both first-order and second-order relaxing schemes are presented in this Chapter. The two approaches are compared and conclusions drawn based on obtained numerical results. In Chapter five, a brief remark and general conclusions based on the achieved outcomes were given. Finally, we pointed out the possibilities for future extension of this research as well as challenges that may be encountered.

.

2. Mathematical Framework

2.1 Governing System of Conservation Laws

Conservation laws (CLs) are usually time-dependent systems of partial differential equations. They describe the conservation of quantities such as mass, momentum and energy, and are usually nonlinear if they have to model most of the dynamic situations. These equations are hyperbolic in nature. In one dimensional space, the equations take the form

$$u_t + f(u)_x = 0,\ u(x, t = 0) = u_0(x),\ t \in [0, \infty),\ x \in (-\infty, \infty) \tag{2.1.1}$$

where $u : \mathbb{R}\text{x}\mathbb{R}_+ \to \mathbb{R}^m$ is a vector with m conserved quantities u_j, and $f : \mathbb{R}^m \to \mathbb{R}^m$ is the vector-valued function called the flux function, in which each jth component $f_j(u)$ is a function of components u_j of u. The equation is called scalar when $m = 1$. Equations of type (2.1.1) often describe transport phenomena and they are popularly referred to as the Cauchy problems.

If we integrate equation (2.1.1) over a given subdomain $[x_1, x_2]$, we obtain

$$\frac{d}{dt}\int_{x_1}^{x_2} u(x,t)dx = \int_{x_1}^{x_2} u_t(x,t)dx \tag{2.1.2}$$

$$= -\int_{x_1}^{x_2} f(u(x,t))_x dx$$

$$= f(u(x_1,t) - f(u(x_2,t)) = [\text{inflow at } x_1] - [\text{outflow at } x_2]. \tag{2.1.3}$$

Hence, the primal formulation of the typical conservation law (2.1.1) stipulates that the time rate of change in the amount of quantity u inside any given interval $[x_1, x_2]$ is balanced by the rate of flux of this quantity through the boundary points of the subdomain. The only change in u is due to the quantity entering or leaving the domain of interest through the boundaries.

The more general system (2.1.1) is called *hyperbolic* if the mxm Jacobian matrix of its flux function $f(u)$, for values of

$$u = \begin{bmatrix} u_1 \\ u_2 \\ . \\ . \\ . \\ u_m \end{bmatrix},\ \text{and } f(u) = \begin{bmatrix} f_1 \\ f_2 \\ . \\ . \\ . \\ f_m \end{bmatrix} \tag{2.1.4}$$

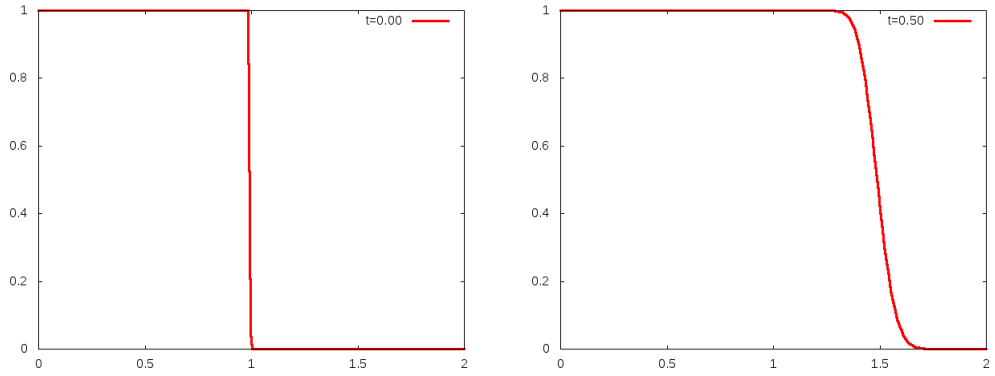

Figure 2.1: Initial solution and final solution at time = 0.5 for the linear advection equation

given by

$$\mathbf{a}(\mathbf{u}) = \frac{\partial \mathbf{f}}{\partial \mathbf{u}} = \begin{bmatrix} \frac{\partial f_1}{\partial u_1} & \cdots & \frac{\partial f_1}{\partial u_m} \\ \frac{\partial f_2}{\partial u_1} & \cdots & \frac{\partial f_2}{\partial u_m} \\ . & . & . \\ . & . & . \\ . & . & . \\ \frac{\partial f_m}{\partial u_1} & \cdots & \frac{\partial f_m}{\partial u_m} \end{bmatrix} \tag{2.1.5}$$

has real eigenvalues and a complete set of m linearly independent eigenvectors corresponding to these eigenvalues (i.e., the Jacobian matrix is diagonalizable). If eigenvalues are distinct, the general system (2.1.1) is said to be strictly hyperbolic.

By explicit differentiation of the second term in (2.1.1), that is

$$\frac{\partial f(u)}{\partial x} = a(u)u_x, \tag{2.1.6}$$

equation (2.1.1) can be written in a quasi-linear (nonconservative) form

$$u_t + a(u)u_x = 0. \tag{2.1.7}$$

When $f(u)_x = au_x$ in (2.1.1) with a a constant, we have a linear system.

Hyperbolic PDEs are used to model transport systems whose conserved information is carried from one point to another within those systems. Solutions to HCLs may be visualized as propagating waves, Figure 2.1. When the system is nonlinear, even if initial conditions are smooth, characteristics can intersect causing the profiles to generate jump discontinuities which propagate as shocks (the wave compresses in one part and stretches on in another), see Figure 2.2. In many cases smooth solutions do not exist, and solutions are sometimes multi-valued.

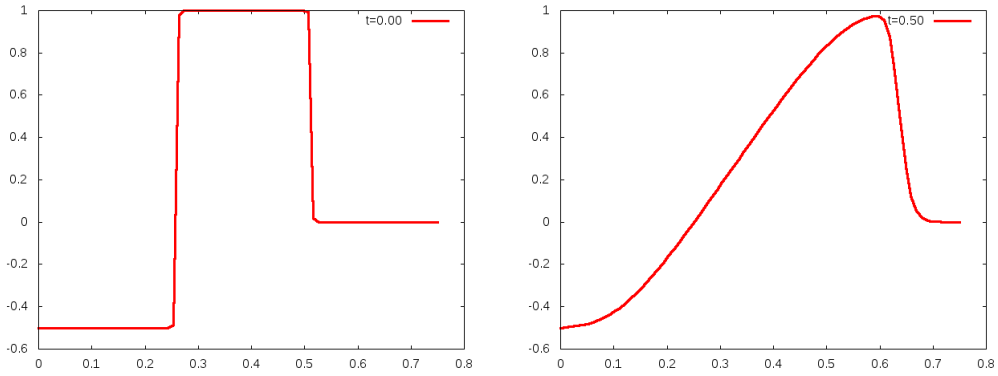

Figure 2.2: Initial and final solution of the Inviscid Burgers' equation at time t = 0.5

Discontinuities in the solutions of nonlinear hyperbolic conservation laws pose serious difficulties which the classical approaches cannot handle. As a result, a number of mathematicians and scientists researching in the field of HCLs started to consider what are called weak solutions, which allow for the development of discontinuous waves. The problem is further complicated due to the fact that in the context of weak solutions, the uniqueness is lost. Several approaches have been developed which set up proper criteria for identifying admissible weak solutions. The most common approach is to use vanishing viscosity [33] and entropy functions [75]. To be able to design efficient numerical methods for HCLs, we need a clear understanding of their analytical structures. In the next section, we discuss briefly ideas related to hyperbolic systems.

2.2 General Hyperbolic Systems

Hyperbolic systems arise in many disciplines especially where the wave motion or advective transport phenomena are involved. Such disciplines include; fluid dynamics, traffic flows, acoustics, elastodynamics, optics, geophysics, biomechanics, the theory of elasticity, electromagnetic waves, direct and inverse scattering and general theory of relativity [70, 77] and many other areas [49]. Hyperbolic systems are basically waves, usually formulated mathematically in terms of time dependent PDEs. The simplest of all hyperbolic systems is the equation (2.1.7) when a is constant. Detailed analysis on the general hyperbolic system framework is found in many books [70, 75, 77, 114, 125].

2.2.1 Linear hyperbolic systems

Linear hyperbolic system

$$u_t + Au_x = 0, u(x,0) = u_0(x) \tag{2.2.1}$$

where $u : \mathbb{R} \times \mathbb{R}_+ \to \mathbb{R}^m$ and $A \in \mathbb{R}^{m\times m}$ is a constant matrix, is called a system of conservation laws with the flux function $f(u) = Au$. The system is called *hyperbolic* if A is *diagonalisable* with real eigenvalues; and is called *strictly hyperbolic* when eigenvalues are distinct. This system is simple and serves as a model for studying more general hyperbolic systems.

2.2.2 Nonlinear hyperbolic systems

The most outstanding challenge many scientists and researchers face when solving nonlinear hyperbolic systems is the tendency of their solutions to develop shock waves. These waves normally develop as abrupt jumps. Therefore, the most distinguished nonlinear feature is the breaking of the solution waves into shocks. The simplest of the nonlinear hyperbolic system is the first-order PDE (2.1.7).

2.2.3 Diagonalization of hyperbolic systems

Matrix (or systems) diagonalization is important in physics and engineering and it has common applications in such areas as stability analysis, the physics of rotating bodies and small oscillations of vibrating systems. In order to analyze and solve the general system (2.2.1), it had been found useful to transform the dependent variables $u(x,t)$ to another set of dependent variables $v(x,t)$.

In order to be able to illustrate the concept of diagonalization and make this transformation, we consider an arbitrary matrix A in a general linear hyperbolic system (2.2.1). A matrix A is said to be diagonalizable if it can be expressed as

$$A = RDR^{-1} \tag{2.2.2}$$

where $D = (\lambda_1, \ldots, \lambda_m)$ is a diagonal matrix of eigenvalues and $R = [r_1, \ldots, r_m]$ is the matrix of right eigenvectors corresponding to the eigenvalues λ_i of A. From (2.2.2), $AR = RD$; that's

$$Ar_p = r_p\lambda_p \text{ where } p = 1, \ldots, m.$$

A system (2.2.1) is said to be diagonalizable if the coefficient matrix A is diagonalizable.

2.2.4 Transform to characteristic variables

The concept of characteristic variables can be well understood by considering the general linear hyperbolic framework (2.2.1). We follow the same presentation style adapted by Toro [125] and LeVeque [75] for this discussion.

Multiplying (2.2.1) by R^{-1} and substituting $A = RDR^{-1}$ we get

$$R^{-1}u_t + R^{-1}(RDR^{-1})u_x = 0. \tag{2.2.3}$$

Since R^{-1} exists, we can define new set of dependent variables $v = (v_1, \ldots, v_m)$, and through transforming $v = R^{-1}u$, we have

$$v_t + Dv_x = 0. \tag{2.2.4}$$

The new variables v are called *characteristic variables*. D is diagonal, so (2.2.4) results (decouples) into m independent scalar equations

$$(v_p)_t + \lambda_p (v_p)_x = 0, \ p = 1, \ldots, m. \tag{2.2.5}$$

Each of these equations is a linear advection equation with a constant coefficient, whose solution (by method of characteristics) is

$$v_p(x,t) = v_p(x - \lambda_p t, 0). \tag{2.2.6}$$

When we write the system (2.2.4) in full it becomes

$$\begin{bmatrix} v_1 \\ v_2 \\ . \\ . \\ . \\ v_m \end{bmatrix}_t + \begin{bmatrix} \lambda_1 & \ldots & 0 \\ 0 & \ldots & 0 \\ . & . & . \\ . & . & . \\ . & . & . \\ 0 & \ldots & \lambda_m \end{bmatrix} \begin{bmatrix} v_1 \\ v_2 \\ . \\ . \\ . \\ v_m \end{bmatrix}_x = 0. \tag{2.2.7}$$

These are governing PDEs in terms of characteristic variables. The characteristic speed is λ_i and there are m characteristic curves satisfying m ordinary differential equations (ODEs)

$$x_t = \lambda_p, p = 1, \ldots, m. \tag{2.2.8}$$

This is useful information that is needed for transformation of a relaxation system (2.5.2). In the next section, we considered what is called weak solutions to (2.1.1).

2.3 Weak Solutions

We consider a Cauchy (initial-value problem (IVP)) for scalar conservation laws in one space dimension

$$\begin{cases} u_t + f(u)_x = 0 \text{ in } \mathbb{R} \times (0, \infty) \\ u(x,t) = u_0(x) \text{ on } \mathbb{R} \times t = 0, \end{cases} \tag{2.3.1}$$

$f : \mathbb{R} \to \mathbb{R}$ and $u_0 : \mathbb{R} \to \mathbb{R}$ are given and the unknown is, $u(x,t) = u : \mathbb{R} \times [0, \infty) \to \mathbb{R}$. As it is known, the method of characteristics (MOC) is the classical method for solving the

IVP for the general first-order PDE with two independent variables. The goal of the MOC when applied to a PDE is to reduce it to an ODE along some characteristic curves, and the ODE can then be integrated to obtain the desired solution. Singularities are inevitable to the solution of the hyperbolic conservation law (2.3.1), and it is proven in literature [42] that, there does not, in general, exist a smooth solution of (2.3.1) for all times $t > 0$; smooth solution can only exist locally. Since we are interested in the global behavior of this solution, we need to re-formulate the problem by setting a general framework that allows some sort of generalized or weak solutions. Weak solutions are not classical [4], not necessarily differentiable, and they satisfy CLs point-wise. Weak solutions are also not necessarily unique and they may not be physical. Due to that, extra conditions such as Oleinik entropy condition [97] and Lax's entropy condition [68], which narrows down weak solutions; singling out admissible ones may need to be imposed. The reader may refer to various existing standard literature such as [33, 42] for classical treatment of weak solutions.

Since we cannot in general find a classical solution of (2.3.1), we must devise some means to solve for a more general solution u which is the solution of an IVP (2.3.1). We can achieve this by *temporarily* assuming u is smooth and multiply the PDE (2.3.1) by an arbitrary test function Φ with continuous first derivatives, in $\mathbb{R}$ and then to integrate by parts, so that we can transfer the derivatives onto Φ. Our test function

$$\begin{cases} \Phi : \mathbb{R} \times [0, \infty) \to \mathbb{R} \text{ is smooth, with} \\ \text{compact support,} \end{cases} \tag{2.3.2}$$

that means the function vanishes outside or on the boundaries of the compact subset of the domain of interest. Now we multiply the PDE (2.3.1) by Φ. Integrating the equation (2.3.3),

$$0 = \int_0^\infty \int_{-\infty}^\infty (u_t + f(u)_x)\Phi dx dt \tag{2.3.3}$$

by parts (Using Fubini's Theorem), we have

$$-\int_0^\infty \int_{-\infty}^\infty u\Phi_t dx dt + \int_{-\infty}^\infty u\Phi|_0^\infty dx - \int_0^\infty \int_{-\infty}^\infty f(u)\Phi_x dx dt + \int_0^\infty f(u)\Phi|_{-\infty}^\infty dt = 0. \tag{2.3.4}$$

We assume that Φ vanishes near the boundaries of $\mathbb{R}$, and with the initial condition $u = u_0(x)$ on $\mathbb{R} \times \{t = 0\}$, we obtain the identity

$$\int_0^\infty \int_{-\infty}^\infty u\Phi_t + f(u)\Phi_x dx dt + \int_{-\infty}^\infty u_0(x)\Phi(x, 0) dx = 0. \tag{2.3.5}$$

Weak solutions will be employed in the derivation of the adjoint systems to the relaxation systems that we consider in the subsequent sections.

2.4 Relaxation Approaches

The aim of relaxation approach is to transform a nonlinear conservation law into a system of linear convective equations with a nonlinear source term. A good approximation to the original conservation law is achieved by solving relaxation system for a positive parameter $\epsilon \ll 1$. Such relaxation systems are stiff. The relaxation method replaces a nonlinear system by a semilinear system with great advantage that it can be solved numerically by avoiding computationally costly Riemann solvers. Here, we have considered two classes of relaxation approaches, namely the relaxation approximation [64] and the discrete kinetic model [5] for the purpose of optimization.

2.5 JIN XIN Relaxation Approximation Methods

We choose relaxation approach [6, 10, 28, 64, 116] because of its simplicity and easy generalization; that is, the system is easily extended to high-order schemes or multi-dimensional systems and their solutions can be treated similarly like in scalar $1D$ case. It has also been noted that, relaxation schemes preserve the hyperbolic structure on the expense of additional terms. However, semi-linearity is perhaps the most attractive feature of relaxation structure which allow for Riemann-solvers free treatment. We consider the model Riemann - Cauchy problem (the IVP with piecewise constant data), $1D$ scalar HCL of the form

$$\frac{\partial u}{\partial t} + \frac{\partial f(u)}{\partial x} = 0;\ x \in \mathbb{R},\ t \geq 0, u \in \mathbb{R} \tag{2.5.1}$$

with initial data $u(x,0) = u_0(x)$.

To obtain a relaxation system, we introduce a linear system with a **stiff** lower order term

$$\begin{cases} \frac{\partial u}{\partial t} + \frac{\partial v}{\partial x} = 0 \\ \frac{\partial v}{\partial t} + a\frac{\partial u}{\partial x} = -\frac{1}{\epsilon}(v - f(u)) \end{cases} \tag{2.5.2}$$

where ϵ is the small positive parameter called *relaxation rate*, v is the artificial variable and a is a positive constant (characteristic speed) of the relaxation system (2.5.2); satisfying the sub-characteristic condition

$$a - (f'(u))^2 \geq 0. \tag{2.5.3}$$

In the limit $\epsilon \to 0$, the relaxation system (2.5.2) can be approximated to

$$v = f(u),\ \frac{\partial u}{\partial t} + \frac{\partial f(u)}{\partial x} = 0. \tag{2.5.4}$$

We can use Chapman-Enskog expansion to show that condition (2.5.3) must hold [116].

2.5.1 Chapman-Enskog analysis for JIN XIN relaxation system

We take the first order approximation for v,

$$v^\epsilon = f(u^\epsilon) + \epsilon v_1; \tag{2.5.5}$$

thus

$$v_x^\epsilon = f(u^\epsilon)_x + \epsilon (v_1)_x. \tag{2.5.6}$$

Substituting (2.5.6) into the first equation of system (2.5.2), we have

$$u_t^\epsilon + f(u^\epsilon)_x + \epsilon (v_1)_x = 0,$$

$$\Longrightarrow \; u_t^\epsilon + f(u^\epsilon)_x = -\epsilon (v_1)_x. \tag{2.5.7}$$

Substituting (2.5.5) into the second equation of (2.5.2)

$$(f(u^\epsilon) + \epsilon v_1)_t + a u_x^\epsilon + \frac{1}{\epsilon}(f(u^\epsilon) + \epsilon v_1 - f(u^\epsilon)) = 0, \tag{2.5.8}$$

$$f(u^\epsilon)_t + \epsilon (v_1)_t + a u_x^\epsilon + v_1 = 0, \tag{2.5.9}$$

$$f(u^\epsilon)_t + a u_x^\epsilon + v_1 = \mathcal{O}(\epsilon). \tag{2.5.10}$$

We redefine $f(u^\epsilon)$ so as to eliminate its derivative with respect to t, this goes as follows:

$$\frac{\partial f}{\partial u^\epsilon}\frac{\partial u^\epsilon}{\partial t} + a u_x^\epsilon + v_1 = \mathcal{O}(\epsilon). \tag{2.5.11}$$

Using $u_t^\epsilon = -v_x^\epsilon$,

$$\frac{\partial f}{\partial u^\epsilon}\left(-\left[f(u^\epsilon) + \epsilon v_1\right]\right)_x + a u_x^\epsilon + v_1 = \mathcal{O}(\epsilon), \tag{2.5.12}$$

$$-\frac{\partial f}{\partial u^\epsilon}\frac{\partial f}{\partial x} - \epsilon \frac{\partial f}{\partial u^\epsilon}\frac{\partial v_1}{\partial x} + a u_x^\epsilon + v_1 = \mathcal{O}(\epsilon), \tag{2.5.13}$$

$$-\frac{\partial f}{\partial u^\epsilon}\frac{\partial f}{\partial u^\epsilon}\frac{\partial u^\epsilon}{\partial x} - \epsilon \frac{\partial f}{\partial u^\epsilon}\frac{\partial v_1}{\partial x} + a u_x^\epsilon + v_1 = \mathcal{O}(\epsilon). \tag{2.5.14}$$

Therefore,

$$-f'(u^\epsilon)^2 u_x^\epsilon + a u_x^\epsilon = \mathcal{O}(\epsilon) - v_1. \tag{2.5.15}$$

Substituting (2.5.7) into (2.5.15) and dropping the $\mathcal{O}(\epsilon)$ term, we have the second order PDE for u^ϵ, i.e.,

$$u_t^\epsilon + f(u^\epsilon)_x = -\epsilon \left[\left(f'(u^\epsilon)^2 - a\right) u_x^\epsilon\right]_x. \tag{2.5.16}$$

Hence the relaxation system (2.5.2) converges to the system of conservation laws (2.5.1) iff the sub-characteristic condition (2.5.3) is satisfied.

2.5.2 Diagonalization of JIN XIN relaxation system

We consider a system of hyperbolic conservation laws in one space dimension,

$$\frac{\partial u}{\partial t} + \frac{\partial f(u)}{\partial x} = 0, \ x \in \mathbb{R}, \ t > 0 \tag{2.5.17}$$

where $u \in \mathbb{R}^m$, $f(u) \in \mathbb{R}^m$ and $f(u)$ is assumed to be a smooth function. Through relaxing system (2.5.17), we have what we call a *relaxation* system,

$$\begin{cases} \frac{\partial u}{\partial t} + \frac{\partial v}{\partial x} = 0, \\ \frac{\partial v}{\partial t} + A\frac{\partial u}{\partial x} = -\frac{1}{\epsilon}(v - f(u)) \end{cases} \tag{2.5.18}$$

where $v \in \mathbb{R}^m$, $A = \text{diag}(a_1, a_2, \ldots, a_m)$ is a positive diagonal matrix, and ϵ is the relaxation rate.

We are looking for the characteristic variables of the system (2.5.18). To do so, we have to diagonalize the relaxation system (2.5.18).

First we need to transform relaxation system (2.5.18) into the form:

$$\vec{U}_t + \vec{F}(\vec{U})_x = -\frac{1}{\epsilon}\vec{G}(\vec{U}) \tag{2.5.19}$$

$$\text{where } \vec{U} = \begin{pmatrix} u \\ v \end{pmatrix}. \tag{2.5.20}$$

We write the linear hyperbolic part (left side of (2.5.19)) in the form below:

$$\begin{pmatrix} u \\ v \end{pmatrix}_t + \begin{pmatrix} 0 & I \\ A & 0 \end{pmatrix} \begin{pmatrix} u \\ v \end{pmatrix}_x = -\frac{1}{\epsilon}\vec{G}(\vec{U}). \tag{2.5.21}$$

In compact form, (2.5.21) can be re-written as

$$\vec{U}_t + \tilde{A}\vec{U}_x = -\frac{1}{\epsilon}\vec{G}(\vec{U}) \tag{2.5.22}$$

with

$$\tilde{A} = \begin{pmatrix} 0 & I \\ A & 0 \end{pmatrix}. \tag{2.5.23}$$

The linear hyperbolic part of (2.5.22),

$$\vec{U}_t + \tilde{A}\vec{U}_x = 0, \ \vec{U}(x, 0) = \vec{U}_o(x) \tag{2.5.24}$$

where $\vec{U} : \mathbb{R} \times \mathbb{R}_+ \to \mathbb{R}^{2m}$ and $\vec{F}(\vec{U}) = \tilde{A}\vec{U}$

is said to be diagonalizable if the coefficient matrix $\tilde{A}$ is diagonalizable.

We now make a local transformation to the hyperbolic system (2.5.24) by computing its characteristic variables. To be able to do that, we follow the same presentation style adapted by [125] and [75].

2.5.3 Characteristic variables for JIN XIN relaxation system

In this section we will again consider a scalar conservation law for clarity. Extension to a system is straight-forward. We consider the general linearized hyperbolic system

$$\begin{bmatrix} u \\ v \end{bmatrix}_t + \begin{bmatrix} 0 & 1 \\ a & 0 \end{bmatrix} \begin{bmatrix} u \\ v \end{bmatrix}_x = 0. \tag{2.5.25}$$

We define characteristic variables

$$\vec{V} = (V_1, V_2)^T = R^{-1}\vec{U} \tag{2.5.26}$$

where R is the matrix of right eigenvectors and R^{-1} is its inverse. We solve for eigenvalues of the matrix

$$\begin{bmatrix} 0 & 1 \\ a & 0 \end{bmatrix}, \tag{2.5.27}$$

$\lambda_p, \;\; p = 1, 2.$

Thus $\lambda_{1,2} = \pm a^{\frac{1}{2}}$.

The matrix of right eigenvectors associated with $\lambda_{1,2} = \pm a^{\frac{1}{2}}$ is given by

$$R = \begin{bmatrix} r_1 & r_2 \end{bmatrix} = \begin{bmatrix} -a^{-\frac{1}{2}}\omega & a^{-\frac{1}{2}}\bar{\omega} \\ \omega & \bar{\omega} \end{bmatrix}. \tag{2.5.28}$$

Note: characteristic variables $\vec{V} = (V_1, V_2)^T = R^{-1}\vec{U}$.

But

$$R^{-1} = \frac{1}{\left(-a^{-\frac{1}{2}}\omega\bar{\omega} - a^{-\frac{1}{2}}\omega\bar{\omega}\right)} \begin{bmatrix} \bar{\omega} & -a^{-\frac{1}{2}}\bar{\omega} \\ -\omega & -a^{-\frac{1}{2}}\omega \end{bmatrix}. \tag{2.5.29}$$

So

$$\vec{V} = \begin{bmatrix} \frac{1}{2a^{-\frac{1}{2}}\omega} & \frac{1}{2\omega} \\ \frac{1}{2a^{-\frac{1}{2}}\bar{\omega}} & \frac{1}{2\bar{\omega}} \end{bmatrix} \begin{bmatrix} u \\ v \end{bmatrix}, \tag{2.5.30}$$

$$= \left(\frac{v}{2\omega} - \frac{u}{2a^{-\frac{1}{2}}\omega}, \;\; \frac{v}{2\bar{\omega}} + \frac{u}{2a^{-\frac{1}{2}}\bar{\omega}}\right) = (V_1, V_2). \tag{2.5.31}$$

Choosing $\omega = \bar{\omega} = \frac{1}{2}$, we have

$$\vec{V} = (V_1, V_2) = \left(v - a^{\frac{1}{2}}u, \;\; v + a^{\frac{1}{2}}u\right). \tag{2.5.32}$$

We re-write system (2.5.25) as

$$\begin{bmatrix} v - a^{\frac{1}{2}}u \\ v + a^{\frac{1}{2}}u \end{bmatrix}_t + \begin{bmatrix} -a^{\frac{1}{2}} & 0 \\ 0 & a^{\frac{1}{2}} \end{bmatrix} \begin{bmatrix} v - a^{\frac{1}{2}}u \\ v + a^{\frac{1}{2}}u \end{bmatrix}_x = 0. \tag{2.5.33}$$

Next we introduce a different relaxation system presented in [5, 88, 92] namely the discrete kinetic system. This relaxation system is simply a BGK model [14] considered in the next section.

2.6 A BGK Model

Consider a general system of conservation laws

$$\partial_t u + \sum_{j=1}^{D} \partial_j F_j(u) = 0, \tag{2.6.1}$$

where

$$(x,t) \in \mathbb{R}^D \times [0,\infty),\ u = u(x,t) \in U \text{ a convex subset of } \mathbb{R}^m, \tag{2.6.2}$$

$F_j : U \to \mathbb{R}^m,\ j = 1,\dots,D$, are smooth functions.
A BGK model is a system

$$\partial_t f_i + \lambda_i \partial_x f_i = \frac{1}{\epsilon}(M_i(u) - f_i),\ i = 1,\dots,L, \tag{2.6.3}$$

with $\epsilon > 0$, $L \geq N$ and for each $i \in \{1,\dots,L\}$,

$$f_i = (f_i^1,\dots,f_i^m) \in \mathbb{R}^m; \tag{2.6.4}$$

$$\lambda_i = (\lambda_{i1},\dots,\lambda_{iD}) \in \mathbb{R}^D; \tag{2.6.5}$$

$$M_i(u) : \mathbb{R}^m \to \mathbb{R}^m. \tag{2.6.6}$$

Let $u := \sum_i^L f_i$,
and assume the components of the Maxwellians, M_i, are denoted by

$$M_i^1,\dots,M_i^m,\ i = 1,\dots,L. \tag{2.6.7}$$

Consider the consistency conditions

$$\sum_{i=1}^{L} M_i(u) = u, \tag{2.6.8}$$

$$\sum_{i=1}^{L} \lambda_{ij} M_i(u) = F_j(u), \ j = 1, \ldots, D. \tag{2.6.9}$$

Consider also solutions f^ϵ of (2.6.3) (suppose that they form a bounded sequence, independent of ϵ, and that $u^\epsilon \to u$, as $\epsilon \to 0$). Then from (2.6.3),

$$M(u^\epsilon) \to M(u) \text{ and } f^\epsilon \to M(u). \tag{2.6.10}$$

If we sum (2.6.3) over i, we obtain,

$$\partial_t \sum_{i=1}^{L} f_i + \sum_{i=1}^{L} \sum_{j=1}^{D} \lambda_{ij} \partial_j f_i = \frac{1}{\epsilon} (\sum_{i=1}^{L} M_i(u) - \sum_{i=1}^{L} f_i). \tag{2.6.11}$$

From the analysis above, we can write (2.6.1) as

$$\partial_t u^\epsilon + \sum_{j=1}^{D} \partial_j \left(\sum_{i=1}^{L} \lambda_{ij} M_i(u) \right) = 0. \tag{2.6.12}$$

Using condition (2.6.9), we obtain (2.6.1) by allowing $\epsilon \to 0$ in equation (2.6.12).

The flux F_j, the fixed velocities λ_i, and the Maxwellians M_i are usually chosen to satisfy the compatibility conditions (2.6.8) and (2.6.9).

Normally, discrete kinetic system can be treated in a similar manner like a BGK model. In the next section, we introduce the problem that we have considered for optimization in conjuction with adjoint-based method, which is also discussed in the subsequent sections.

2.7 Problem Formulation and Adjoint Approach to Optimization

We are interested in minimizing the objective functional

$$J(u(x, T; u_0)(u_0), u_0; u_d) = \frac{1}{2} \int_\Omega |u(x, T; u_0) - u_d(x)|^2 d\Omega \tag{2.7.1}$$

subject to a system of HCL (2.1.1), where u is the solution of (2.1.1) at a terminal time T, u_0 is the initial condition and u_d is the target solution.

Our aim is to compute the optimal initial values $u_0(x)$ that will generate optimal solution $u(., T)$ which matches to a given target solution u_d at terminal time T.

The approach used is presently known as the method of Lagrange multipliers, named after its developer, Joseph Louis Lagrange (1736 - 1813), to formulate the problem (2.7.1) as an unconstrained optimal control problem. Hence we need to optimize

$$L(u(x, T; u_0)(u_0), u_0, \lambda; u_d) = J(u(x, T; u_0)(u_0), u_0; u_d) + \lambda \left(\frac{\partial u}{\partial t} + \frac{\partial f(u)}{\partial x} \right), \tag{2.7.2}$$

where λ is the co-state variable. The term optimal control refers to the fact that one is trying to determine some control parameter which causes a process to minimize (maximize) some performance measure at the same time satisfying a set of physical constraints. In this case, the optimization cycle for the adjoint-based method for the minimization of the problem (2.7.1), needs two solutions from two systems of hyperbolic conservation laws, the state systems (flow equations) and the adjoint systems to the relaxation systems (2.5.2, 2.6.3). The adjoint systems are derived using the formal Lagrangian approach. This is carried out in the next two subsections.

2.7.1 Derivation of the optimality system from JIN XIN relaxation system

We are interested in the optimization of the objective function

$$J(u(x,T),u_0;u_d)=\frac{1}{2}\int_\Omega |u(x,T;u_0)-u_d(x)|^2 d\Omega \tag{2.7.3}$$

constrained by relaxation system in (2.5.18), where u_0 is the control variable, $u(x,T;u_0)$ the solution at time T with initial condition u_0 and u_d is the desired profile. We want to solve this optimization problem by using the adjoint approach. Problem (2.7.3) can thus be written as an unconstrained optimal control problem,

$$L=L(u(x,T),u_0,\lambda;u_d)=J(u(x,T),u_0;u_d)+\int_0^T\int_\Omega \lambda \begin{bmatrix} u_t & + & v_x & \\ v_t & + & au_x & +\frac{1}{\epsilon}(v-f(u)) \end{bmatrix} dxdt \tag{2.7.4}$$

where $\lambda=[p,q]^T$ is the co-state variable which is assumed to be a smooth function with compact support in Ω and $\lambda=0$ on the boundaries of Ω. To derive the optimality system, we set first variations of L with respect to each of the variables λ, u, v and u_0 equal to zero.

For convenience, we assume that p and q are smooth functions and integrate by parts, the second term on the left side of (2.7.4) there by transferring the derivatives onto p and q. Setting the first partial derivative of L in (2.7.4) with respect to $\lambda=[p,q]^T$ equal to zero, we have the relaxation system (2.5.18). After integrating

$$L=J(u(x,T),u_0;u_d)+\int_0^T\int_\Omega \left[p(u_t+v_x)+q(v_t+au_x+\frac{1}{\epsilon}(v-f(u)))\right] dxdt; \tag{2.7.5}$$

by parts, we have

$$\begin{aligned} L = J(u(x,T),u_0;u_d) &+ \int_\Omega up|_0^T dx - \int_\Omega\int_0^T up_t dtdx + \int_0^T pv|_{\partial\Omega} dt \\ &- \int_0^T\int_\Omega vp_x dxdt + \int_\Omega vq|_0^T dx - \int_\Omega\int_0^T vq_t dtdx + a\int_0^T qu|_{\partial\Omega} dt \\ &- a\int_0^T\int_\Omega uq_x dxdt + \int_0^T\int_\Omega \frac{q}{\epsilon}(v - f(u))dxdt. \end{aligned} \tag{2.7.6}$$

Assume, that u and v vanish at the boundaries of Ω, then

$$\begin{aligned} L = J(u(x,T),u_0;u_d) &+ \int_\Omega \left[u_T p_T - u_0 p_0\right] dx - \int_\Omega\int_0^T up_t dtdx - \int_0^T\int_\Omega vp_x dxdt \\ &+ \int_\Omega \left[v_T q_T - v_0 q_0\right] dx - \int_\Omega\int_0^T vq_T dtdx - a\int_0^T\int_\Omega uq_x dxdt \\ &+ \int_0^T\int_\Omega \frac{q}{\epsilon}(v - f(u))dxdt. \end{aligned} \tag{2.7.7}$$

To get the adjoint system we set the first partial derivatives of L with respect to u and v equal to zero from (2.7.7) above.

Thus,

$$\begin{aligned} \frac{\partial L}{\partial u} &= \frac{\partial J}{\partial u(x,T)}\frac{\partial u(x,T)}{\partial u} - \int_\Omega\int_0^T p_t dtdx - a\int_0^T\int_\Omega q_x dxdt - \int_0^T\int_\Omega \frac{\partial f(u)}{\partial u}\frac{q}{\epsilon}dxdt \\ &= 0, \end{aligned} \tag{2.7.8}$$

results to

$$-p_t - aq_x = f'(u)\frac{q}{\epsilon},\ p(x,t=T) = p_T(x). \tag{2.7.9}$$

Again,

$$\frac{\partial L}{\partial v} = -\int_0^T\int_\Omega p_x dxdt - \int_\Omega\int_0^T q_t dtdx + \int_0^T\int_\Omega \frac{q}{\epsilon}dxdt = 0, \tag{2.7.10}$$

yields

$$-q_t - q_x = -\frac{q}{\epsilon},\ q(x,t=T) = q_T(x). \tag{2.7.11}$$

Therefore, we have the system of adjoint equations:

$$\begin{aligned} -p_t - aq_x = f'(u)\frac{q}{\epsilon},\ p(x,t=T) = p_T(x), \\ -q_t - q_x = -\frac{q}{\epsilon},\ q(x,t=T) = q_T(x), \end{aligned} \tag{2.7.12}$$

with terminal conditions

$$p_T(x) = u_T(x) - u_d, \; q_T(x) = 0 \tag{2.7.13}$$

resulting from setting $\frac{\partial L}{\partial u_T} = 0$ and $\frac{\partial L}{\partial v_T} = 0$.

Setting the partial derivative of L with respect to u_0 equal to zero, gives the optimality condition

$$\frac{\partial J}{\partial u_0} = \int_\Omega \left[p_0 - \frac{\partial f(u_0)}{\partial u_0} \frac{q_0}{\epsilon} \right] dx. \tag{2.7.14}$$

This simplifies to the gradient

$$J_{u_0} = p_0 + f(u_0) q_0. \tag{2.7.15}$$

The relaxation system (2.5.18), with the initial conditions, adjoint equations (2.7.12) and the gradient (2.7.15) together with the terminal conditions (2.7.13) form what we call the optimality system.

2.7.2 Derivation of the adjoint system for the discrete kinetic model

We adapt the same approach, we have used to derive the optimality system for the relaxation approximation above. Consider the Maxwellians of the form

$$M_i(u) = \alpha_i u + \beta_i A(u), \tag{2.7.16}$$

$$= \alpha_i \sum_{j=1}^{N} f_j + \beta_i \sum_{j=1}^{N} \lambda_j f_j, \tag{2.7.17}$$

and a discrete kinetic model

$$f_{it} + \lambda_i f_{ix} = \frac{1}{\epsilon}(M_i(u) - f_i). \tag{2.7.18}$$

We use Lagrangian approach to augment the objective function

$$J(u(x,T)(u_o); u_d) = \frac{1}{2} \int_\Omega |u(x,T) - u_d|^2 d\Omega, \tag{2.7.19}$$

that is,

$$\begin{aligned} L &= L(u(x,T)(u_0), p_i; u_d) \\ &= J(u(x,T)(u_0); u_d) + \int_0^T \int_\Omega p_i \left[f_{it} + \lambda_i f_{ix} - \frac{1}{\epsilon}(M_i(u) - f_i) \right] dxdt. \end{aligned} \tag{2.7.20}$$

We introduce the Maxwellians and re-write the Lagrangian functional

$$L = J(u(x,T)(u_0); u_d) + \int_0^T \int_\Omega p_i \left[f_{it} + \lambda_i f_{ix} - \frac{1}{\epsilon} \left(\sum_{j=1}^{n} \alpha_i f_j + \sum_{j=1}^{N} \beta_i \lambda_j f_j - f_i \right) \right] dxdt. \tag{2.7.21}$$

Let us integrate

$$\int_0^T \int_\Omega p_i \left[f_{it} + \lambda_i f_{ix} - \frac{1}{\epsilon} \left(\sum_{j=1}^{n} \alpha_i f_j + \sum_{j=1}^{N} \beta_i \lambda_j f_j - f_i \right) \right] dxdt$$

by parts by assuming that $p_i's$ are smooth functions and transfer derivatives onto $p_i's$. After integrating, we can re-write equation (2.7.21) as follows,

$$\begin{aligned} L = J(u(x,T)(u_0);u_d) + \int_\Omega p_i f_i|_0^T dx - \int_\Omega \int_0^T f_i p_{it} dt dx + \int_0^T p_i \lambda_i f_i|_{\partial\Omega} dt - \int_0^T \int_\Omega \lambda_i f_i p_{ix} dx dt \\ - \int_0^T \int_\Omega \frac{1}{\epsilon} p_i \left[\sum_{j}^{N} \alpha_i f_j + \sum_{j}^{N} \beta_i \lambda_j f_j - f_i \right] dxdt. \end{aligned} \tag{2.7.22}$$

Assume that $f_i's$ vanish at the boundaries of Ω, then

$$\begin{aligned} L = J(u(x,T)(u_0);u_d) + \int_\Omega \left[p_{iT} f_{iT} - p_{i0} f_{i0} \right] dx - \int_\Omega \int_0^T f_i p_{it} dt dx - \int_0^T \int_\Omega \lambda_i f_i p_{ix} dx dt \\ - \int_0^T \int_\Omega \frac{p_i}{\epsilon} \left[\sum_{j=1}^{N} \alpha_i f_j + \sum_{j=1}^{N} \beta_i \lambda_j f_j - f_i \right] dxdt. \end{aligned} \tag{2.7.23}$$

Setting the first partial derivative of L with respect to p_i equals to zero, we have the relaxation system (2.7.18).

Similarly,

$$\begin{aligned} \frac{\partial L}{\partial f_i} &= -\int_\Omega \int_0^T p_{it} dt dx - \int_0^T \int_\Omega \lambda_i p_{ix} dx dt - \int_0^T \int_\Omega \frac{1}{\epsilon} \left[\sum_{i=1}^{N} \alpha_i p_i + \sum_{i=1}^{N} \beta_i \lambda_i p_i - p_i \right] dxdt \\ &= 0, \end{aligned} \tag{2.7.24}$$

implies that

$$-\int_\Omega \int_0^T p_{it} dt dx - \int_0^T \int_\Omega \lambda_i p_{ix} dx dt - \int_0^T \int_\Omega \frac{1}{\epsilon} \left[\sum_{i=1}^{N} \alpha_i p_i + \sum_{i=1}^{N} \beta_i \lambda_i p_i - p_i \right] dxdt = 0. \tag{2.7.25}$$

We finally end up with the adjoint equation

$$-p_{it} - \lambda_i p_{ix} = \frac{1}{\epsilon} \left[\sum_{i=1}^{N} (\alpha_i p_i + \beta_i \lambda_i p_i) - p_i \right], \tag{2.7.26}$$

$$p_i(x,T) = M_i(u_T, u_d), \ i = 1, \ldots, L. \tag{2.7.27}$$

Up to this point, we have briefly pointed out mathematical framework related to HCLs and adjoint-based optimization in general. This framework serves as a foundation for the numerical solution of HCLs as well as for the optimization process. In the next Chapter, we consider the discretization methods for the relaxations systems (2.5.2, 2.6.3), and also for the derived adjoint systems (2.7.12, 2.7.26). The subsequent Chapter is thus devoted to discussing effective numerical schemes for solutions of relaxation systems and adjoint equations which we used for optimization.

3. Discretizations of the Relaxation Systems

Due to the fact that conservation laws like the Euler Equations are nonlinear, it may not be possible to obtain explicit solution formulae. Sometimes explicit solutions for Riemann problems may be computed in terms of shocks, rarefaction waves and compound shocks. The procedure is usually tedious, and it may be extremely difficult for more complicated Riemann data. Therefore, there is a need to develop efficient numerical methods to approximate or simulate solutions of hyperbolic conservation laws. However, in order to obtain numerical solutions, the first step is to discretize the continuous PDEs (HCLs in this case) to obtain their discrete versions. This Chapter is therefore focused on discretizations of both flow and adjoint equations for the two relaxation models under consideration. In our solution approach, we used the semi-discrete method in combination with the Implicit-Explicit (IMEX) [10, 102] Runge-Kutta schemes. To achieve second-order accuracy in space, we employed a combination of semi-discrete scheme (Method of lines) and the MUSCL approach following the work of Van Leer [73]. We started by considering the discretization of the relaxation method considered in [64], and then the discrete kinetic model [5, 6, 92]. Derived numerical schemes will be tested for the 1D solutions of scalar and systems of HCLs.

3.1 Construction of the First-order JIN XIN Relaxing Scheme

We develop a numerical discretization, first order in time and space for the relaxation system discussed in [6]. We employ the method of lines (MOL) [63], where we first consider spatial discretization of a system while retaining it continuous in time. For time discretization, we employ TVD Runge-Kutta time discretizations method. We follow similar trend for the discretization of discrete kinetic model.

3.1.1 Spatial discretization

We start the discretization process by considering the following definitions: We denote by h_j a grid point, with grid spacing $h_j = x_{j+\frac{1}{2}} - x_{j-\frac{1}{2}}$, where $x_{j+\frac{1}{2}} = jh_j + \frac{1}{2}h_j$, and a uniform discrete time step, $\triangle t = t^{n+1} - t^n$ for $n = 0, 1, 2 \ldots$. Next we approximate $w^n_{j+\frac{1}{2}} = w(x_{j+\frac{1}{2}}, t^n)$, and define

$$D_x w_j = \frac{w_{j+\frac{1}{2}} - w_{j-\frac{1}{2}}}{h_j}. \tag{3.1.1}$$

Proceeding with the method of lines (MOL) to treat spatial and time discretization separately, we write system (2.5.2) with discretized space in conserved form

$$\begin{cases} \frac{\partial u_j}{\partial t} + \frac{1}{h_j}\left(v_{j+\frac{1}{2}} - v_{j-\frac{1}{2}}\right) = 0 \\ \frac{\partial v_j}{\partial t} + \frac{1}{h_j}a\left(u_{j+\frac{1}{2}} - u_{j-\frac{1}{2}}\right) = -\frac{1}{\epsilon}(v_j - f_j), \end{cases} \tag{3.1.2}$$

where

$$f_j = \frac{1}{h_j}\int_{x_{j-\frac{1}{2}}}^{x_{j+\frac{1}{2}}} f(u)dx = f\left(\frac{1}{h_j}\int_{x_{j-\frac{1}{2}}}^{x_{j+\frac{1}{2}}} udx\right) + \mathcal{O}(h^2) \tag{3.1.3}$$

$$= f(u_j) + \mathcal{O}(h^2), \tag{3.1.4}$$

which is the averaged quantity. With an accuracy of $\mathcal{O}(h^2)$, system (3.1.2) can be written as

$$\begin{cases} \frac{\partial u_j}{\partial t} + \frac{1}{h_j}\left(v_{j+\frac{1}{2}} - v_{j-\frac{1}{2}}\right) = 0 \\ \frac{\partial v_j}{\partial t} + \frac{1}{h_j}a\left(u_{j+\frac{1}{2}} - u_{j-\frac{1}{2}}\right) = \frac{1}{\epsilon}(v_j - f(u_j)). \end{cases} \tag{3.1.5}$$

We have seen that by the method of characteristics, the relaxation system (2.5.2) has two characteristics variables (2.5.32),

$$v \pm a^{\frac{1}{2}}u \tag{3.1.6}$$

with characteristics speeds respectively, $\pm a^{\frac{1}{2}}$.

Applying the first order upwind scheme to (3.1.6) gives,

$$\begin{cases} (v + a^{\frac{1}{2}}u)_{j+\frac{1}{2}} = (v + a^{\frac{1}{2}}u)_j = v_j + a^{\frac{1}{2}}u_j \\ (v - a^{\frac{1}{2}}u)_{j+\frac{1}{2}} = (v - a^{\frac{1}{2}}u)_{j+1} = v_{j+1} - a^{\frac{1}{2}}u_{j+1}. \end{cases} \tag{3.1.7}$$

Solving (3.1.7) for unknowns $u_{j+\frac{1}{2}}$ and $v_{j+\frac{1}{2}}$, we have

$$\begin{cases} u_{j+\frac{1}{2}} = \frac{1}{2}(u_j + u_{j+1}) - \frac{1}{2}a^{-\frac{1}{2}}(v_{j+1} - v_j) \\ v_{j+\frac{1}{2}} = \frac{1}{2}(v_j + v_{j+1}) - \frac{1}{2}a^{\frac{1}{2}}(u_{j+1} - u_j), \end{cases} \tag{3.1.8}$$

and plugging (3.1.8) into (3.1.2) gives the first order semi-discrete upwind approximation to (2.5.2),

$$\begin{cases} \frac{\partial u_j}{\partial t} + \frac{1}{2h_j}(v_{j+1} - v_{j-1}) - \frac{1}{2h_j}a^{\frac{1}{2}}(u_{j+1} - 2u_j + u_{j-1}) = 0 \\ \frac{\partial v_j}{\partial t} + a\frac{1}{2h_j}(u_{j+1} - u_{j-1}) - \frac{1}{2h_j}a^{\frac{1}{2}}(v_{j+1} - 2v_j + v_{j-1}) = -\frac{1}{\epsilon}(v_j - f(u_j)). \end{cases} \tag{3.1.9}$$

3.1.2 TVD Runge-Kutta time discretization

We consider an Implicit-Explicit (IMEX) algorithm presented in [10] for the time discretization of the relaxation system (2.5.2). This algorithm takes two steps: implicit step for stiff ordinary differential equation (ODE), and an explicit step for the system of advection equations, see for example a more recent work on TVD Runge-Kutta time discretizations construction by Pareschi for relaxation systems [103, 104].

Before discretizing system (2.5.2), we split the system into two parts: a system of "stiff" ODE,

$$\begin{cases} u_t = 0 \\ v_t = -\frac{1}{\epsilon}(v - f(u)); \end{cases} \tag{3.1.10}$$

and a non-stiff advection system,

$$\begin{cases} u_t + v_x = 0 \\ v_t + a u_x = 0. \end{cases} \tag{3.1.11}$$

Following the same discretization as in [10, 64], we proceed as follows: starting with initial conditions $u_j^n,\ v_j^n = f(u_j^*)$,

$$u_j^* = u_j^n,\ v_j^* = v_i^n - \frac{\triangle t}{\epsilon}(v_j^* - f(u_j^*)), \tag{3.1.12}$$

$$u_j^{(1)} = u_j^* - \triangle t D_x^* v_j^*,\ v_j^{(1)} = v_j^* - \triangle t a D_x^* u_j^*, \tag{3.1.13}$$

$$u_j^{n+1} = u_j^n,\ v_j^{n+1} = v_j^n. \tag{3.1.14}$$

We can explicitly write

$$v^* = \left(\frac{\epsilon}{\epsilon - \triangle t}\right)\left(v_j^n - \frac{\triangle t}{\epsilon} f(u_j^*)\right), \tag{3.1.15}$$

$$u_j^{(1)} = u_j^* - \frac{\triangle t}{2h_j}(v_{j+1}^* - v_{j-1}^*) + \frac{\triangle t}{2h_j}\sqrt{a}(u_{j+1}^* - 2u_j^* + u_{j-1}^*), \tag{3.1.16}$$

$$v_j^{(1)} = v_j^* - \frac{a\triangle t}{2h_j}(u_{j+1}^* - u_{j-1}^*) + \frac{\triangle t}{2h_j}\frac{a}{\sqrt{a}}(v_{j+1}^* - 2v_j^* + v_{j-1}^*); \tag{3.1.17}$$

$$v_j^{**} = v_j^{(1)} - \frac{\triangle t}{\epsilon}(v_j^{**} - f_j(u_j^{**})) - 2\frac{\triangle t}{\epsilon}(v_j^* - f_j(u_j^*)) \tag{3.1.18}$$

$$v_j^{**} = \left(\frac{\epsilon}{\epsilon + \triangle t}\right)\left(v_j^{(1)} + \frac{\triangle t}{\epsilon} f_j(u_j^{**})\right) - 2\left(\frac{\triangle t}{\epsilon + \triangle t}\right)(v_j^* - f_j(u_j^*)). \tag{3.1.19}$$

Then u and v can be updated as

$$u_j^{(2)} = u_j^{**} - \frac{\triangle t}{2h_j}(v_{j+1}^{**} - v_{j-1}^{**}) + \frac{\triangle t}{2h_j}\sqrt{a}(u_{j+1}^{**} - 2u_j^{**} + u_j^{**}), \tag{3.1.20}$$

$$v_j^{(2)} = v_j^{**} - \frac{\triangle t}{2h_j}a(u_{j+1}^{**} - u_{j-1}^{**}) + \frac{\triangle t}{2h_j}\frac{a}{\sqrt{a}}(v_{j+1}^{**} - 2v_j^{**} + v_{j-1}^{**}). \tag{3.1.21}$$

In the following Section, we derive the discrete version of the adjoint relaxation system (2.7.12). Analogously to the flow equations, discretization process for both space and time is achieved separately, and then, the two semi-discrete schemes are merged to obtain a full discrete scheme.

3.2 First-order Discretization of the Adjoint System

We employ similar approach for the discretization of the adjoint system as we did for the forward equations, following the same method by [10]. The adjoint system is solved backward in time.

3.2.1 Spatial discretization

We consider the set of adjoint equations (2.7.12) and write them as a linear system,

$$\begin{bmatrix} p \\ q \end{bmatrix}_t - \begin{bmatrix} 0 & 1 \\ a & 0 \end{bmatrix}\begin{bmatrix} p \\ q \end{bmatrix}_x = 0. \tag{3.2.1}$$

As it is shown in [10], the characteristic variables $p \pm \sqrt{a}q$ satisfy

$$-\partial_t(p \pm \sqrt{a}q) \mp a\partial_x(p \pm \sqrt{a}q) = 0, \tag{3.2.2}$$

$$\partial_t(-p \mp \sqrt{a}(-q)) \mp a\partial_x(-p \pm \sqrt{a}(-q)) = 0. \tag{3.2.3}$$

Remember that the adjoint equation is solved backward in time, thus an upwind discretization for the linear system (3.5.29) advects $p \pm \sqrt{a}q$ and $-p \pm \sqrt{a}(-q)$ with velocity $\mp\sqrt{a}$. Therefore,

$$(p + \sqrt{a}q)_{j+\frac{1}{2}} = p_{j+1} + \sqrt{a}q_{j+1}, \ (p - \sqrt{a}q)_{j+\frac{1}{2}} = p_j - \sqrt{a}q_j, \tag{3.2.4}$$

and finally, we have

$$\begin{aligned} p_{j+\frac{1}{2}} &= \frac{1}{2}(p_j + p_{j+1}) + \frac{\sqrt{a}}{2}(q_{j+1} - q_j), \\ q_{j+\frac{1}{2}} &= \frac{1}{2}(q_{j+1} + q_j) + \frac{1}{2\sqrt{a}}(p_{j+1} - p_j). \end{aligned} \tag{3.2.5}$$

Substituting $-p$ for p and $-q$ for q, we obtain,

$$\begin{aligned} p_{j+\frac{1}{2}} &= -\frac{p_j + p_{j+1}}{2} - \sqrt{a}\frac{q_{j+1} - q_j}{2}, \\ q_{j+\frac{1}{2}} &= -\frac{q_j + q_{j+1}}{2} - \frac{p_{j+1} - p_j}{2\sqrt{a}}. \end{aligned} \tag{3.2.6}$$

In the following Subsection, we derive a discrete TVD Runge-Kutta type time discretization scheme. Finite-difference equations (3.2.6) are incorporated in this discretization process to have a full discrete scheme.

3.2.2 TVD Runge-Kutta time discretization for the adjoint system

The adjoint scheme is therefore given by,

$$p_j^{(1)} = p_j^{n+1},\ q_j^{(1)} = q_j^{n+1}, \tag{3.2.7}$$

$$p_j^* = p_j^{(1)} + \frac{\triangle t}{\epsilon} q_j^* f_j(u_j^*) - \triangle t a D_x^* q_j^*, \tag{3.2.8}$$

where

$$D_x^* q_j^{(1)} = \frac{1}{h_j}\left(q_{j+\frac{1}{2}}^{(1)} - q_{j-\frac{1}{2}}^{(1)}\right), \tag{3.2.9}$$

and

$$q_{j+\frac{1}{2}}^{(1)} = -\frac{q_j^{(1)} + q_{j+1}^{(1)}}{2} - \frac{p_{j+1}^{(1)} - p_j^{(1)}}{2\sqrt{a}}, \tag{3.2.10}$$

$$q_{j-\frac{1}{2}}^{(1)} = -\frac{q_j^{(1)} + q_{j-1}^{(1)}}{2} - \sqrt{a}\frac{p_j^{(1)} - p_{j-1}^{(1)}}{2}. \tag{3.2.11}$$

Thus,

$$p_j^* = p_j^{(1)} + \frac{\triangle t}{\epsilon} q_j^* f_j(u_j^*) + \frac{1}{2}\frac{\triangle t}{h_j} a\left(q_{j+1}^{(1)} - q_{j-1}^{(1)}\right) + \frac{1}{2}\frac{\triangle t}{h_j}\frac{a}{\sqrt{a}}\left(p_{j+1}^{(1)} - 2p_j^{(1)} + p_{j-1}^{(1)}\right). \tag{3.2.12}$$

Similarly,

$$q_j^* = q_j^{(1)} - \frac{\triangle t}{\epsilon} q_j^* - \triangle t D_x^* p_j^{(1)}, \tag{3.2.13}$$

where

$$D_x^* p_j^{(1)} = \frac{1}{h_j}\left(p_{j+\frac{1}{2}}^{(1)} - p_{j-\frac{1}{2}}^{(1)}\right), \tag{3.2.14}$$

$$p_{j+\frac{1}{2}}^{(1)} = -\frac{p_j^{(1)} + p_{j+1}^{(1)}}{2} - \sqrt{a}\frac{q_{j+1}^{(1)} - q_j^{(1)}}{2},\ p_{j-\frac{1}{2}}^{(1)} = -\frac{p_j^{(1)} + p_{j-1}^{(1)}}{2} - \frac{q_j^{(1)} - q_{j-1}^{(1)}}{2\sqrt{a}}. \tag{3.2.15}$$

Hence,

$$q_j^* = q_j^{(1)} - \frac{\triangle}{\epsilon} q_j^* + \frac{1}{2}\frac{\triangle t}{h_j}\left(p_{j+1}^{(1)} - p_{j-1}^{(1)}\right) + \frac{\sqrt{a}}{2}\frac{\triangle t}{h_j}\left(q_{j+1}^{(1)} - 2q_j^{(1)} + q_{j-1}^{(1)}\right) \tag{3.2.16}$$

or explicitly,

$$q_j^* = \left(\frac{\epsilon}{\epsilon+\triangle t}\right) q_j^{(1)} + \left(\frac{\epsilon}{\epsilon+\triangle t}\right) \frac{\triangle t}{2h_j}\left(p_{j+1}^{(1)} - p_{j-1}^{(1)}\right) + \left(\frac{\epsilon}{\epsilon+\triangle t}\right) \sqrt{a}\frac{1}{2}\frac{\triangle t}{h_j}\left(q_{j+1}^{(1)} - 2q_j^{(1)} + q_{j-1}^{(1)}\right), \tag{3.2.17}$$

$$p_j^n = p_j^*,\ q_j^n = q_j^*. \tag{3.2.18}$$

Next Section discusses what is called MUSCL method, as was first developed by Sweby [124], for construction of higher-order relaxing schemes. Schemes developed using this approach satisfy TVD property and are utmost second-order accurate.

3.3 MUSCL, TVD High Resolution Schemes: JIN XIN Relaxation Scheme

Higher resolution schemes give more appealing results by circumventing some drawbacks such as smearing of solutions at the corners and prevention of oscillations. Construction of TVD or MUSCL schemes uses linear combinations of low order schemes and high order accurate schemes by using some limiter function [78, 119, 124]. In general these schemes give sharper solutions than first-order schemes and improve solutions to at least first-order accuracy across discontinuities.

3.3.1 Construction of MUSCL, TVD second-order in space schemes

We construct a slope limiter type scheme but with enough diffusion to avoid oscillations by following exactly the same approach as presented by [64]. We consider the piecewise linear interpolation to the rth components of $v \pm a^{\frac{1}{2}}u$,

$$(v + \sqrt{a_r}u)_{j+\frac{1}{2}} = (v + \sqrt{a_r}u)_j + \frac{1}{2}h_j\sigma_j^+, \tag{3.3.1}$$

$$(v - \sqrt{a_r}u)_{j+\frac{1}{2}} = (v - \sqrt{a_r}u)_{j-1} + \frac{1}{2}h_{j+1}\sigma_{j+1}^-; \tag{3.3.2}$$

where u and v are respectively, the rth components of U and V, such that $1 \leq r \leq m$, and $\sigma_j^{\pm}$ is the slope of $v \pm \sqrt{a_r}u$ on the jth cell. We use one of the well known Sweby's limiter [124],

$$\sigma_j^{\pm} = \frac{1}{h_j}(v_{j+1} \pm \sqrt{a_r}u_{j+1} - v_j \mp \sqrt{a_r}u_j)\Phi(\theta_j^{\pm}), \tag{3.3.3}$$

where

$$\theta_j^{\pm} = \frac{v_j \pm \sqrt{a_r}u_j - v_{j-1} \mp \sqrt{a_r}u_{j-1}}{v_{j+1} \pm \sqrt{a_r}u_{j+1} - v_j \mp \sqrt{a_r}u_j} \tag{3.3.4}$$

and the minmod slope $\Phi(\theta) = \max(0, \min(1, \theta))$, where

$$\text{minmod}(a, b) = \frac{\text{sgn}(a) + \text{sgn}(b)}{2} \min(|a|, |b|). \tag{3.3.5}$$

From (3.3.1)

$$u_{j+1} = \frac{1}{2}(u_j + u_{j+1}) - \frac{1}{2\sqrt{a_r}}(v_{j+1} - v_j) + \frac{1}{4\sqrt{a_r}}(h_j\sigma_j^+ + h_{j+1}\sigma_{j+1}^-), \tag{3.3.6}$$

$$v_{j+1} = \frac{1}{2}(v_j + v_{j+1}) - \frac{\sqrt{a_r}}{2}(u_{j+1} - u_j) + \frac{1}{4}(h_j\sigma_j^+ - h_{j+1}\sigma_{j+1}^-). \tag{3.3.7}$$

We also have

$$u_{j-\frac{1}{2}} = \frac{1}{2}(u_{j-1} + u_j) - \frac{1}{2\sqrt{a_r}}(v_j - v_{j-1}) + \frac{1}{4\sqrt{a_r}}(h_{j-1}\sigma_{j-1}^+ + h_j\sigma_j^-), \tag{3.3.8}$$

and

$$v_{j-\frac{1}{2}} = \frac{1}{2}(v_{j-1} + v_j) - \frac{\sqrt{a_r}}{2}(u_j + u_{j-1}) + \frac{1}{4}(h_{j-1}\sigma_{j-1}^+ - h_j\sigma_j^-). \tag{3.3.9}$$

Substituting terms from (3.3.6 - 3.3.9) into the system

$$\begin{cases} \frac{\partial u_j}{\partial t} + \frac{1}{h_j}(v_{j+\frac{1}{2}} - v_{j-\frac{1}{2}}) \\ \frac{\partial v_j}{\partial t} + \frac{a}{h_j}(u_{j+\frac{1}{2}} - u_{j-\frac{1}{2}}) = -\frac{1}{\epsilon}(v_j - f(u_j)), \end{cases} \tag{3.3.10}$$

we have

$$\frac{\partial u_j}{\partial t} + \frac{1}{h_j}(v_{j+1} - v_{j-1}) - \frac{\sqrt{a_r}}{2h_j}(u_{j+1} - 2u_j + u_{j-1}) - \frac{1}{4h_j}(h_{j+1}\sigma_{j+1}^- - h_j(\sigma_j^+ + \sigma_j^-) + h_{j-1}\sigma_{j-1}^+) = 0, \tag{3.3.11}$$

and

$$\begin{aligned} &\frac{\partial v_j}{\partial t} + \frac{\sqrt{a_r}}{2h_j}(u_{j+1} - u_{j-1}) - \frac{\sqrt{a_r}}{2h_j\sqrt{a_r}}(v_{j+1} - 2v_j + v_{j-1}) \\ &+ \frac{a_r}{4h_j\sqrt{a_r}}(h_{j+1}\sigma_{j+1}^- + h_j(\sigma_j^+ - \sigma_j^-) - h_{j-1}\sigma_{j-1}^+) = -\frac{1}{\epsilon}(v_j - f(u_j)). \end{aligned} \tag{3.3.12}$$

Equations (3.3.11, 3.3.12), though in semi-discrete form but actually take the form of ODEs. In the next paragraph, we obtain a full discrete scheme by appropriately applying TVD Runge-Kutta method for time discretizations.

3.3.2 TVD, Runge-Kutta second-order in time discretization

We follow the same Runge-Kutta time discretization algorithm as for the first-order scheme. The discretization proceeds as follows:

$$u^* = u^n,\ v^n = f(u^*), \tag{3.3.13}$$

$$v^* = v^n + \frac{\triangle t}{\epsilon}(v^* - f(u^*)), \tag{3.3.14}$$

$$v^* = \left(\frac{\epsilon}{\epsilon - \triangle t}\right)(v^n - \frac{\triangle t}{\epsilon}f(u^*)), \tag{3.3.15}$$

$$u^{(1)} = u^* - \triangle t D_+ v^* = u^* - \frac{\triangle t}{h_j}\left(v^*_{j+\frac{1}{2}} - v^*_{j-\frac{1}{2}}\right), \tag{3.3.16}$$

$$v^{(1)} = v^* - \triangle t a D_+ u^* = v^* - \triangle t a \frac{1}{h_j}\left(u^*_{j+\frac{1}{2}} - u^*_{j-\frac{1}{2}}\right). \tag{3.3.17}$$

Defining fluxes at the cell boundaries as in (3.1.8), we re-write (3.3.16) and (3.3.17) above as

$$\begin{aligned} u^{(1)} = u^* &- \frac{\triangle t}{2h_j}\left(v^*_{j+1} - v^*_{j-1}\right) + \frac{\sqrt{a_r}\triangle t}{2h_j}\left(u^*_{j+1} - 2u^*_j + u^*_{j-1}\right) \\ &+ \frac{\triangle t}{4h_j}\left(h_{j+1}\sigma^{-*}_{j+1} - h_j(\sigma^{+*}_j + \sigma^{-*}_j) + h_{j-1}\sigma_{j-1}\sigma^{+*}_{j-1}\right), \end{aligned} \tag{3.3.18}$$

$$\begin{aligned} v^{(1)} = v^* &- \frac{a\triangle t}{2h_j}\left(u^*_{j+1} - u^*_{j-1}\right) + \frac{a\triangle t}{2\sqrt{a_r}h_j}\left(v^*_{j+1} - 2v^*_j + v^*_{j-1}\right) \\ &- \frac{a\triangle t}{4\sqrt{a_r}h_j}\left(h_{j+1}\sigma^{-*}_{j+1} + h_j(\sigma^{+*}_j - \sigma^{-*}_j) - h_{j-1}\sigma^{+*}_{j-1}\right). \end{aligned} \tag{3.3.19}$$

Again, we write

$$u^{**} = u^{(1)}, \tag{3.3.20}$$

$$v^{**} = \left(\frac{\epsilon}{\epsilon + \triangle t}\right)\left(v^{(1)} + \frac{\triangle t}{\epsilon}f(u^{**})\right) - \left(\frac{2\triangle t}{\epsilon + \triangle t}\right)(v^* - f(u^*)), \tag{3.3.21}$$

$$\begin{aligned} u^{(2)} &= u^{**} - \frac{\triangle t}{h_j}(v^{**}_{j+\frac{1}{2}} - v^{**}_{j-\frac{1}{2}}) \\ &= u^{**} - \frac{\triangle t}{2h_j}(v^{**}_{j+1} - v^{**}_{j-1}) + \frac{\sqrt{a_r}\triangle t}{2h_j}(u^{**}_{j+1} - 2u^{**}_j + u^{**}_j) \\ &\quad + \frac{\triangle t}{4h_j}\left(h_{j+1}\sigma^{-**}_{j+1} - h_j(\sigma^{+**}_j + \sigma^{-**}_j) + h_{j-1}\sigma^{+**}_{j-1}\right), \end{aligned} \tag{3.3.22}$$

$$\begin{aligned} v^{(2)} &= v^{**} - \frac{a\triangle t}{h_j}(u^{**}_{j+\frac{1}{2}} - u^{**}_{j-\frac{1}{2}}) \\ &= v^{**} - \frac{a\triangle t}{2h_j}(u^{**}_{j+1} - u^{**}_{j-1}) + \frac{a_r\triangle t}{2\sqrt{a_r}h_j}(v^{**}_{j+1} - 2v^{**}_j + v^{**}_{j-1}) \\ &\quad - \frac{a_r\triangle t}{4\sqrt{a_r}h_j}\left(h_{j+1}\sigma^{-**}_{j+1} + h_j(\sigma^{+**}_j - \sigma^{-**}_j) - h_{j-1}\sigma^{+**}_{j-1}\right), \end{aligned} \tag{3.3.23}$$

and then,

$$u^{n+1} = \frac{1}{2}(u^n + u^{(2)}),\ v^{n+1} = \frac{1}{2}(v^n + v^{(2)}). \tag{3.3.24}$$

Next, we discretize the adjoint equations 2.7.12. These equations are a set of HCLs, therefore, as for the first-order adjoint discretization, the resulting scheme is relaxing, but it is solved backward in time.

3.4 Discretization of the Adjoint Equation, Second-order in Time and Space

We consider the discretization of the adjoint equation, second-order in time and space. Basically, the discretization is the same as for the first order scheme. We review the derivation of this scheme, and materials and the presentation style are adapted from [10].

3.4.1 Spatial discretization

We present a second-order in space accurate discretization of the adjoint equations derived under subsection (2.7.1). We recall the finite difference approximation derived previously (3.2.5) by considering the characteristic variables $p \pm \sqrt{a}q$, that is,

$$\begin{aligned} p_{j+\frac{1}{2}} &= \frac{1}{2}(p_j + p_{j+1}) + \frac{\sqrt{a}}{2}(q_{j+1} - q_j), \\ q_{j+\frac{1}{2}} &= \frac{1}{2}(q_{j+1} + q_j) + \frac{1}{2\sqrt{a}}(p_{j+1} - p_j). \end{aligned} \tag{3.4.1}$$

Using the polynomial Γ, the procedure is formulated as follows:

$$(p + \sqrt{a}q)_{j+\frac{1}{2}} = (p + \sqrt{a}q)^+_{j+\frac{1}{2}} = \Gamma_{j+1}(x_{j+\frac{1}{2}}; \Phi^+), \tag{3.4.2}$$

$$(p - \sqrt{a}q)_{j+\frac{1}{2}} = (p - \sqrt{a}q)^-_{j+\frac{1}{2}} = \Gamma_j(x_{j+\frac{1}{2}}; \Phi^-), \tag{3.4.3}$$

from which we obtain

$$p_{j+1} = \frac{1}{2}\left(\Gamma_j(x_{j+\frac{1}{2}}; \Phi^-) + \Gamma_{j+1}(x_{j+\frac{1}{2}}; \Phi^+)\right) \tag{3.4.4}$$

$$q_{j+1} = \frac{1}{2\sqrt{a}}\left(\Gamma_{j+1}(x_{j+\frac{1}{2}}; \Phi^+) - \Gamma_j(x_{j+\frac{1}{2}}; \Phi^-)\right). \tag{3.4.5}$$

The superscripts + and − correspond to the right and left cell of a cell boundary at $x_{j+\frac{1}{2}}$. The first-order scheme can, therefore, be represented by the polynomial taking the form:

$$\Gamma_j(x;\Phi) = \Phi \tag{3.4.6}$$

which are polynomials defined in terms of characteristic variables. The second-order scheme applies polynomials taking the form:

$$\Gamma_j(x;\Phi) = \Phi_j + \sigma(\Phi_j)(x - x_j) \tag{3.4.7}$$

where

$$\Phi_j^- = p_j - \sqrt{a}q_j,\ \Phi_j^+ = p_j + \sqrt{a}q_j. \tag{3.4.8}$$

Thus the second-order terms can be formulated as follows:

$$\begin{aligned}
p_{j+\frac{1}{2}} &= \frac{1}{2}\left((\Gamma_j(x_{j+\frac{1}{2}};\Phi^-) + \Gamma_{j+1}(x_{j+\frac{1}{2}};\Phi^+)\right) \\
&= \frac{1}{2}\left(\Phi_j^- + \sigma(\Phi_j^-)(x_{j+\frac{1}{2}} - x_j) + \Phi_{j+1}^+ + \sigma(\Phi_{j+1}^+)(x_{j+\frac{1}{2}} - x_{j+1})\right) \\
&= \frac{1}{2}\left(\Phi_j^- + \frac{1}{2}\sigma(\Phi_j^-) + \Phi_{j+1}^+ - \frac{1}{2}\sigma(\Phi_{j+1}^+)\right) \\
&= \frac{1}{2}\left(p_j - \sqrt{a}q_j + \frac{1}{2}\sigma_j^- + p_{j+1} + \sqrt{a}q_{j+1} - \frac{1}{2}\sigma_{j+1}^+\right) \\
&= \frac{1}{2}\left(p_j + p_{j+1} + \sqrt{a}(q_{j+1} - q_j) + \frac{1}{2}(\sigma_j^- - \sigma_{j+1}^+)\right);
\end{aligned} \tag{3.4.9}$$

similarly,

$$\begin{aligned}
q_{j+\frac{1}{2}} &= \frac{1}{2\sqrt{a}}\left((\Gamma_{j+1}(x_{j+\frac{1}{2}};\Phi^+) - \Gamma_j(x_{j+\frac{1}{2}};\Phi^-)\right) \\
&= \frac{1}{2\sqrt{a}}\left(\Phi_{j+1}^+ + \sigma(\Phi_{j+1}^+)(x_{j+\frac{1}{2}} - x_{j+1}) - \Phi_j^- - \sigma(\Phi_j^-)(x_{j+\frac{1}{2}} - x_j)\right) \\
&= \frac{1}{2\sqrt{a}}\left(\Phi_{j+1}^+ - \frac{1}{2}\sigma(\Phi_{j+1}^+) - \Phi_j^- - \frac{1}{2}\sigma(\Phi_j^-)\right) \\
&= \frac{1}{2\sqrt{a}}\left(p_{j+1} + \sqrt{a}q_{j+1} - \frac{1}{2}\sigma_{j+1}^+ - p_j + \sqrt{a}q_j - \frac{1}{2}\sigma_j^-\right) \\
&= \frac{1}{2\sqrt{a}}\left(-p_j + p_{j+1} + \sqrt{a}(q_{j+1} + q_j) - \frac{1}{2}(\sigma_{j+1}^+ + \sigma_j^-)\right) \\
&= \frac{1}{2}(q_{j+1} + q_j) + \frac{1}{2\sqrt{a}}(-p_j + p_{j+1}) - \frac{1}{4\sqrt{a}}(\sigma_{j+1}^+ + \sigma_j^-).
\end{aligned} \tag{3.4.10}$$

Replacing p by $-p$ and q by $-q$, we have

$$p_{j+\frac{1}{2}} = \frac{1}{2}\left(-p_j - p_{j+1} + \sqrt{a}(-q_{j+1} + q_j) + \frac{1}{2}(\sigma_j^- - \sigma_{j+1}^+)\right), \tag{3.4.11}$$

$$q_{j+\frac{1}{2}} = \frac{1}{2}(-q_{j+1} - q_j) + \frac{1}{2\sqrt{a}}(p_j - p_{j+1}) - \frac{1}{4\sqrt{a}}(\sigma_{j+1}^+ + \sigma_j^-) \tag{3.4.12}$$

where

$$\begin{aligned} \sigma_j^- &= (\Phi_{j+1}^- - \Phi_j^-)\phi(\theta_j^-) \\ &= (p_{j+1} - \sqrt{a}q_{j+1} - p_j + \sqrt{a}q_j)\phi(\theta_j^-), \end{aligned} \tag{3.4.13}$$

$$\begin{aligned} \sigma_{j+1}^+ &= (\Phi_{j+2}^+ - \Phi_{j+1}^+)\phi(\theta_{j+1}^+) \\ &= (p_{j+2} + \sqrt{a}q_{j+2} - p_{j+1} - \sqrt{a}q_{j+1})\phi(\theta_{j+1}^+). \end{aligned} \tag{3.4.14}$$

Furthermore,

$$\phi(\theta_j^\pm) = \phi\left(\frac{\Phi_j^\pm - \Phi_{j-1}^\pm}{\Phi_{j+1}^\pm - \Phi_j^\pm}\right). \tag{3.4.15}$$

Again replace p by $-p$ and q by $-q$, and re-write:

$$\begin{aligned} \sigma_j^- &= \left[-p_{j+1} + \sqrt{a}q_{j+1} + p_j - \sqrt{a}q_j\right]\phi\left(\frac{-p_j + \sqrt{a}q_j + p_{j-1} - \sqrt{a}q_{j-1}}{-p_{j+1} + \sqrt{a}q_{j+1} + p_j - \sqrt{a}q_j}\right) \\ &= \left[-(p_{j+1} - \sqrt{a}q_{j+1}) - (-(p_j - \sqrt{a}q_j))\right]\phi\left[\frac{-(p_j - \sqrt{a}q_j) - (-(p_{j-1} - \sqrt{a}q_{j-1}))}{-(p_{j+1} - \sqrt{a}q_{j+1}) - (-(p_j - \sqrt{a}q_j))}\right]; \end{aligned} \tag{3.4.16}$$

$$\begin{aligned} \sigma_{j+1}^+ &= \left[-p_{j+2} - \sqrt{a}q_{j+2} + p_{j+1} + \sqrt{a}q_{j+1}\right]\phi\left[\frac{-p_{j+1} - \sqrt{a}q_{j+1} + p_j + \sqrt{a}q_j}{-p_{j+2} - \sqrt{a}q_{j+2} + p_{j+1} + \sqrt{a}q_{j+1}}\right] \\ &= \left[-(p_{j+2} + \sqrt{a}q_{j+2}) - (-(p_{j+1} + \sqrt{a}q_{j+1}))\right] \\ &\quad \times \phi\left[\frac{-(p_{j+1} + \sqrt{a}q_{j+1}) - (-(p_j + \sqrt{a}q_j))}{-(p_{j+2} + \sqrt{a}q_{j+2}) - (-(p_{j+1} + \sqrt{a}q_{j+1}))}\right]. \end{aligned} \tag{3.4.17}$$

To conform with the format of the adjoint equations, equations (3.4.11) and (3.4.12) are written as

$$p_{j+\frac{1}{2}} = -\left[\frac{1}{2}(p_j + p_{j+1}) - \frac{\sqrt{a}}{2}(q_j - q_{j+1}) - \frac{1}{4}(\sigma_j^- - \sigma_{j+1}^+)\right], \tag{3.4.18}$$

$$q_{j+\frac{1}{2}} = -\left[\frac{1}{2}(q_{j+1} + q_j) - \frac{1}{2\sqrt{a}}(p_j - p_{j+1}) + \frac{1}{4\sqrt{a}}(\sigma_{j+1}^+ + \sigma_j^-)\right]. \tag{3.4.19}$$

3.4.2 Time discretizations

We now turn to the second-order TVD Runge-Kutta time discretization to construct an algorithm for the solution of the adjoint equations. Similar to the first-order adjoint, discretization takes two steps, explicit step for convective equation and implicit step for the stiff ODE part,

but we can reformulate the scheme and write all steps as explicit as possible. The Runge-Kutta type discretization for the adjoint system we are reviewing was first published in [10]. Obviously, we have:

$$p_j^{(2)} = \frac{1}{2}p_j^{n+1},\ q_j^{(2)} = \frac{1}{2}q_j^{n+1}; \tag{3.4.20}$$

$$\begin{aligned} q_j^{**} = &\left(\frac{\epsilon}{\epsilon+\triangle t}\right) q_j^{(2)} + \left(\frac{\epsilon}{\epsilon+\triangle t}\right)\frac{\triangle t}{2h_j}\left[(p_{j+1}^{(2)} - p_{j+1}^{(2)}) + \sqrt{a}(q_{j+1}^{(2)} - 2q_j^{(2)} + q_{j-1}^{(2)})\right] \\ &+ \left(\frac{\epsilon}{\epsilon+\triangle t}\right)\frac{\triangle t}{4h_j}\left[\sigma_{j-1}^{-} - (\sigma_j^{+} + \sigma_j^{-}) + \sigma_{j-1}^{+}\right] \end{aligned} \tag{3.4.21}$$

$$\begin{aligned} p_j^{**} = &p_j^{(2)} + q_j^{**}\frac{\triangle t}{\epsilon}f^{'}(u_j^{**}) + a\frac{\triangle t}{2h_j}\left[(q_{j+1}^{(2)} - q_{j-1}^{(2)}) + \frac{1}{\sqrt{a}}(p_{j+1}^{(2)} - 2p_j^{(2)} + p_{j-1}^{(2)})\right] \\ &- \frac{a}{\sqrt{a}}\frac{\triangle t}{4h_j}\left[\sigma_{j-1}^{-} + (\sigma_j^{+} - \sigma_j^{-}) - \sigma_{j+1}^{+}\right]; \end{aligned} \tag{3.4.22}$$

$$p_j^{(1)} = p_j^{**},\ q_j^{(1)} = q_j^{**}; \tag{3.4.23}$$

$$\begin{aligned} q_j^{*} = &\left(\frac{\epsilon}{\epsilon+\triangle t}\right) q_j^{(1)} - \left(\frac{\epsilon}{\epsilon+\triangle t}\right)\frac{2\triangle t}{\epsilon}q_j^{**} \\ &+ \left(\frac{\epsilon}{\epsilon+\triangle t}\right)\frac{\triangle t}{2h_j}\left[(p_{j+1}^{(1)} - p_{j-1}^{(1)}) + \sqrt{a}(q_{j+1}^{(1)} - 2q_j^{(1)} + q_{j-1}^{(1)})\right] \\ &+ \left(\frac{\epsilon}{\epsilon+\triangle t}\right)\frac{\triangle t}{4h_j}\left[\sigma_{j-1}^{-} - (\sigma_j^{+} + \sigma_j^{-}) + \sigma_{j+1}^{+}\right], \end{aligned}$$

$$\begin{aligned} p_j^{*} = &p_j^{(1)} - \frac{\triangle t}{\epsilon}f^{'}(u_j^{**})(q_j^{*} - 2q_j^{**}) \\ &+ a\frac{\triangle t}{2h_j}\left[(q_{j+1}^{(1)} - q_{j-1}^{(1)}) + \frac{1}{\sqrt{a}}(p_{j+1}^{(1)} - 2p_j^{(1)} + p_{j-1}^{(1)})\right] \\ &- \frac{a}{\sqrt{a}}\frac{\triangle t}{4h_j}\left[\sigma_{j-1}^{-} + (\sigma_j^{+} - \sigma_j^{-}) - \sigma_{j+1}^{+}\right], \end{aligned}$$

$$p_j^{n} = \frac{1}{2}p_j^{n+1} + p_j^{*},\ q_j^{n} = \frac{1}{2}q_j^{n+1} + q_j^{*} \tag{3.4.24}$$

There is an alternative reformulation provided in [10] which can also be considered.

We adapt similar procedures in order to develop relaxing schemes for discrete kinetic relaxation system as for JIN XIN relaxation system. In the sequel, therefore, we discuss the derivations of relaxing schemes up to second -order in time and space for the kinetic flow equation and for its dual adjoint equation as well. Our intention is to realize both JIN XIN and kinetic relaxing schemes through numerical experimentations.

3.5 Relaxing Scheme for the Discrete Kinetic Relaxation system

We consider discretization of a BGK-like model

$$\partial_t f_i^\epsilon + \lambda_i \partial_x f_i^\epsilon = \frac{1}{\epsilon}(M_i(Pf^\epsilon) - f_i^\epsilon),\ i \in \{1, \dots, N\}, \tag{3.5.1}$$

which is the model based on a kinetic approximation of the problem (2.6.1) with initial conditions

$$f^\epsilon(x, 0) = f_0^\epsilon(x) = M_i(u^0), \tag{3.5.2}$$

where M_i are Lipschitz (piecewise C^1) continuous functions called Maxwellians, defined on $\mathbb{R}^m$, and other conditions are satisfied as discussed under Section (2.6).

3.5.1 Discretization of the discrete kinetic model, first-order in time and space

For spatial discretization of the discrete kinetic model, we use the results discussed under subsection (3.1.1), the outcome is a simple upwinding. For the Runge-Kutta time discretization scheme, we employ the operator splitting approach and split the relaxation system (2.7.18) into stiff ODE and an advection system. Considering Maxwellian functions $M_i(u) = \alpha_i u + \beta_i A(u)$, $M_i(u) \in \mathbb{R}^m, (i = 1, 2, 3)$, we have for stiff ODE,

$$u_j^* = u_j^n,\ f_{j,i}^n = M_{j,i}(u_j^*), \tag{3.5.3}$$

$$\partial_t f_i = \frac{1}{\epsilon}(M_i(u) - f_i), \implies f_{j,i}^* = f_{j,i}^n + \frac{\triangle t}{\epsilon}(M_{j,i}(u_j^*) - f_{j,i}^*). \tag{3.5.4}$$

And for advection system,

$$\partial_t f_i + \lambda_i \nabla_x f_i = 0, \tag{3.5.5}$$

$$\begin{aligned} f_{j,i}^{n+\frac{1}{2}} &= f_{j,i}^n + \triangle t D_x^* f_i^* \\ &= f_{j,i}^n - \lambda_i \frac{\triangle t}{h_j}(f_{j+1,i}^* - f_{j-1,i}^*) + \frac{|\lambda_i|}{2}(f_{j+1,i}^* - 2f_{j,i}^* + f_{j-1,i}^*), \end{aligned} \tag{3.5.6}$$

$$u_j^{n+1} = \sum_j f_{j,i}^{n+\frac{1}{2}},\ f_{j,i}^n = M_{j,i}(u_j^{n+1}). \tag{3.5.7}$$

For practical reasons, for example for two-velocities (N = 2) discrete kinetic model, we can choose Maxwellians to take the form [5],

$$M_i(u) = \frac{1}{2}\left(u \pm \frac{A(u)}{\lambda_i}\right)\ \lambda_1 = \lambda,\ \lambda_2 = -\lambda. \tag{3.5.8}$$

3.5.2 Spatial discretization for the discrete kinetic model, second-order in space

We consider the discretization constructed by MUSCL method (reconstruction-transport-projection method) on transport part that is presented in [5]. There slope limiters are constructed by using piecewise linear function. However, reconstruction is made with particular interest on boundary coefficients, therefore, in our case we only draw information that are valuable for our construction.

We define $\chi_i = |\lambda|\frac{\triangle t}{h_j}$.

For positive velocity λ_i, and for all $j \geq 0$, we find that

$$f_{j,i}^{n+\frac{1}{2}} = (1-\chi_i) f_{j,i}^n + \chi_i f_{j-1,i}^n - h_j \frac{\chi_i(1-\chi_i)}{2} \left(\sigma_{j,i} - \sigma_{j-1,i}\right). \tag{3.5.9}$$

For all $j \geq 0$, and for non-positive velocities, λ_i, we have

$$f_{j,i}^{n+\frac{1}{2}} = (1-\chi_i) f_{j,i}^n + \chi_i f_{j+1,i}^n - h_j \frac{\chi_i(1-\chi_i)}{2} \left(\sigma_{j+1,i} - \sigma_{j,i}\right). \tag{3.5.10}$$

We use a minmod slope for all $j \geq 0$,

$$\sigma_{i,j}^n = \text{minmod}\left(X_{1,i,j}\frac{\triangle f_{j+\frac{1}{2},i}^n}{h_j}, X_{2,i,j}\frac{\triangle f_{j-\frac{1}{2},i}^n}{h_j}\right) \tag{3.5.11}$$

where

$$\text{minmod}(a,b) = \frac{\text{sgn}(a)+\text{sgn}(b)}{2}\min(|a|,|b|), \tag{3.5.12}$$

and

$$\triangle f_{j+\frac{1}{2},i}^n = f_{j+1,i}^n - f_{j,i}^n,\ \triangle f_{j-\frac{1}{2},i}^n = f_{j,i}^n - f_{j-1,i}^n. \tag{3.5.13}$$

$X_{1,i,j}$ and $X_{2,i,j}$ can be chosen according to [5].

3.5.3 Second-order Runge-Kutta time discretizations for the discrete kinetic model

We applied a 3-velocities model relaxation system, corresponding to $\lambda_1 = -\lambda_2 = \lambda > 0$ and $\lambda_0 = 0$, which was proposed in [7],

$$\begin{aligned}
\partial_t f_{i+}^\epsilon \quad + \quad \lambda_i \partial_x f_{i+}^\epsilon \quad &= \quad \tfrac{1}{\epsilon}(M_{i+}(u) - f_{i+}^\epsilon), \\
\partial_t f_{i0}^\epsilon \quad &= \quad \tfrac{1}{\epsilon}(M_{i0}(u) - f_{i0}^\epsilon), \\
\partial_t f_{i-}^\epsilon \quad - \quad \lambda_i \partial_x f_{i-}^\epsilon \quad &= \quad \tfrac{1}{\epsilon}(M_{i-}(u) - f_{i-}^\epsilon),\ i = 1, \ldots, N.
\end{aligned} \tag{3.5.14}$$

For simplicity we drop superscript ϵ and subscript i writing respectively, equations associated with λ_1, λ_0 and λ_2 as

$$\begin{aligned} \partial_t f_+ \quad + \quad \lambda \partial_x f_+ \quad &= \quad \tfrac{1}{\epsilon}(M_+(u) - f_+), \\ \partial_t f_0 \quad &= \quad \tfrac{1}{\epsilon}(M_0(u) - f_0), \\ \partial_t f_- \quad - \quad \lambda \partial_x f_- \quad &= \quad \tfrac{1}{\epsilon}(M_-(u) - f_-). \end{aligned} \tag{3.5.15}$$

For Runge-Kutta time discretization, we split the system above into two parts: the collision/stiff ODE part

$$\begin{aligned} \partial_t f_+ \quad &= \quad \tfrac{1}{\epsilon}(M_+(u) - f_+), \\ \partial_t f_0 \quad &= \quad \tfrac{1}{\epsilon}(M_0(u) - f_0), \\ \partial_t f_- \quad &= \quad \tfrac{1}{\epsilon}(M_-(u) - f_-), \end{aligned} \tag{3.5.16}$$

and the transport system

$$\begin{aligned} \partial_t f_+ \quad + \quad \lambda \partial_x f_+ \quad &= \quad 0, \\ \partial_t f_0 \quad &= \quad 0, \\ \partial_t f_- \quad - \quad \lambda \partial_x f_- \quad &= \quad 0. \end{aligned} \tag{3.5.17}$$

As for the first-order scheme, we then develop an Explicit-Implicit scheme, which takes two stages, one for stiff part and another for advection system, therefore, for $u_j^n = u_j^*$,

$$\partial_t f_+ = \frac{1}{\epsilon}(M_+(u) - f_+),\ \partial_t f_0 = \frac{1}{\epsilon}(M_0(u) - f_0),\ \partial_t f_- = \frac{1}{\epsilon}(M_-(u) - f_-), \tag{3.5.18}$$

$$\begin{aligned} f_{j,+}^* \quad &= \quad f_{j,+}^n \quad - \quad \tfrac{1}{\epsilon}(M_{j,+}(u_j^*) - f_{j,+}^*), \\ f_{j,0}^* \quad &= \quad f_{j,0}^n \quad - \quad \tfrac{1}{\epsilon}(M_{j,0}(u_j^*) - f_{j,0}^*), \\ f_{j,-}^* \quad &= \quad f_{j,-}^n \quad - \quad \tfrac{1}{\epsilon}(M_{j,-}(u_j^*) - f_{j,-}^*), \end{aligned} \tag{3.5.19}$$

$$\begin{aligned} f_{j,+}^{(1)} &= f_{j,+}^* - \triangle t \lambda D_x f_{j,+}^* \\ &= f_{j,+}^* - \chi_i (f_{j,+}^* - f_{j-1,+}^*) - h_j \frac{\chi_i(1-\chi_i)}{2} \left(\sigma_{j,+}^* - \sigma_{j-1,+}^*\right), \end{aligned} \tag{3.5.20}$$

$$\begin{aligned} f_{j,-}^{(1)} &= f_{j,-}^{*} + \triangle t \lambda D_x f_{j,-}^{*} \\ &= f_{j,-}^{*} + \chi_i (f_{j+1,-}^{*} - f_{j,-}^{*}) - h_j \frac{\chi_i(1-\chi_i)}{2} \left(\sigma_{j+1,-}^{*} - \sigma_{j,-}^{*}\right), \end{aligned} \tag{3.5.21}$$

$$\begin{aligned} f_{j,+}^{**} &= f_{j,+}^{(1)} + \tfrac{\triangle t}{\epsilon}(M_{j,+}(u_j^{**}) - f_{j,+}^{**}) + \tfrac{2\triangle t}{\epsilon}(M_{j,+}(u_j^{*}) - f_{j,+}^{*}), \\ f_{j,0}^{**} &= f_{j,0}^{(1)} + \tfrac{\triangle t}{\epsilon}(M_{j,0}(u_j^{**}) - f_{j,0}^{**}) + \tfrac{2\triangle t}{\epsilon}(M_{j,0}(u_j^{*}) - f_{j,0}^{*}), \\ f_{j,-}^{**} &= f_{j,-}^{(1)} + \tfrac{\triangle t}{\epsilon}(M_{j,-}(u_j^{**}) - f_{j,-}^{**}) + \tfrac{2\triangle t}{\epsilon}(M_{j,-}(u_j^{*}) - f_{j,-}^{*}), \end{aligned} \tag{3.5.22}$$

$$\begin{aligned} f_{j,+}^{(2)} &= f_{j,+}^{**} - \triangle t \lambda D_x f_{j,+}^{**} \\ &= f_{j,+}^{**} - \chi_i (f_{j,+}^{**} - f_{j-1,+}^{**}) - h_j \frac{\chi_i(1-\chi_i)}{2} \left(\sigma_{j,+}^{**} - \sigma_{j-1,+}^{**}\right), \end{aligned} \tag{3.5.23}$$

$$\begin{aligned} f_{j,-}^{(2)} &= f_{j,-}^{**} + \triangle t \lambda D_x f_{j,-}^{**} \\ &= f_{j,-}^{**} + \chi_i (f_{j+1,-}^{**} - f_{j,-}^{**}) - h_j \frac{\chi_i(1-\chi_i)}{2} \left(\sigma_{j+1,-}^{**} - \sigma_{j,-}^{**}\right), \end{aligned} \tag{3.5.24}$$

$$f_{j,+}^{n+1} = \frac{1}{2}(f_{j,+}^{(2)} + f_{j,+}^{n}), \;\; f_{j,-}^{n+1} = \frac{1}{2}(f_{j,-}^{(2)} + f_{j,-}^{n}), \;\; f_{j,0}^{n+1} = f_{j,0}^{**} \tag{3.5.25}$$

where

$$u_j^{n+1} = \frac{1}{2}\sum_i (f_{j,i}^{(2)} + f_{j,i}^{n}). \tag{3.5.26}$$

3.5.4 Time and space adjoint discretizations of discrete kinetic model, second-order

We consider the discretization of the adjoint system (2.7.26) (derived under Subsection 2.7.2),

$$-\partial_t p_i - \lambda_i \partial_x p_i = \frac{1}{\epsilon}(M_i(u) - f_i) \;\; i = 1, \ldots, 3. \tag{3.5.27}$$

If we write the system in an extended form

$$\begin{aligned} -\partial_t p_+ + \lambda \partial_x p_+ &= \tfrac{1}{\epsilon}(M_+(u) - f_+) \\ -\partial_t p_0 &= \tfrac{1}{\epsilon}(M_0(u) - f_0) \\ -\partial_t p_- - \lambda \partial_x p_- &= \tfrac{1}{\epsilon}(M_-(u) - f_-), \end{aligned} \tag{3.5.28}$$

we see that the linear transport system of adjoint equations

$$-\begin{bmatrix} p_+ \\ p_0 \\ p_- \end{bmatrix}_t - \begin{bmatrix} \lambda & 0 \\ 0 & 0 \\ 0 & -\lambda \end{bmatrix} \begin{bmatrix} p_+ \\ p_0 \\ p_- \end{bmatrix}_x = 0, \tag{3.5.29}$$

is analogous to the system (3.5.29), so it is possible to derive its characteristic variables by selecting appropriate values for the scaling factors. Therefore, it is enough to conclude that, by following analysis under Subsection 3.4.1, we can deduce flux-differences at the cell boundaries for the adjoint system (3.5.28) to be

$$\begin{aligned}(p_{j+\frac{1}{2},+} - p_{j-\frac{1}{2},-}) = &-\frac{1}{2}\left[(p_{j+1,+} - p_{j-1,+}) + \lambda(p_{j+1,+} - 2p_{j,+} + p_{j-1,+})\right] \\ &- \frac{1}{4}\left[(\sigma^+_{j+1,+} - (\sigma^+_{j,+} + \sigma^-_{j,+}) + \sigma^-_{j-1,+})\right],\end{aligned} \tag{3.5.30}$$

$$\begin{aligned}(p_{j+\frac{1}{2},-} - p_{j-\frac{1}{2},-}) = &-\frac{1}{2}\left[(p_{j+1,-} - p_{j-1,-}) + \frac{1}{\lambda}(p_{j+1,-} - 2p_{j,-} + p_{j-1,-})\right] \\ &- \frac{1}{4\lambda}\left[(\sigma^+_{j+1,-} - (\sigma^+_{j,-} - \sigma^-_{j,-}) - \sigma^-_{j-1,-})\right].\end{aligned} \tag{3.5.31}$$

Thus, second-order Runge-Kutta time discretization for the adjoint system (3.5.28) would be

$$p^{(2)}_{j,+} = \frac{1}{2}p^{n+1}_{j,+},\ p^{(2)}_{j,-} = \frac{1}{2}p^{n+1}_{j,-}, \tag{3.5.32}$$

$$\begin{aligned}p^{**}_{j,+} &= p^{(2)}_{j,+} - \frac{\triangle t}{\epsilon}\left(M_{j,+}(u^{**}_j) - f^{**}_{j,+}\right) - \lambda\triangle t D_x p^{(2)}_{j,+} \\ &= p^{(2)}_{j,+} - \frac{\triangle t}{\epsilon}\left(M_{j,+}(u^{**}_j) - f^{**}_{j,+}\right) \\ &\quad + \lambda\frac{\triangle t}{2h_j}\left[(p^{(2)}_{j+1,+} - 2p^{(2)}_{j-1,+}) + \lambda(p^{(2)}_{j+1,+} - 2p^{(2)}_{j,+} + p^{(2)}_{j-1,+})\right] \\ &\quad + \lambda\frac{\triangle t}{4h_j}\left[\sigma^{+(2)}_{j+1,+} - (\sigma^{+(2)}_{j,+} + \sigma^{-(2)}_{j,+}) + \sigma^{-(2)}_{j-1,+}\right],\end{aligned} \tag{3.5.33}$$

$$\begin{aligned}p^{**}_{j,-} &= p^{(2)}_{j,-} + \frac{\triangle t}{\epsilon}\left(M_{j-}(u^{**}_j) - f^{**}_{j,-}\right) + \lambda\triangle t D_x p^{(2)}_{j,-} \\ &= p^{(2)}_{j,-} + \frac{\triangle t}{\epsilon}\left(M_{j-}(u^{**}_j) - f^{**}_{j,-}\right) \\ &\quad - \lambda\frac{\triangle t}{2h_j}\left[(p^{(2)}_{j+1,-} - p^{(2)}_{j-1,-}) + \frac{1}{\lambda}(p^{(2)}_{j+1,-} - 2p^{(2)}_{j,-} + p^{(2)}_{j-1,-})\right] \\ &\quad - \frac{\triangle t}{4h_j}\left[\sigma^{+(2)}_{j+1,-} - (\sigma^{+(2)}_{j,-} - \sigma^{-(2)}_{j,-}) - \sigma^{-(2)}_{j-1,-}\right],\end{aligned} \tag{3.5.34}$$

$$p_{j,+}^{(1)} = p_{j,+}^{**},\ p_{j,-}^{(1)} = p_{j,-}^{**}, \tag{3.5.35}$$

$$\begin{aligned} p_{j,+}^{*} &= p_{j,+}^{(1)} - \frac{1}{\epsilon}\left(M_{j,+}(u_j^{*}) - f_{j,+}^{*}\right) + \frac{2\triangle t}{\epsilon}\left(M_{j,+}(u_j^{**}) - f_{j,+}^{**}\right) - \lambda \triangle t D_x p_{j,+}^{(1)} \\ &= p_{j,+}^{(1)} - \frac{1}{\epsilon}\left(M_{j,+}(u_j^{*}) - f_{j,+}^{*}\right) + \frac{2\triangle t}{\epsilon}\left(M_{j,+}(u_j^{**}) - f_{j,+}^{**}\right) \\ &\quad + \lambda \frac{\triangle t}{2h_j}\left[(p_{j+1,+}^{(1)} - 2p_{j-1,+}^{(1)}) + \lambda(p_{j+1,+}^{(1)} - 2p_{j,+}^{(1)} + p_{j-1,+}^{(1)})\right] \\ &\quad + \lambda \frac{\triangle t}{4h_j}\left[\sigma_{j+1,+}^{+(1)} - (\sigma_{j,+}^{+(1)} + \sigma_{j,+}^{-(1)}) + \sigma_{j-1,+}^{-(1)}\right], \end{aligned} \tag{3.5.36}$$

$$\begin{aligned} p_{j,-}^{*} &= p_{j,-}^{(1)} - \frac{\triangle t}{\epsilon}\left(M_{j,-}(u_j^{*}) - f_{j,-}^{*}\right) + \frac{2\triangle t}{\epsilon}\left(M_{j,-}(u_j^{**}) - f_{j,-}^{**}\right) + \lambda \triangle t D_x p_{j,-}^{(1)} \\ &= p_{j,-}^{(1)} - \frac{\triangle t}{\epsilon}\left(M_{j,-}(u_j^{*}) - f_{j,-}^{*}\right) + \frac{2\triangle t}{\epsilon}\left(M_{j,-}(u_j^{**}) - f_{j,-}^{**}\right) \\ &\quad - \lambda \frac{\triangle t}{2h_j}\left[(p_{j+1,-}^{(1)} - p_{j-1,-}^{(1)}) + \frac{1}{\lambda}(p_{j+1,-}^{(1)} - 2p_{j,-}^{(1)} + p_{j-1,-}^{(1)})\right] \\ &\quad - \frac{\triangle t}{4h_j}\left[\sigma_{j+1,-}^{+(1)} - (\sigma_{j,-}^{+(1)} - \sigma_{j,-}^{-(1)}) - \sigma_{j-1,-}^{-(1)}\right], \end{aligned} \tag{3.5.37}$$

$$p_{j,+}^{n} = \frac{1}{2}(p_{j,+}^{n+1} + p_{j,+}^{*}),\ p_{j,-}^{n} \frac{1}{2}(p_{j,-}^{n+1} + p_{j,-}^{*}). \tag{3.5.38}$$

As for all other numerical schemes, discretized schemes reviewed under this Chapter needs numerical implementation for analysis, visualization and presentation of results. Due to this, it is customary to consider a truncated spatial and time domain of interest for numerical computational purposes. The truncated spatial domain needs to be supplemented at its ends by boundary conditions, which is the subject of the subsequent Section.

3.6 Boundary conditions

Numerical solutions are not computed over the whole domain $\mathbb{R}$. Therefore, we had to truncate a reasonable computational domain of our interest $[x_L, x_R]$. This truncation of course suggests that boundary conditions must be imposed. In our computations, we used two types of boundary conditions: periodic boundary conditions and transparent (non-reflecting Neumann type) boundary conditions.

3.6.1 Periodic boundary conditions

In this case, the scheme requires two ghost cells, one on the left of the domain and another one on the right. This means if we consider our truncated domain to be $[x_L, x_R]$, then the two ghost

cells are respectively $x_L - \triangle x$ and $x_R + \triangle x$ on the left and right sides. Therefore, numerically we set $u_0^n = u_N^n$ and $u_{N+1}^n = u_1^n$.

3.6.2 Transparent boundary conditions

Transparent (non-reflecting Neumann type) boundary conditions are usually imposed such that, the values of the cell next to the boundary are the same as for the ghost cells, i.e., $u_0^n = u_1^n$, $u_{N+1}^n = u_N^n$.
We have described the imposition of the boundary conditions using macroscopic variable u, similar imposition is to be considered with the microscopic variables.

3.6.3 Algorithm for gradient computing

The optimal control method under consideration involves the computation of the cost functional 2.7.1 gradient. This gradient is used to modify the design variable (in our case initial condition) which adjusts in such a way to produce optimal solution that matches the given target. To compute the gradient of the 2.7.1 and incorporate it in the optimal control method, we need to follow the following procedures:

- We first linearize the nonlinear CLs (2.1.1) to have its relaxation form 2.5.18;
- Derive its adjoint system;
- Solve for the flow variable $u(., T)$ forward in time;
- Use the solution of the flow variable above at the terminal time T to solve for the adjoint variable backward in time;
- Use the adjoint variable and the control variable u_0 to evaluate the gradient of the cost functional (2.7.1), $\nabla_{u_0} J$;
- Update the control variable by using the gradient obtained above and the chosen step size by making a step in the negative gradient direction,

$$u_{0_{new}} = u_{0_{old}} - \alpha \nabla_{u_0} J; \tag{3.6.1}$$

- Repeat processes (3-6) until a minimization is reached.

This algorithm gives a brief overview of the adjoint-based optimization. We specifically applied this algorithm to optimize the Euler Equations of Gas dynamics that models transportation of gases in pipelines [9, 11, 12]. To insure convergence of the optimization process some rules,

such as Armijo step-size rule described in [8], have been considered to automatically choose the optimal value of α by making step towards the steepest descent direction.

Derivation of relaxing schemes from relaxation systems of hyperbolic conservation laws, has been the major focus of this Chapter. These schemes were tested for the numerical solutions of linear, nonlinear scalar and systems of hyperbolic conservation laws. Accurate solutions of HCLs has been a central point to our research because they form important components of the adjoint-based optimization procedure being discussed. Numerical tests for both solutions of HCLs and for the adjoint-based optimization method are discussed in the next Chapter.

4. Numerical Results

This Chapter deals with the numerical findings as a result of implementation of the two relaxing schemes derived under Chapter 3 which include simulations of the solutions and optimization results for scalar and systems of HCLs. We have considered the advection equation, the inviscid Burgers' Equation and the systems of HCLs, specifically, system of Euler Equations. We first looked for their solutions and then employed adjoint-based control summarized by the algorithm 3.6.3 as an optimal control strategy. Two relaxing schemes: The JIN XIN scheme described in [64] and the discrete kinetic scheme presented in [5, 92] are compared for both solutions of HCLs and for the problem of optimization as well. Schemes developed are TVD, based on the method of lines associated with Runge-Kutta type time discretizations. Second-order accuracy in solution is achieved through second-order MUSCL type space discretization coupled with a second-order Runge-Kutta time splitting scheme using minmod slope limiter introduced by Sweby in [124].

All numerical results that will be presented in a sequel are performed with *intel core i*5, 2.67 GHZ, and 4G RAM machine, and programs developed using Python scripting language. Briefly, this chapter is devoted to present, describe and analyze numerical results obtained from our experiments.

4.1 Numerical Discretizations of Spatial and Temporal Domains

We take the first step to discretize both the time and spatial domains. We consider a bounded domain of $\mathbb{R}$, $[x_L, x_R]$. For the sake of simplicity, the domain $[x_L, x_R]$ is divided uniformly into a sequence of $M+1$ points, $m = 0, \ldots, M$, such that $x_0 = x_L$, $x_M = x_R$; with a mesh size $\triangle x = \frac{1}{M}$. The temporal domain is considered to be $[0, T]$, discretized into N time levels, t^n, with time step, $\triangle t = t^{n+1} - t^n$, and the horizon time is given by $T = N\triangle t$. Our interest is to have the approximation of the form u_j^n.

4.2 General Descriptions

We computed the approximate solutions for both scalar and systems of HCLs on a uniform mesh, with 200, 400, 800, and 1600 grid points and present results for different values of time. We choose fixed time step $\triangle t$ and spatial step $\triangle x$ related by the stability condition $\triangle t = \text{CFL}\triangle x/\sqrt{a_{\max}}$, where CFL is the Courant-Friedrichs-Lewy number, and $a_{\max}$ is the maximum of the characteristic speeds. Without loss of generality, we considered solutions on the spatial computational domain $[0, 1]$, and a mesh with $M+1$ grid points. Where possible, numerical

solutions are compared with exact solution or a reference (depicted by red solid line) solved with the number of grid points $M = 1600$.

For the two relaxing schemes, JIN XIN and the discrete kinetic scheme, the macroscopic variable u is linked to microscopic f_i by the Maxwellians

$$M_i(u) = \alpha_i u + \beta_i A(u), \tag{4.2.1}$$

$$= \alpha_i \sum_{j=1}^{N} f_j + \beta_i \sum_{j=1}^{N} \lambda_j f_j, \tag{4.2.2}$$

where Maxwellians must be monotone preserving according to [5]. Next, we define the following variables related to discrete kinetic schemes, that will be used throughout the course of this Chapter: for a system with two velocity model we have $\lambda_1 = -\lambda_2$, while for three velocities discrete kinetic scheme, we have $\lambda_3 = -\lambda_1$, where λ_2 is set to 0. Furthermore, we set $\alpha = \alpha_1 = \alpha_3$, $\alpha_2 = 1 - 2\alpha$; $\beta = \beta_2$,

$$\beta_1 = \frac{1}{2}\left(-\frac{1}{\lambda_3} - \beta\right); \beta_3 = \frac{1}{2}\left(\frac{1}{\lambda_3} - \beta\right). \tag{4.2.3}$$

For two velocity model, we obviously have the diagonal relation

$$M_i(u) = \frac{1}{2}\left(u \pm \frac{A_i(u)}{\lambda_i}\right), \ \lambda_1 = \lambda, \ \lambda_2 = -\lambda \tag{4.2.4}$$

between macroscopic u and Maxwellians. Here, we restrict numerical results for discrete kinetic model to two or three velocities scheme. A relaxation rate $\epsilon = 10^{-8}$ is considered for both schemes.

In the sequel, we start to present numerical results obtained with the schemes we have derived in Chapter 3 for various HCLs problems. The aim is to develop accurate numerical solutions to be incorporated during adjoint-based optimal control process.

4.3 Numerical Experiments for Scalar HCLs

We start by presenting numerical solutions for the linear, and then nonlinear scalar HCLs, for both JIN XIN [64] and discrete kinetic [5] relaxation models. We have chosen to start with the solutions of the model linear and nonlinear scalar HCLs which serve as prototype to generalization to systems of HCLs and multi-dimensional problems.

4.3.1 Numerical experiments for scalar linear HCLs

We consider the numerical solution of the one-dimensional version of the linear transport equation

$$u_t + a u_x = 0, \ \forall (x,t) \in \mathbb{R} \times \mathbb{R}_+ \tag{4.3.1}$$

with initial condition $u(x,0) = u_0(x)$.

To be specific, we consider the linear transport equation (4.3.1) with initial data

$$u_0(x) = \sin(2\pi x). \tag{4.3.2}$$

Solution of the HCL (4.3.1) is implemented with periodic boundary conditions for $a = 1$ over time $T = 1$ and the computational domain $[0, 1]$ using the two relaxing schemes described in [64] and [5]. We repeat this experiment for the second-order relaxing schemes. Obviously, solutions displayed in Figure 4.1(a) for the first-order scheme, and in Figure 4.1(b) for the second-order scheme are good approximations.

Again, we solve the transport equation (4.3.1) for discontinuous initial Riemann data defined as

$$u_0(x) = \begin{cases} 2 \text{ if } x < 0.5 \\ 1 \text{ if } x > 0.5, \end{cases} \tag{4.3.3}$$

implemented over time $T = 0.3$ for $a = 1$, but this time together with transparent boundary conditions. First-order, Figure 4.2(c) and second-order, Figure 4.2(d) numerical solutions for both relaxing schemes are quite well approximated.

4.3.2 Numerical experiments for scalar nonlinear HCLs

Most natural phenomena can be described by nonlinear models. In such models, the velocity field, for example, a simple case $a(x,t) = u(x,t)$ depends on the solution itself. Hence the quasilinear transport equation (4.3.1) becomes

$$u_t + uu_x = 0. \tag{4.3.4}$$

If we assume that the solution u is smooth, equation (4.3.4) is equivalent to the equation

$$u_t + \left(\frac{1}{2}u^2\right)_x = 0, \tag{4.3.5}$$

which is a *conservative* form of (4.3.4). The HCLs (4.3.5) is called inviscid Burgers Equation.

To start with, we consider the model nonlinear HCL (4.3.5), i.e.,

$$u_t + f(u)_x = 0, \;\; f(u) = \frac{1}{2}u^2 \tag{4.3.6}$$

with smooth initial data

$$u_0 = \frac{1}{2} + \sin(x), \;\; x \in [0, 2\pi] \tag{4.3.7}$$

for $a = 1.3$ over different time periods of $T = \frac{\pi}{4}$ and $T = 2.0$. Computational domain is taken to be $[0, 1]$.

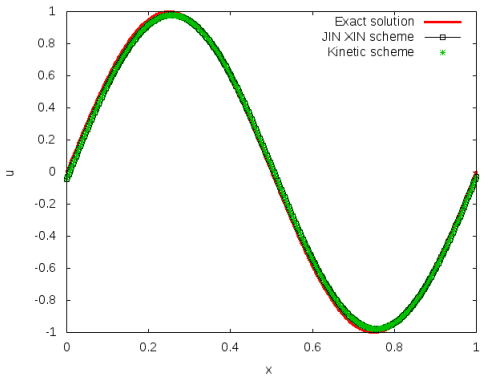

(a) First-order smooth solution with initial data (4.3.2), $T = 1$

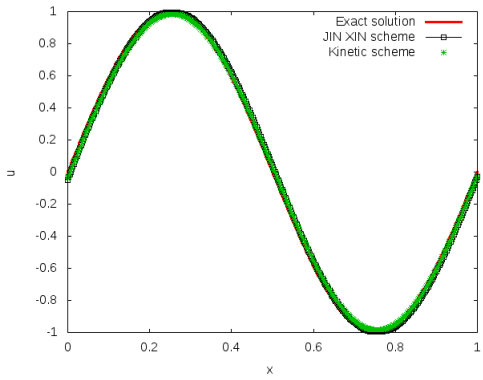

(b) Second-order test, same parameters as for 4.1(a)

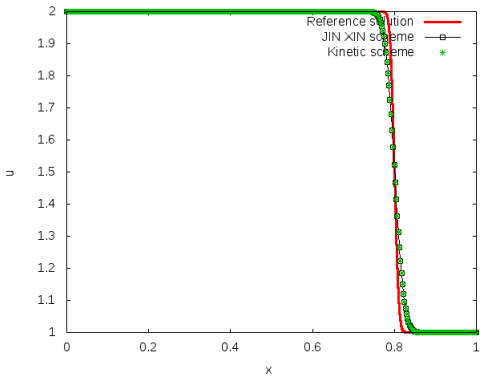

(c) First-order shock solution with initial data (4.3.3), $T = 0.3$

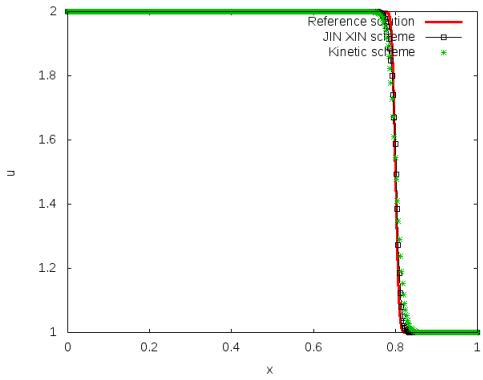

(d) Second-order test, same parameters as for 4.1(c)

Figure 4.1: Solution of the linear advection equation (4.3.1) for JIN XIN scheme (black solid line with squares at data points), kinetic scheme (green asterisk), and a reference solution (red solid line) for $a = 1$, $M = 400$ and $\epsilon = 10^{-8}$. The x-axis represents the space variable x and the y-axis represents the advected quantity, u.

Here we have tested the two relaxation approaches with HCL (4.3.6) for smooth initial data (4.3.7) implemented together with periodic boundary conditions. We first display a smooth solution at some finite time, $T = \frac{\pi}{4}$, Figure 4.2(a), and then we allow the solution to evolve over a bit larger time, $T = 2.0$, so that it develops a shock, Figure 4.2(b). These results are obtained with the first-order relaxing schemes. We then repeat the previous experiments with the second-order relaxing schemes and display results in Figures 4.2(c), 4.2(d), computed respectively, over $T = \frac{\pi}{4}$ and $T = 2$. As depicted by Figures, both solutions are close approximations of the true solution.

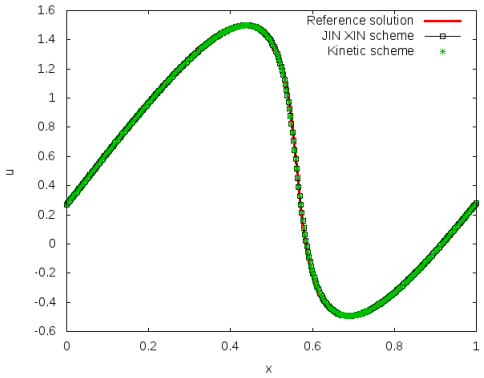

(a) Smoot solution at time, $T = \frac{\pi}{4}$, first-order test

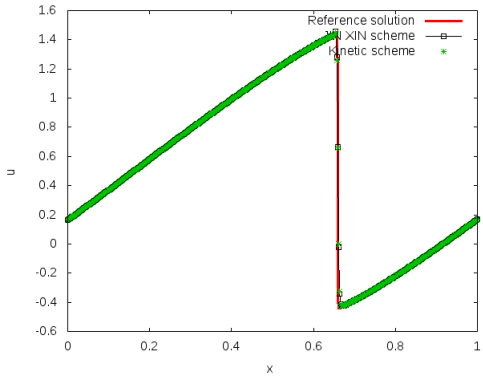

(b) Shock solution at time, $T = 2$, first-order test

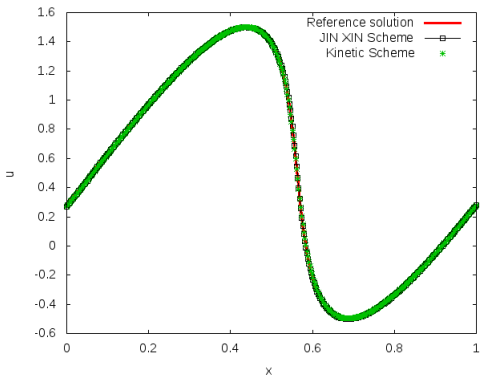

(c) Smooth solution, $T = \frac{\pi}{4}$, second-order test

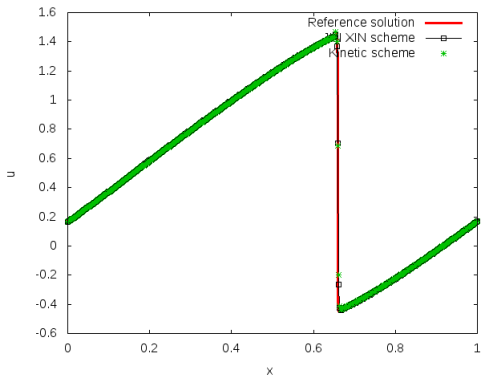

(d) Shock solution, $T = 2$, second-order test

Figure 4.2: Solution of the Burgers' Equation using JIN XIN scheme (black solid line with squares at data points), kinetic scheme (green asterisk), and a reference solution (red solid line) for $a = 1.3$, $M = 400$ and $\epsilon = 10^{-8}$. The x-axis represents the space variable x and the y-axis represents the conserved quantity, u.

Next, we consider a discontinuous initial Riemann data

$$u(x,0) = \begin{cases} 1 \text{ if } x < 0.5 \\ 0 \text{ if } x > 0.5. \end{cases} \tag{4.3.8}$$

This time, the HCL (4.3.6) is solved over $T = 0.5$ together with transparent boundary conditions, where $a = 1$. We obtain good results with first-order relaxing scheme, Figure 4.3(a) and second-order relaxing scheme as well, Figure 4.3(b).

Finally we consider the last example under this Section for discontinuous initial Riemann data given by

$$u(x,0) = \begin{cases} -1 \text{ if } x < 0.5 \\ 1 \text{ if } x > 0.5, \end{cases} \tag{4.3.9}$$

implemented with transparent boundary conditions over time period $T = 0.2$. Again, we take $a = 1$. Well approximated solutions with the first and second order schemes for this set of data are, respectively shown in Figures 4.2(c) and 4.2(d).

We have tested the two relaxing schemes, first and second order in time and space for the solutions of the linear and nonlinear HCLs evolved from two types of data: smooth sine wave and the Riemann data. As we have seen, two types of solutions are depicted: smooth and discontinuous ones. Here, a pair of solutions, one with and another one without shock both evolving from smooth initial data (4.3.7) is depicted by Figure 4.2. Discontinuous solutions evolved from a pair of discontinuous Riemann data (4.3.8, 4.3.9) are illustrated by Figure 4.3. Solutions to both schemes are very well approximated, and in the case of solution in which discontinuity, (Figures 4.2(b), 4.2(d)) would arise after a finite time, care is well taken and the solution is non-oscillatory as well.

4.4 Numerical Solutions for Systems of HCLs

Systems of conservation laws occur in many natural interesting phenomena and are useful for the modeling of complex physical systems, especially those which involve interaction of many unknowns. Systems of HCLs are, therefore, one of the suitable tools for modeling physical dynamical systems, in areas such as CFD and aerodynamic designs. Here, we considered the solution of 1D system of Euler Equations, and in particular, applied this solution for illustration of the optimization process under consideration.

We solved numerically the nonlinear $m \times m$ system

$$u_t + f(u)_x = 0, \tag{4.4.1}$$

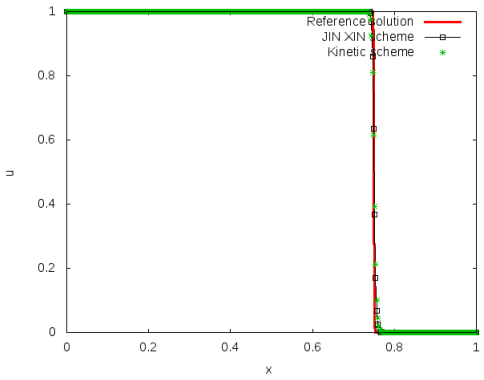

(a) Shock solution with initial Riemann data (4.3.8) at time, $T = 0.5$, first-order test

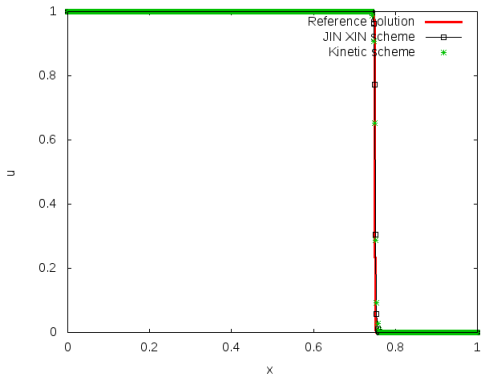

(b) Shock solution with initial Riemann data (4.3.8), $T = 0.5$, second-order test

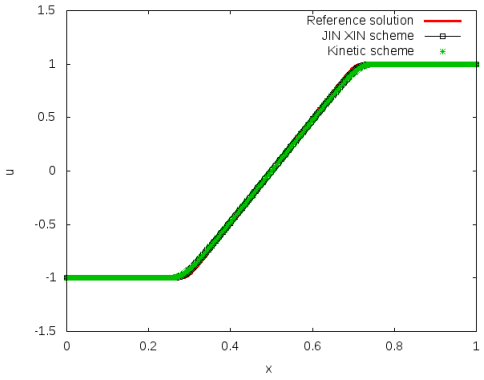

(c) Rarefaction wave solution with initial Riemann data 4.3.9 at time, $T = 0.2$, first-order test

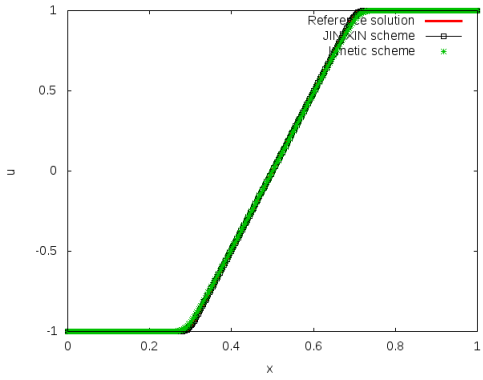

(d) Rarefaction wave solution with initial Riemann data (4.3.9), $T = 0.2$, second-order test

Figure 4.3: First and second-order numerical solutions for JIN XIN and discrete kinetic relaxing schemes. The x-axis represents the space variable x and the y-axis represents the velocity field, u.

of HCLs in one space dimension, where

$$u = [u^1, \ldots, u^m]^T \tag{4.4.2}$$

is the vector of unknown conserved variables, and

$$f = [f^1, \ldots, f^m]^T \tag{4.4.3}$$

is the vector of flux functions. When $m = 1$, the system (4.4.1) reduces to scalar HCL.

We have begun the solution of nonlinear systems of HCLs by first considering a linear system

$$u_t + Au_x = 0, \tag{4.4.4}$$

which is the simplest case of (4.4.1). Specifically, we consider the one-dimensional wave equation

$$u_{tt} - a^2 u_{xx} = 0, \ (x,t) \in (0;L) \times \mathbb{R}^+, \tag{4.4.5}$$

$$u(x,0) = u_0(x), \ u_t(x,0) = u_1(x), \ x \in [0;L]. \tag{4.4.6}$$

The wave equation (4.4.5) can be transformed into a system of first-order equations by making change of variables $v = u_x$, and $w = -u_t$. With these changes, the wave equation (4.4.5) reduces to

$$v_t + aw_x = 0 \tag{4.4.7}$$

$$w_t + av_x = 0, \ (x,t) \in (0;L) \times \mathbb{R}^+, \tag{4.4.8}$$

supplemented with initial conditions

$$v(x,0) = v_0(x) = 0, \tag{4.4.9}$$

$$w(x,0) = -\frac{1}{a}\int_0^x u_1(s)ds + c, \ u_1(x) = \sin(\pi x), \ x \in [0;L]. \tag{4.4.10}$$

We solved the system of equations (4.4.7) with boundary conditions for $L = 1$ (see Figure 4.4). Accurate numerical solution solved with suitable initial and boundary conditions

$$u(x,0) = 0, \ u_t(x,0) = 0 \tag{4.4.11}$$

$$u(0,t) = 0; \ u(\pi,t) = 0, \tag{4.4.12}$$

can be compared to analytical solution $u(x,t) = \frac{1}{a}\sin(at)\sin(x)$.

Good approximations for both schemes are obtained for the solution of the problem discussed above. Our intention here is that, the linear model equation provides crucial information for generalization to nonlinear systems. Thus, we carried out tests to numerically solve these kind of problems, especially those with propagating discontinuities.

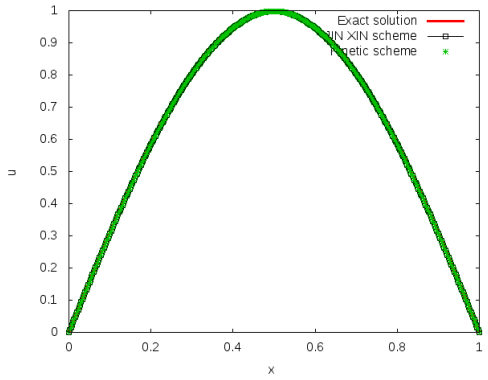

Figure 4.4: Solution of the wave equation (4.4.5), JIN XIN scheme (black solid line with squares at data points), kinetic scheme (green asterisk), and exact solution (red solid line); $T = \frac{\pi}{2}$, $M = 400$, $\epsilon = 10^{-8}$, $a = 1$. The x-axis represents the space variable x and the y-axis represents the wave profile, u.

4.5 Numerical Solutions for Nonlinear Systems of HCLs

We embark to consider relaxing schemes for the solution of the nonlinear systems of HCLs. As we have already explored the development of these schemes, discretization in space is achieved by the operator splitting approach associated with TVD Runge-Kutta type time discretizations up to second-order in time. Second-order accuracy in space is achieved by employing minmod slope limiter through MUSCL reconstruction on the transport part. Other slope-limiters can also be considered. This kind of discretization is suitable for circumventing discontinuities at the same time increasing accuracy. We started by testing comparatively the two first-order relaxing schemes, and then repeat experiments with the examples we have surveyed for the first-order schemes with the second-order in time and space more accurate schemes.

As we have mentioned in the previous sections, our intention has been to solve numerically 1D nonlinear system of HCLs for the purpose of optimization. We devised a means to obtain accurate approximations to solutions of these systems, and emphasized on accuracy as an important ingredient and central tool to optimization process under consideration.

Consider the approximate numerical solution of the 1D Euler Equations of gas dynamics in a conserved form

$$\frac{\partial}{\partial t}\rho + \frac{\partial}{\partial x}m = 0 \tag{4.5.1}$$

$$\frac{\partial}{\partial t}m + \frac{\partial}{\partial x}(\rho u^2 + p) = 0 \tag{4.5.2}$$

$$\frac{\partial}{\partial t}E + \frac{\partial}{\partial x}(u(E + p)) = 0, \tag{4.5.3}$$

where $\rho,\ u,\ m=\rho u,\ p,$ and E are, respectively, the density, velocity, momentun, pressure and total energy of the gas. For a perfect gas, E is related to other quantities by

$$E=\frac{p}{\gamma-1}+\frac{1}{2}\rho u^2 \tag{4.5.4}$$

where γ constitutes the thermodaynamic property of the gas and is the rato of specific heat coefficients.

The system (4.5.1) takes the form

$$u_t+f(u)_x=0, \tag{4.5.5}$$

when we write

$$u=\begin{bmatrix}\rho\\ m\\ E\end{bmatrix},\qquad f(u)=\begin{bmatrix}m\\ \rho u^2+p\\ u(E+p)\end{bmatrix}. \tag{4.5.6}$$

The relaxation system for (4.5.5) takes the form

$$\begin{cases}\frac{\partial u}{\partial t}+\frac{\partial v}{\partial x}=0,\\ \frac{\partial v}{\partial t}+A\frac{\partial u}{\partial x}=-\frac{1}{\epsilon}(v-f(u)),\end{cases} \tag{4.5.7}$$

where $A=\text{diag}\{a_i\}$, $a_i>0$, for $1\le i\le 3$,

and its equivalent discrete kinetic relaxation takes the form (3.5.1).

Mathematical analysis [34, 125] shows that, the relaxation (4.5.7) of the Euler equation (4.5.5) can be decomposed as $A=P\wedge P^{-1}$ where

$$\wedge=\begin{bmatrix}u-a & 0 & 0\\ 0 & u & 0\\ 0 & 0 & u+a\end{bmatrix}, \tag{4.5.8}$$

$$P=\begin{bmatrix}1 & 1 & 1\\ u-a & u & u+a\\ H-au & \frac{1}{2}u^2 & H+au\end{bmatrix}, \tag{4.5.9}$$

and

$$P^{-1}=\begin{bmatrix}\frac{1}{2}(\alpha_1+\frac{u}{a}) & -\frac{1}{2}(\alpha_2 u+\frac{1}{a}) & \frac{\alpha_2}{2}\\ 1-\alpha_1 & \alpha_2 u & -\alpha_2\\ \frac{1}{2}(\alpha_1-\frac{u}{a}) & -\frac{1}{2}(\alpha_2 u-\frac{1}{a}) & \frac{\alpha_2}{2}\end{bmatrix} \tag{4.5.10}$$

such that $\alpha_1 = \frac{(\gamma-1)u^2}{2a^2}$ and $\alpha_2 = \frac{\gamma-1}{a^2}$. Here $a = \sqrt{\gamma\frac{p}{\rho}} = \sqrt{\gamma RT}$ is the local sound speed, H is the Enthalpy, R the universal gas constant and T is the temperature of the gas.

The relaxation system (4.5.7) therefore has three eigenvalues given by

$$\lambda_- = u - a,\ \lambda_0 = u, \lambda_+ = u + a. \tag{4.5.11}$$

For computational tests, we can make the choices according to [64], i.e., $a_1, a_2, a_3 = \sup|u-a|$, $\sup|u|$, $\sup|u+a|$, respectively, or $a_1 = a_2 = a_3 = \max(\sup|u-a|, \sup|u|, \sup|u+a|)$, where sup is an abbreviation for supremum, and supremum is defined as the least upper bound value of a given set. We then solved the two relaxation systems (4.5.7) and (3.5.1) for the parameters of our choice.

4.5.1 Sod Shock Tube Problem

Our computational tests involved experimentation with the Sod's data for the Shock Tube problem. To be able to understand the idea behind the shock tube we had to consider a long 1D tube which is closed at its ends and initially filled with a gas separated by a membrane at the middle. The gas has a high pressure and density in one section of the tube than the other, Figure 4.5. The velocity of the gas is initially zero everywhere. When the membrane is suddenly removed at time $t = 0$, causes the high speed flow of the gas from high to low pressure region, Figure 4.6. Assumming that the net flow is uniform across the tube, there will be variation in only one direction, and this variation can be described or modeled by 1D Euler Equations of gas dynamics considered. Detailed descriptions of the shock tube problem is found in [59, 76].

4.5.2 First and second order numerical tests

We implemented schemes we derived under Chapter 3 with the Riemann data defined in this way: $u_L = (\rho_L,\ v_L,\ p_L)$ corresponds, respectively, to the density, velocity and pressure on the left part of the domain for $0 \leq x < 0.5$; and $u_R = (\rho_R,\ v_R,\ p_R)$ is the data corresponding to density, velocity and pressure on the right part of the domain for $0.5 \leq x \leq 1$. All (unless stated otherwise) tests for the system of the Euler equations are carried for the following set of values: $T = 0.17$, the computational spatial domain $[0, 1]$, $M = 400$ grid points, CFL (Courant-Friedrichs-Lewy) $= 0.75$ and $\epsilon = 10^{-8}$. In addition, for the second-order relaxing schemes we used minmod slope limiter.

We have begun the solution of the Euler equations for the following pair of Riemann data: $u_L = (1.25,\ 0.0,\ 1.2)$, $u_R = (0.25,\ 0.0,\ 0.25)$. We take $a_1 = 1.0,\ a_2 = 2.5,\ a_3 = 5.2$. Results obtained with the first and second order relaxing schemes presented in Figure 4.7 show that the two schemes well agree to each other.

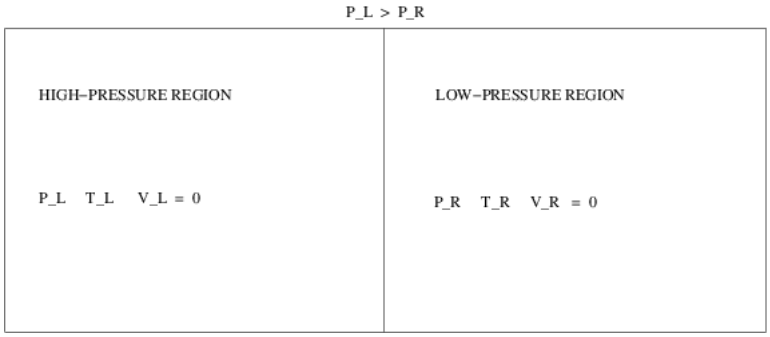

Figure 4.5: Sketch of the initial configuration of the shock tube at time $t = 0$. $P_L,\ T_L,\ V_L$ and $P_R,\ T_R,\ V_R$ are, respectively pressure, temperature and velocity; on the left and right part of the tube.

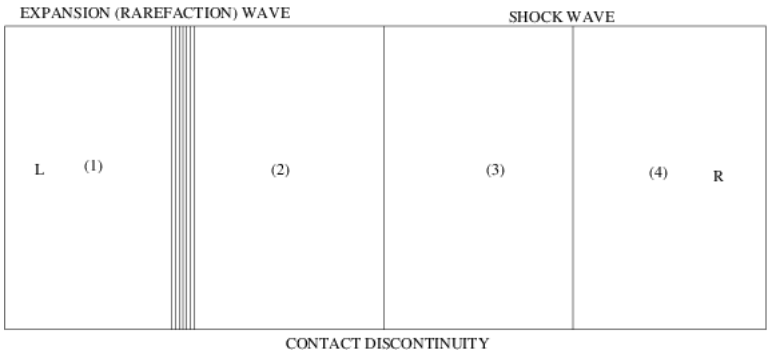

Figure 4.6: Sketch of the shock tube showing waves interaction after the membrane breakdown, $t > 0$.

We consider a second example, solved with initial condition $u_L = (1.45,\ 0.0,\ 1.5)$, $u_R = (0.45,\ 0.0,\ 0.5)$. This time we have chosen $a_1 = 2.2,\ a_2 = 2.5,\ a_3 = 5.0$. Solutions computed over time length $T = 0.17$ are displayed in Figure 4.8. Density, velocity and pressure profiles for both schemes are reasonably equivalent.

Finally, consider the last example evolved from initial data $u_L = (2.5,\ 0.0,\ 2.0)$, $u_R = (0.5,\ 0.0,\ 0.6)$ computed over same time horizon $T = 0.17$ as for previous examples, and present simulated results in Figure 4.9. Simulations show that, solutions obtained with two different relaxing schemes are comparable in terms of appearance and accuracy as well.

These examples demonstrate that the two relaxing schemes under consideration are basically equivalent and give similar results.

We have implemented first and second-order schemes derived under Chapter 3. We observed from a series of figures that second-order solutions are more sharper compared to the first-order ones. As compared, all the numerical results for the two relaxing schemes presented for different meshes show that the two schemes, the JIN XIN and the discrete kinetic reasonably give similar results. We have computed solutions for the meshes of 200, 400, 800, 1600 points for the sake of comparison. Clearly, results show that all schemes convergence with mesh refinement, but beyond 400 grid points, numerical experiments reveal that refinement is no longer necessary as

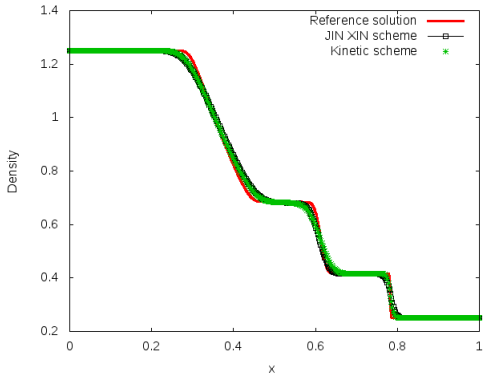

(a) First-order test

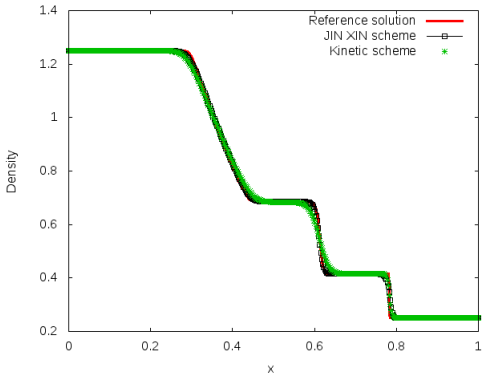

(b) Second-order test

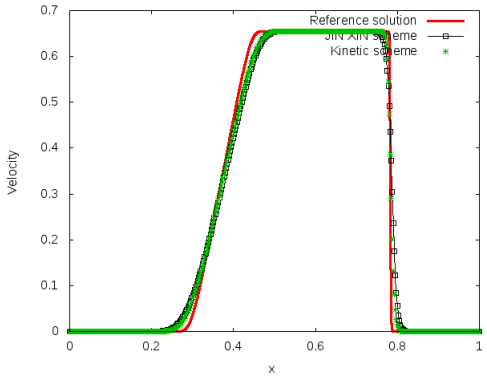

(c) First-order test

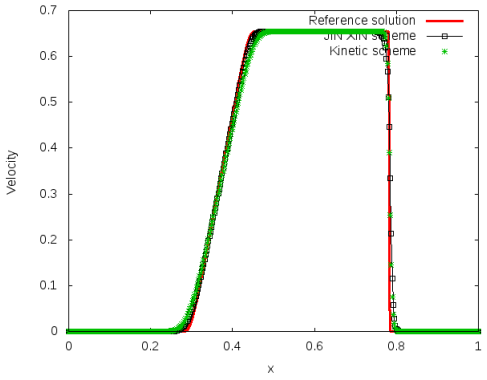

(d) Second-order test

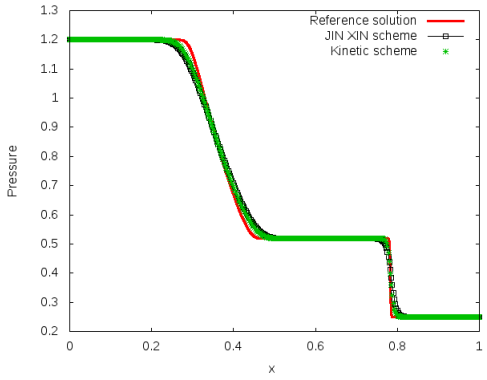

(e) First-order test

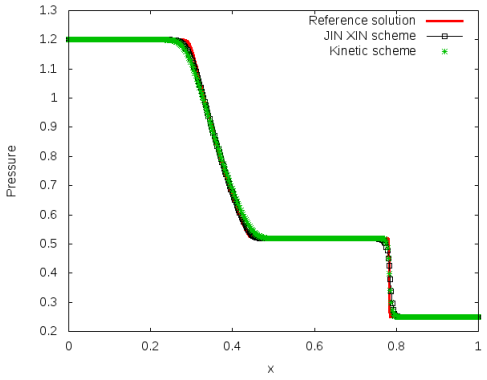

(f) Second-order test

Figure 4.7: First and second order numerical solutions for density, velocity and pressure profiles with JIN XIN and discrete kinetic schemes, for 1D Euler Equations at time, $T = 0.17$, $u_L = (1.25,\ 0.0,\ 1.2)$, $u_R = (0.25,\ 0.0,\ 0.25)$, for $a_1 = 1.0$, $a_2 = 2.5$, $a_3 = 5.2$, $M = 400$ and $\epsilon = 10^{-8}$. The x-axis represents the space variable x and the y-axis represents density (top), velocity (middle) and pressure (bottom).

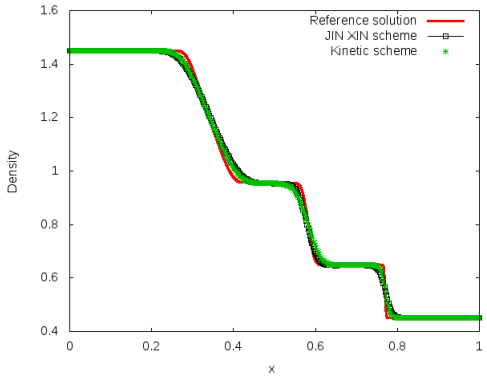

(a) First-order test

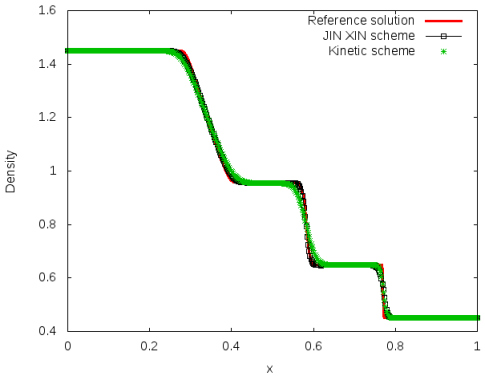

(b) Second-order test

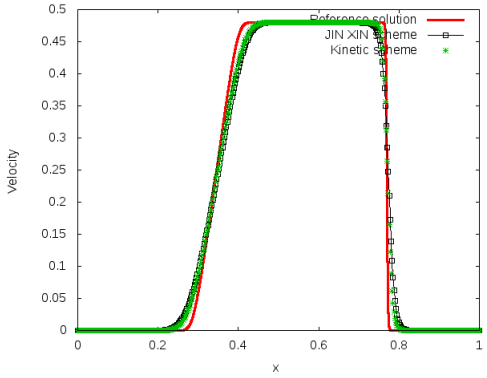

(c) First-order test

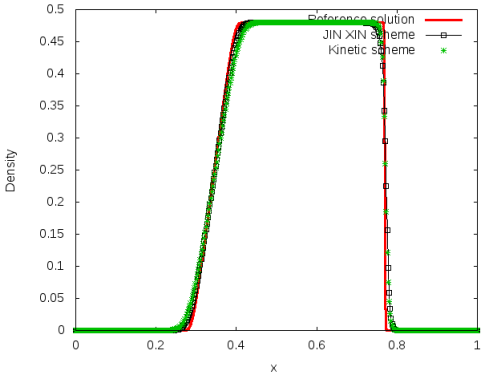

(d) Second-order test

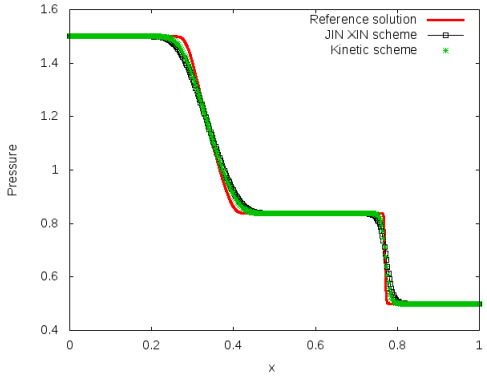

(e) First-order test

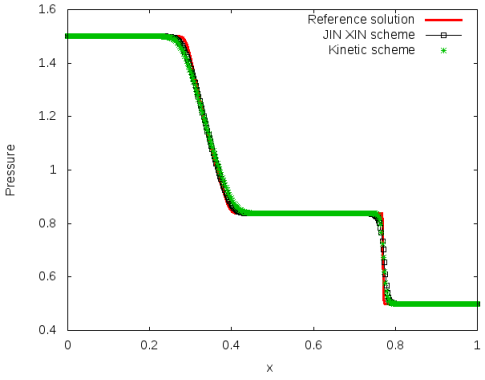

(f) Second-order test

Figure 4.8: First and second order numerical solutions for density, velocity and pressure profiles with JIN XIN and discrete kinetic schemes, for 1D Euler Equations at time, $T = 0.17$, $u_L = (1.45,\ 0.0,\ 1.5)$, $u_R = (0.45,\ 0.0,\ 0.5)$; $a_1 = 2.2,\ a_2 = 2.5,\ a_3 = 5.0$, $M = 400$ and $\epsilon = 10^{-8}$. The x-axis represents the space variable x and the y-axis represents density (top), velocity (middle) and pressure (bottom).

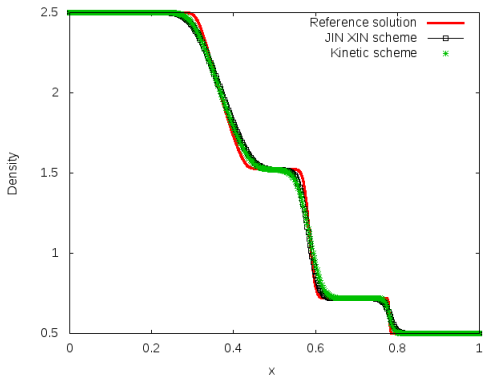

(a) First-order test

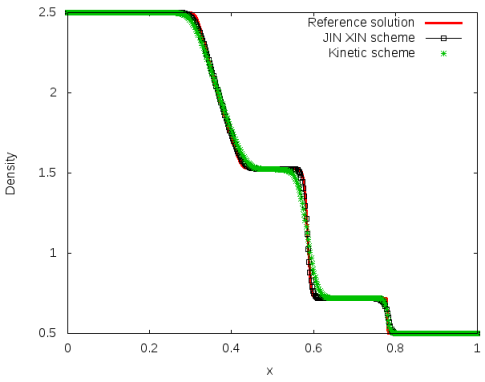

(b) Second-order test

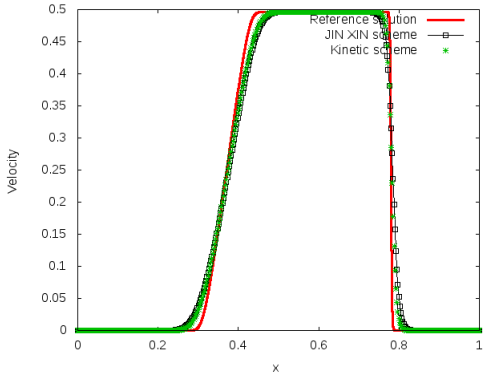

(c) First-order test

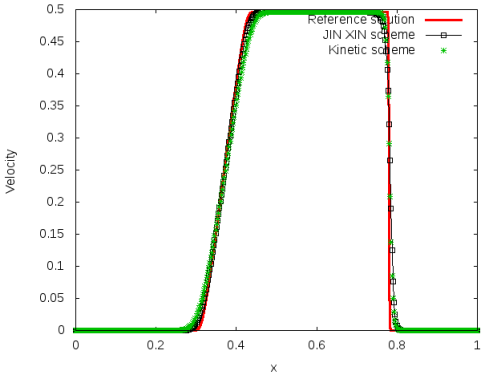

(d) Second-order test

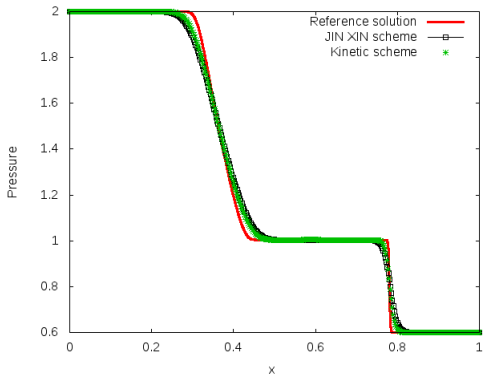

(e) First-order test

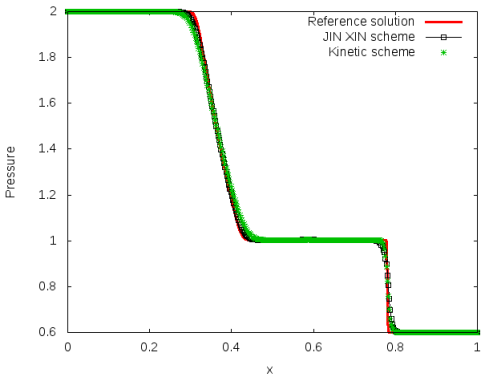

(f) Second-order test

Figure 4.9: First and second order numerical solutions for density, velocity and pressure profiles with JIN XIN and discrete kinetic schemes, for 1D Euler Equations at time, $T = 0.17$, $u_L = (2.5,\ 0.0,\ 2.0)$, $u_R = (0.5,\ 0.0,\ 0.6)$; $a_1 = 3.5,\ a_2 = 4.5,\ a_3 = 5.5$, $M = 400$ and $\epsilon = 10^{-8}$. The x-axis represents the space variable x and the y-axis represents density (top), velocity (middle) and pressure (bottom).

solutions are already sharper at this point (see Figures 4.10, 4.11). Thus, only numerical results for 400 grid points are presented, and this grid could be used for optimization as well. However, one would obviously expect that, decreasing mesh sizes indeed give more accurate results but also leads to a higher run-time. Another observation is that, some set of data introduce more viscosity, see for example in Figure 4.9, considerably smearing contact discontinuities while others produce sharper solutions even for first-order schemes especially with increased grid refinement.

We have numerically demonstrated that the two relaxing schemes discussed in [5] and [64] which we also have surveyed and discussed under Chapter 3 are equivalent. In addition, these numerical results further verify the applicability and the robustness of the methods we have considered. This solution approach is promising, and in the next Section it is considered and employed as an essential tool in an optimization procedure.

4.6 Adjoint-Optimization Tests

We present first-order and second-order optimal control results for scalar nonlinear hyperbolic conservation laws and the one-dimensional systems of Euler Equations for the two relaxing schemes, JIN XIN and discrete kinetic schemes derived under Chapter 3. The optimal control is carried out by matching the numerical solution to the target for a given time length. The minimization process therefore involves the cost functional of L_2 norm of the difference between the computed solution and a desired one. Briefly, optimization process is an implementation of the algorithm described under Subsection 3.6.3. In addition to the algorithm, we employed Wolfe conditions [96, 8] to restrict the choice of the step-size α which is used to modify the functional gradient (2.7.15) that perturb the flow solution. The control parameters are chosen to be initial values of density, velocity and pressure. Existence of the optimal control solution can be conceptualized from numerical displays. We obtained good match between the numerical solution and the desired one for both first and second order schemes.

As described, the optimal control process is of matching type in which we iteratively compute some solution $u(x,T)(u_0)$ (depicted by green solid line) to match with a target solution $u_d(x,T)$. The process starts by choosing some initial guess u_0, and then using the relaxing schemes derived under Chapter 3, we solve the HCL to obtain the solution $u(x,T)$, a function of u_0 at some terminal time T. The functional gradient (2.7.15) is calculated and used at every optimization cycle to modify the design parameter u_0, and each modified u_0 is evolved by the relaxing scheme until the optimal solution $u(x,T)$ that matches the target is attained. The whole optimization process is summarized by the algorithm 3.6.3. We denote by $V(x,T)(u_0)$ the initial solution obtained by solving the flow equation once forward in time, where V is any conserved quantity (density, velocity and pressure for the Euler system of equations). Optimal denotes the numerical

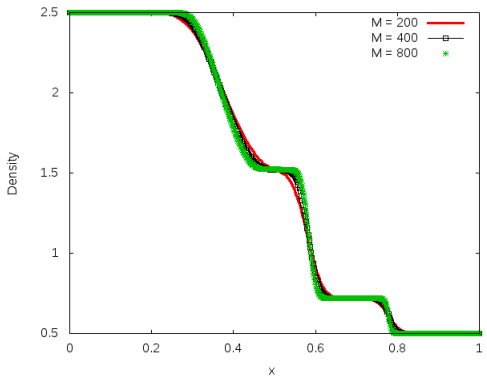

(a) First-order

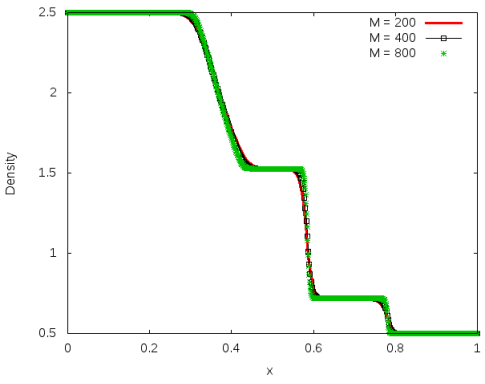

(b) Second-order

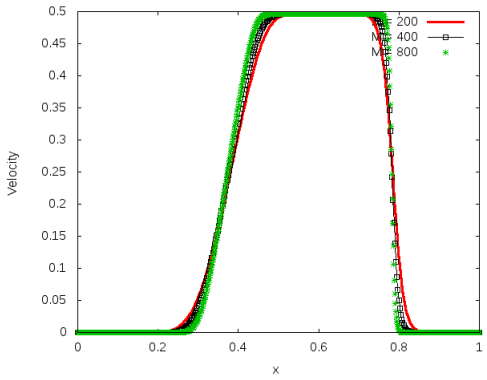

(c) First-order

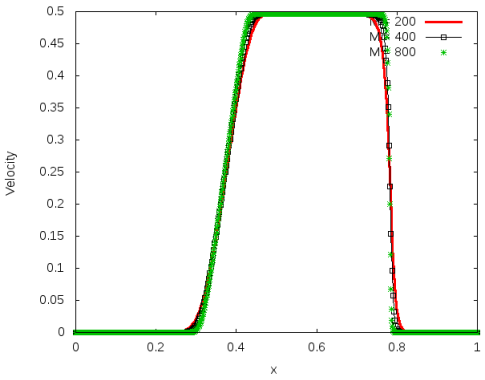

(d) Second-order

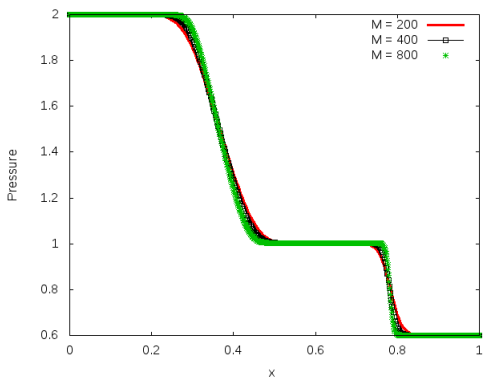

(e) First-order

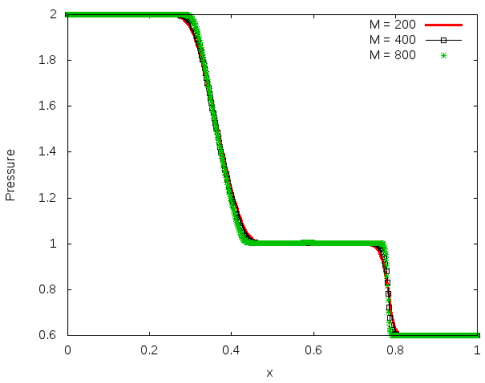

(f) Second-order

Figure 4.10: Comparing first-order and second-order solutions for different grids with JIN XIN scheme; $T = 0.17,\ u_L = (2.5,\ 0.0,\ 2.0),\ u_R = (0.5,\ 0.0,\ 0.6);\ a_1 = 2.0,\ a_2 = 3.5,\ a_3 = 5.5,\ \epsilon = 10^{-8}$. The x-axis represents the space variable x and the y-axis represents density (top), velocity (middle) and pressure (bottom).

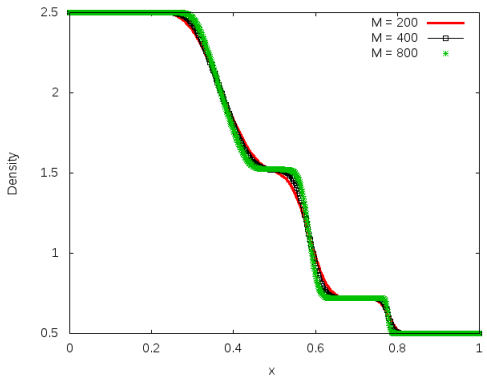

(a) First-order

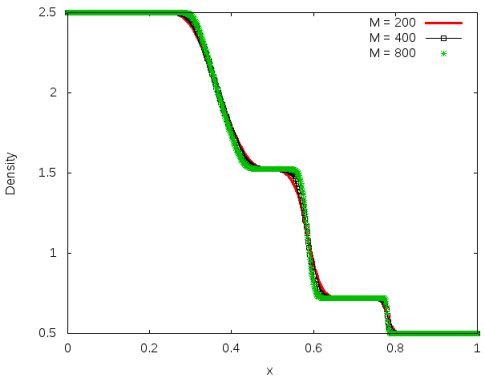

(b) Second-order

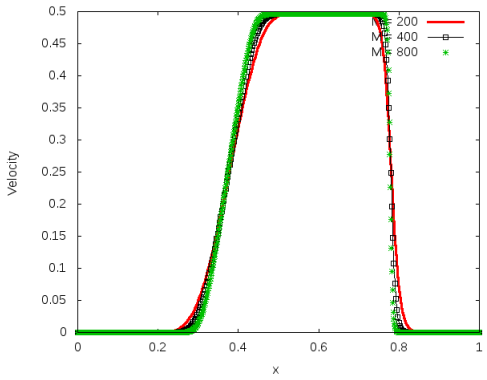

(c) First-order

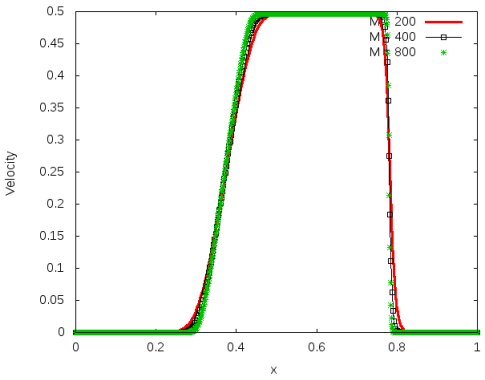

(d) Second-order

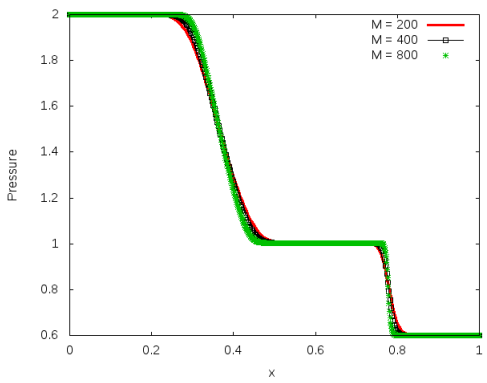

(e) First-order

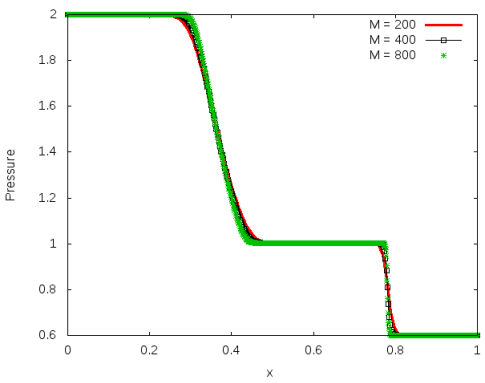

(f) Second-order

Figure 4.11: Comparing first-order and second-order solutions for different grids with discrete kinetic scheme. Same parameters as in Figure 4.10. The x-axis represents the space variable x and the y-axis represents density (top), velocity (middle) and pressure (bottom).

solution that matches the desired profile (solution) and the desired profile is called Target. We used as a stopping criterion the functional (2.7.1) absolute value, $|J(u_0, u_d)| < 10^{-4}$.

4.6.1 Optimization tests for scalar nonlinear HCLs

Under this Subsection, we present optimal control results for scalar nonlinear HCLs. We consider the Burgers' Equation (4.3.4) with Initial condition for the target solution

$$u_0(d) = \frac{1}{2} + \sin(x), \tag{4.6.1}$$

and the design parameter (initial guess) for optimal solution

$$u_0 = \sin(x) \tag{4.6.2}$$

for $x \in [0, 2\pi]$. Optimal control first and second order results for both schemes are, respectively, presented in Figures 4.12 and 4.13. It is clear that we obtained a good match between optimal and the target solutions for this example.

4.6.2 Optimization tests for systems of nonlinear HCLs

In this minimization process, initial guess for the target solution is comprised of the Sod shock tube data for system of Euler Equations,

$$u_L = (1.0,\ 0.0,\ 1.0), u_R = (0.125,\ 0.0,\ 0.1). \tag{4.6.3}$$

The target solution for the initial data (4.6.3) is obtained using $a_1 = 1.0,\ a_2 = 1.68,\ a_3 = 5.045$ over $T = 0.17$. We present optimal control results first-order and second-order in time and space for the two relaxing schemes derived under chapter 3. These results are for the minimization of the problem (2.7.1) with a system of Euler equations (4.5.1) as a constraint.

The first example we considered matches the target to the optimal solution computed from the set of data $u_L = (1.2,\ 0.078,\ 1.2)$, $u_R = (0.325,\ 0.285,\ 0.295)$, $a_1 = 2.183,\ a_2 = 3.004,\ a_3 = 4.286$ over the time $T = 0.17$. The optimal solution for density, pressure and velocity were found to be in a very good agreement with the target for both schemes. First and second order optimal control results for JIN XIN scheme and discrete kinetic scheme are, respectively, potrayed in Figures 4.14, 4.15.

We considered the second example in which also the optimal solutions for the density, velocity and pressure match exactly with the target solutions. Optimal solutions are solved for values of initial condition, $u_L = (1.2,\ 0.2,\ 1.25)$, $u_R = (0.32,\ 0.73,\ 0.32)$, $a_1 = 2.47,\ a_2 = 3.5,\ a_3 = 4.36$. We carried computations over usual time $T = 0.17$. First and second order results for this set of data are displayed in Figure 4.16 for JIN XIN scheme and in Figure 4.17 for discrete kinetic scheme.

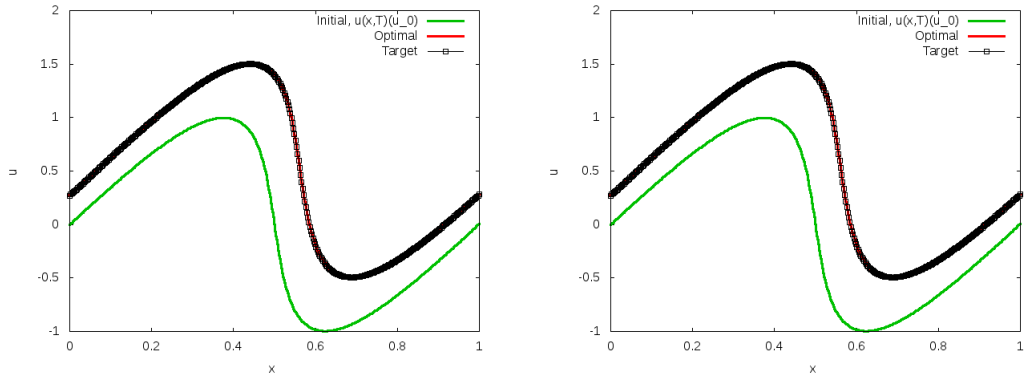

(a) Optimization with smooth solution using JIN XIN scheme, $T = \frac{\pi}{4}$

(b) Optimization with smooth solution using kinetic scheme, $T = \frac{\pi}{4}$

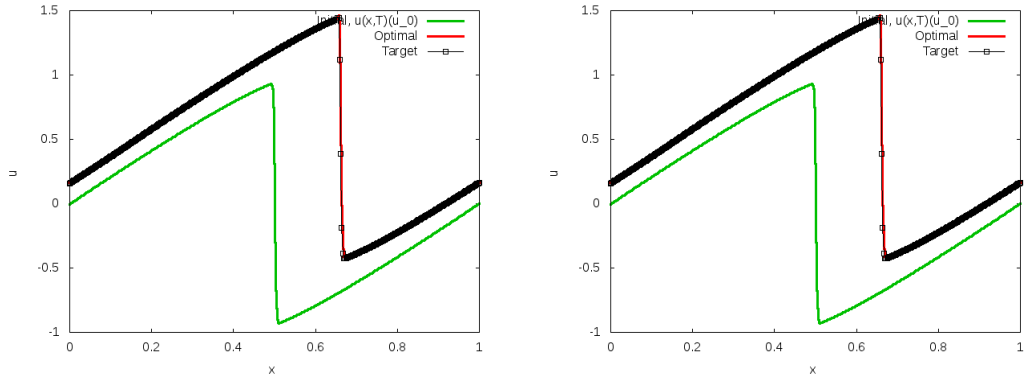

(c) Optimization with shock solution using JIN XIN scheme, $T = 2$

(d) Optimization with shock using kinetic scheme, $T = 2$

Figure 4.12: First-order adjoint-based optimization of scalar nonlinear HCL results for JIN XIN and kinetic schemes, $M = 400$ and $\epsilon = 10^{-8}$. The x-axis represents the space variable x and the y-axis represents the conserved quantity, u.

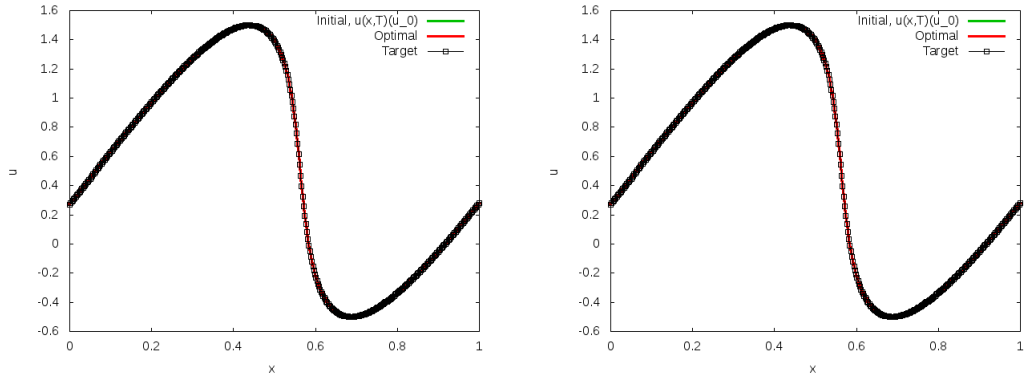

(a) Optimization with smooth solution using JIN XIN scheme, $T = \frac{\pi}{4}$

(b) Optimization with smooth solution using kinetic scheme, $T = \frac{\pi}{4}$

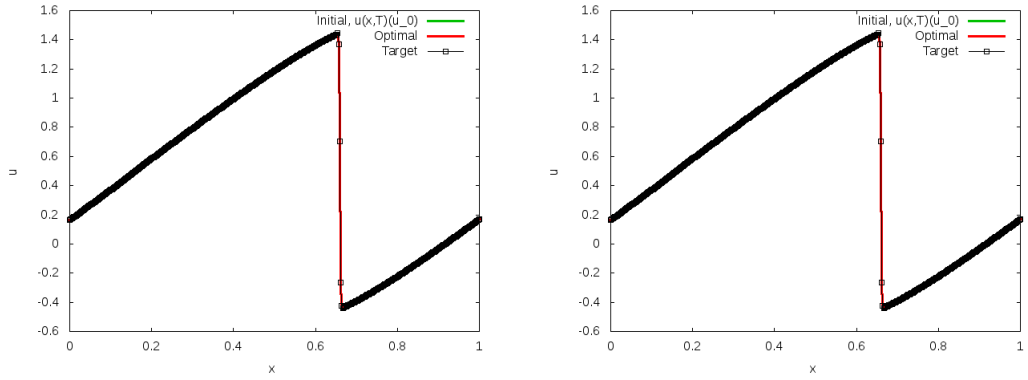

(c) Optimization with shock solution using JIN XIN scheme, $T = 2$

(d) Optimization with shock using kinetic scheme, $T = 2$

Figure 4.13: Same parameters as in Figure 4.12 but second-order tests. The x-axis represents the space variable x and the y-axis represents the conserved quantity, u.

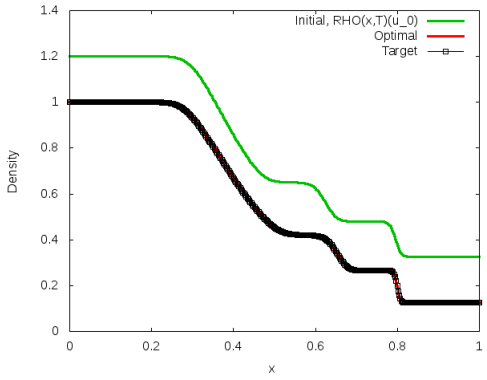

(a) First-order test

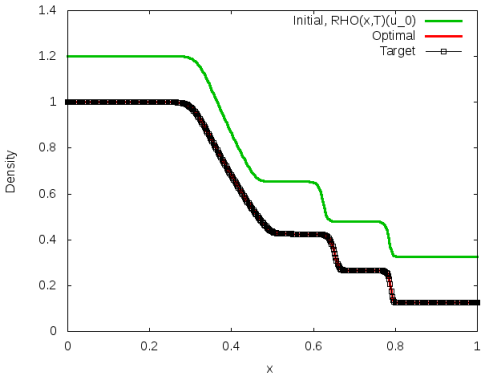

(b) Second-order test

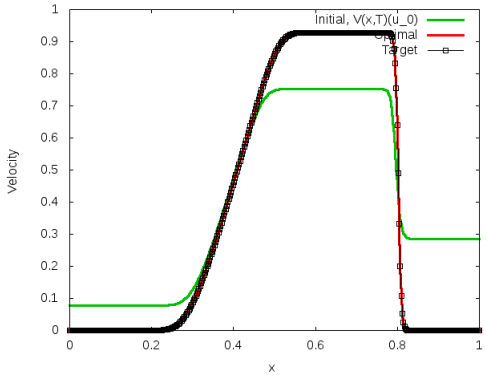

(c) First-order test

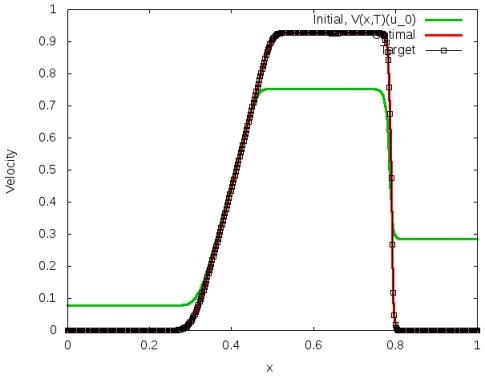

(d) Second-order test

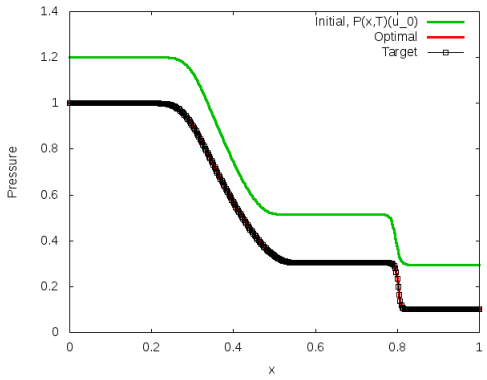

(e) First-order test

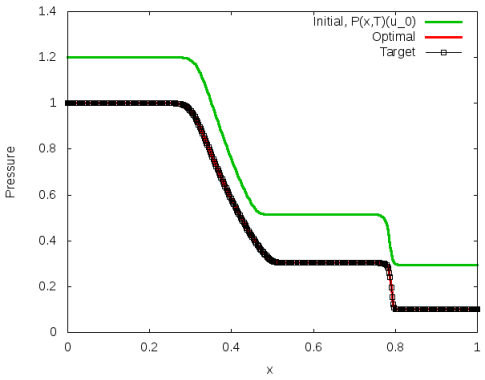

(f) Second-order test

Figure 4.14: First-order (Left) and second-order (Right) 1D Euler Equations optimal control results. The optimal solution is shown by the red solid line and target by black solid line with squares at data points, $T = 0.17$, $u_L = (1.2,\ 0.078,\ 1.2)$, $u_R = (0.325,\ 0.285,\ 0.295)$, $a_1 = 2.183$, $a_2 = 3.004$, $a_3 = 4.286$, $M = 400$ and $\epsilon = 10^{-8}$. The x-axis represents the space variable x and the y-axis represents density (top), velocity (middle) and pressure (bottom).

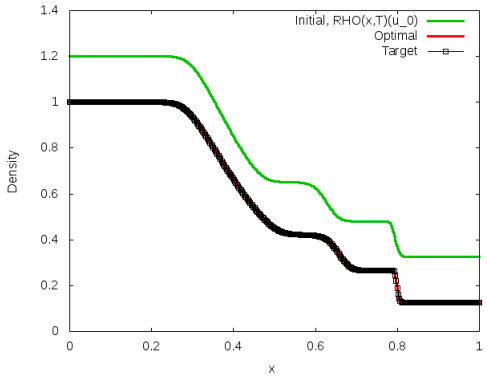

(a) First-order test

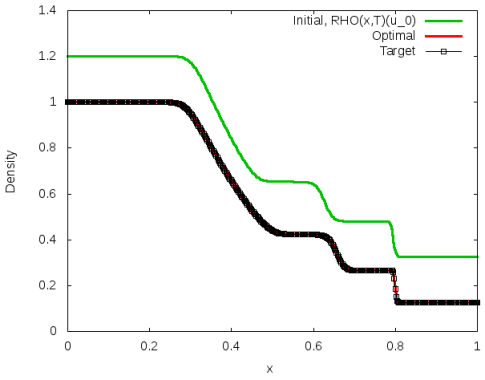

(b) Second-order test

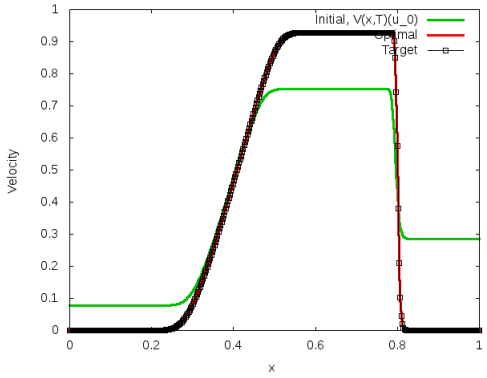

(c) First-order test

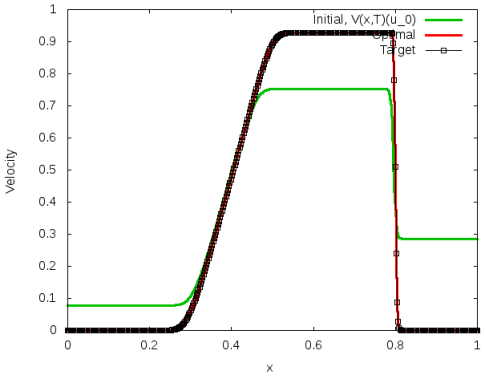

(d) Second-order test

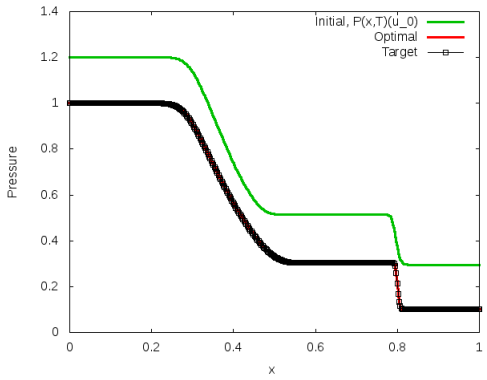

(e) First-order test

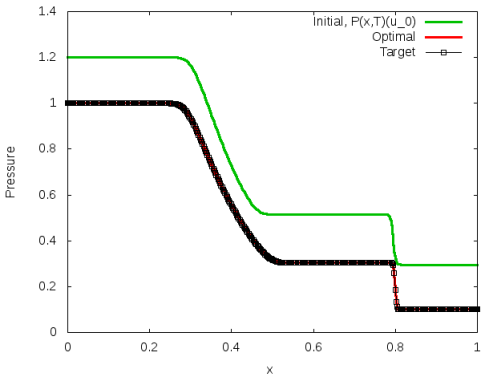

(f) Second-order test

Figure 4.15: First-order (Left) and second-order (Right) 1D Euler Equations optimal control results obtained with discrete kinetic scheme. Optimal solution is depicted by the red solid line and target by black solid line with squares at data points, same parameters as used for Figure 4.14. The x-axis represents the space variable x and the y-axis represents density (top), velocity (middle) and pressure (bottom).

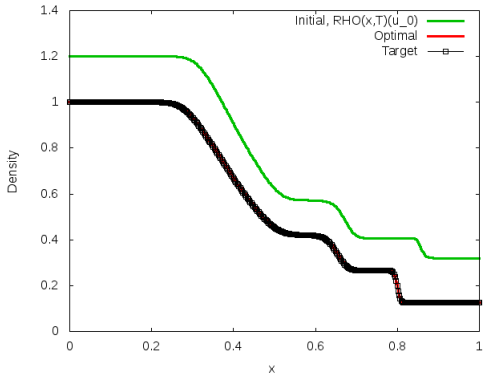

(a) First-order test

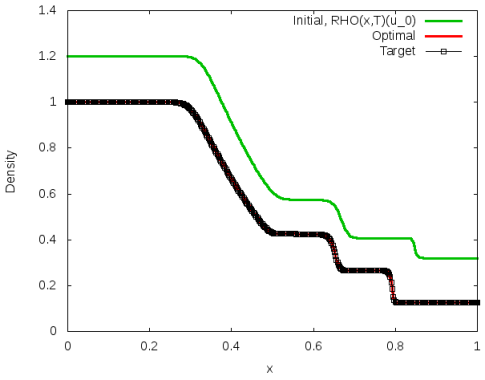

(b) Second-order test

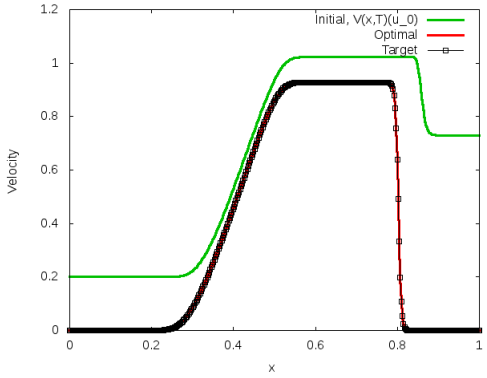

(c) First-order test

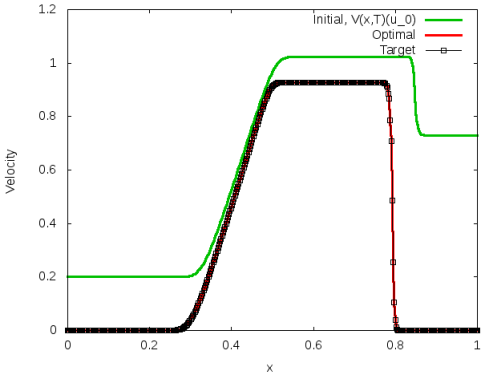

(d) Second-order test

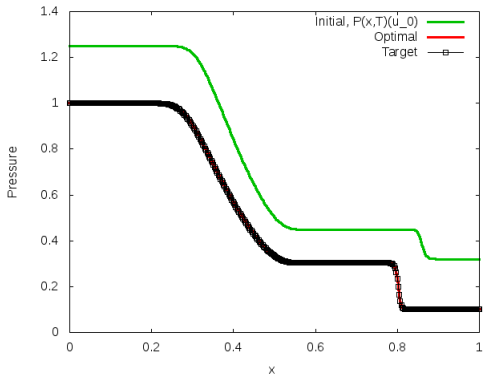

(e) First-order test

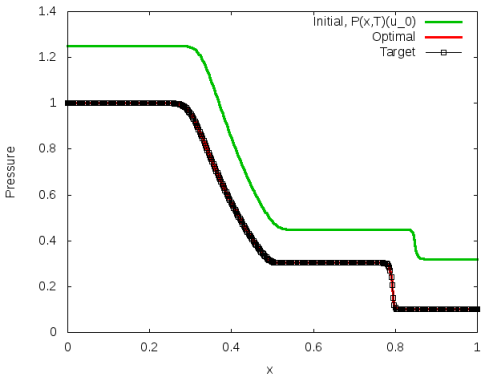

(f) Second-order test

Figure 4.16: First-order (Left) and second-order (Right) 1D Euler Equations optimal control results. Optimal (red solid line) and target (black solid line with squares at data points) solutions, for density, velocity and pressure profiles with JIN XIN scheme at time, $T = 0.17$, $u_L = (1.2,\ 0.2,\ 1.25)$, $u_R = (0.32,\ 0.73,\ 0.32)$, $a_1 = 2.47$, $a_2 = 3.5$, $a_3 = 4.36$, $M = 400$ and $\epsilon = 10^{-8}$. The x-axis represents the space variable x and the y-axis represents density (top), velocity (middle) and pressure (bottom).

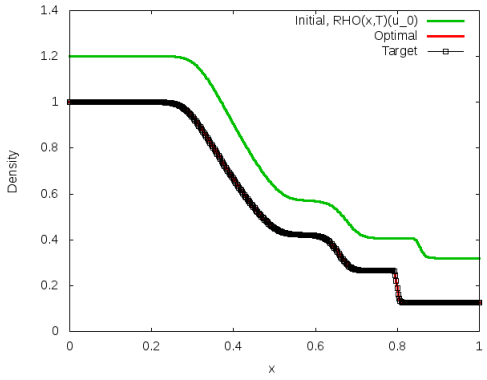

(a) First-order test

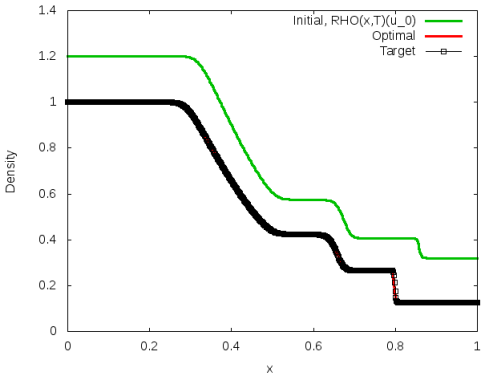

(b) Second-order test

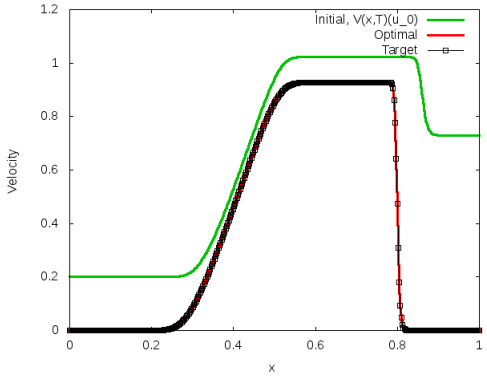

(c) First-order test

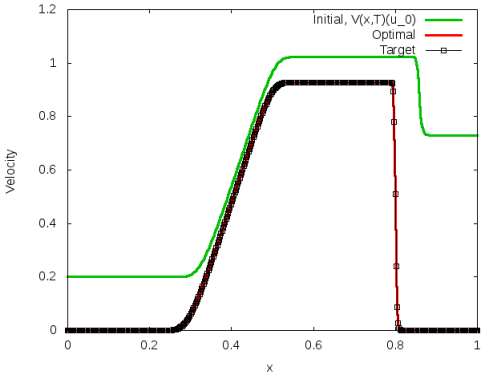

(d) Second-order test

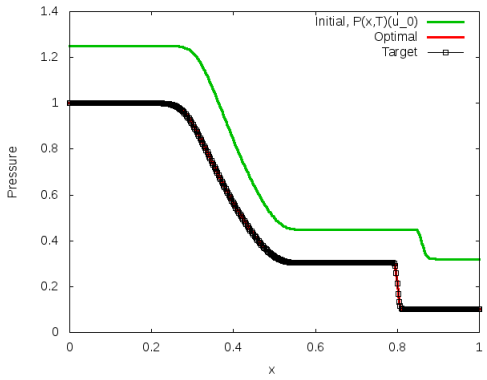

(e) First-order test

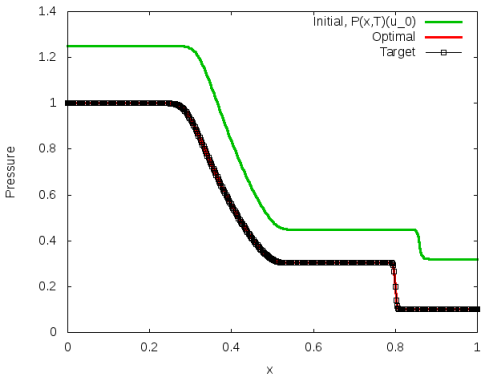

(f) Second-order test

Figure 4.17: First-order (Left) and second-order (Right) 1D Euler Equations optimal control results. Optimal (red solid line) and target (black solid line with squares at data points) solutions, for density, velocity and pressure profiles with discrete kinetic scheme. Same parameters as in Figure 4.16. The x-axis represents the space variable x and the y-axis represents density (top), velocity (middle) and pressure (bottom).

Thirdly, we present results for initial Riemann data $u_L = (1.24,\ 0.1852,\ 1.25)$, $u_R = (0.366,\ 0.629,\ 0.33)$. We chose $a_1 = 1.96,\ a_2 = 2.9,\ a_3 = 4.33$. As for the previous examples, we obtained good match between the optimal and target solutions. Results are visualized in Figures 4.18 and 4.19.

Finally, we considered an example presented in [60]. In this case, initial optimal solutions are solved for values of Sod data initial condition, $u_L = (1.0,\ 0.0,\ 1.0)$, $u_R = (0.125,\ 0.0,\ 0.1)$, and the target is the solution of the initial conditions $u_L = (1.1,\ 0.0,\ 1.1)$, $u_R = (0.2,\ 0.0,\ 0.2)$ for $a_1 = 1.6,\ a_2 = 2.82,\ a_3 = 4,25$. Computations are carried over usual time $T = 0.17$. First and second order results for this example are given in Figure 4.20 for JIN XIN scheme and in Figure 4.21 for discrete kinetic scheme. Good match between optimal and target solutions was observed.

4.7 Functional Convergence

We conclude the analysis of the optimal control results presented above by giving a brief convergence history for the two relaxing schemes. Under this analysis, the representative optimal control example associated with a set of data $u_L = (1.2,\ 0.078,\ 1.2)$, $u_R = (0.325,\ 0.285,\ 0.295)$ whose computations were carried over time $T = 0.17$ is chosen. The two graphs below summarizes the progressive minimization of the cost functional with the number of iterations for both the first-order and second order relaxing schemes. Results show that second-order schemes take few iterations to converge than first-order ones. However, the number of optimization iterations are independent of the grid size.

4.8 Comparison of Computation time

Besides qualitatively and physically comparing optimal control results for the JIN XIN scheme and the discrete kinetic scheme discussed in the previous Sections, we also discuss briefly about the computation time taken for simulation of these results. The time needed for the JIN XIN scheme to converge is larger than that needed for the discrete kinetic scheme. Obviously, time taken for the algorithm to converge for both schemes increase with the number of discretization points, M. The computation time for a representative example is reported in Tables 4.1 and 4.2 for the space discretization with $M = 200,\ 400,\ 800$ grid points against NI, the number of iterations. All computations are performed on a 2.67 GHZ Intel Core dual i5 processor using python 2.5.6.

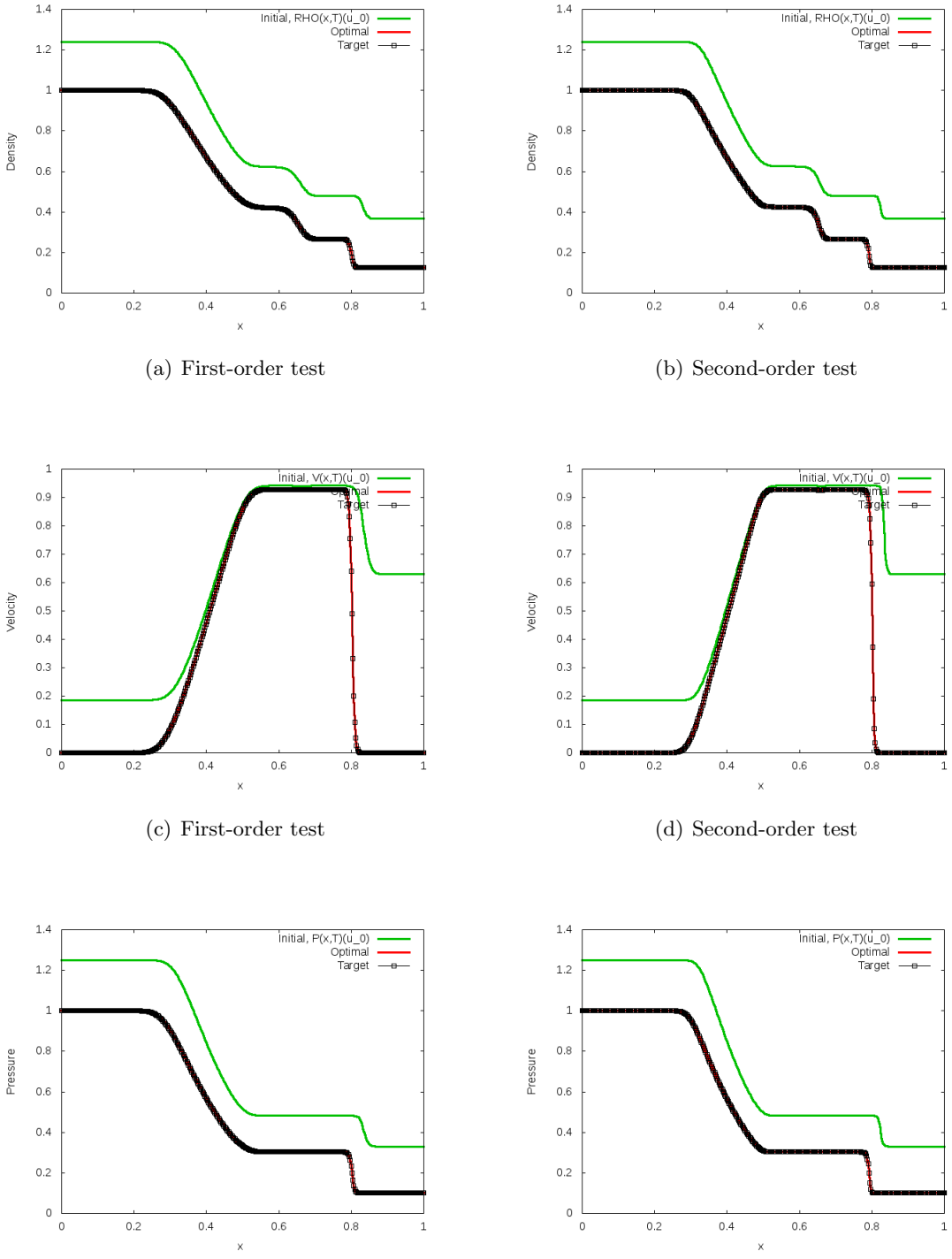

(a) First-order test

(b) Second-order test

(c) First-order test

(d) Second-order test

(e) First-order test

(f) Second-order test

Figure 4.18: First-order (Left) and second-order (Right) 1D Euler Equations optimal control results. Optimal (red solid line) and target (black solid line with squares at data points) solutions, for density, velocity and pressure profiles with JIN XIN scheme at time; $T = 0.17$, $u_L = (1.24,\ 0.1852,\ 1.25)$, $u_R = (0.366,\ 0.629,\ 0.33)$, $a_1 = 1.96,\ a_2 = 2.9,\ a_3 = 4.33$, $M = 400$ and $\epsilon = 10^{-8}$. The x-axis represents the space variable x and the y-axis represents density (top), velocity (middle) and pressure (bottom).

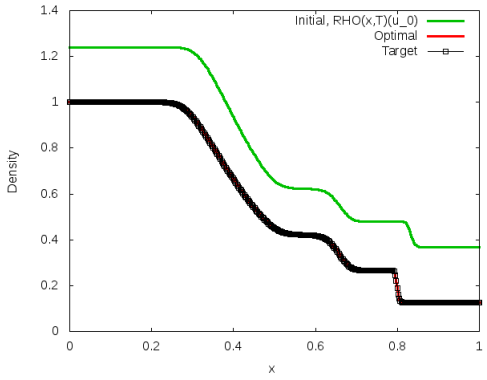

(a) First-order test

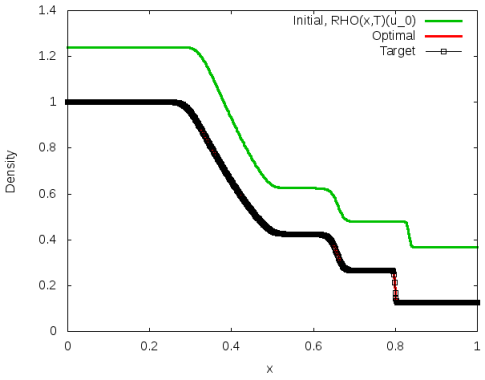

(b) Second-order test

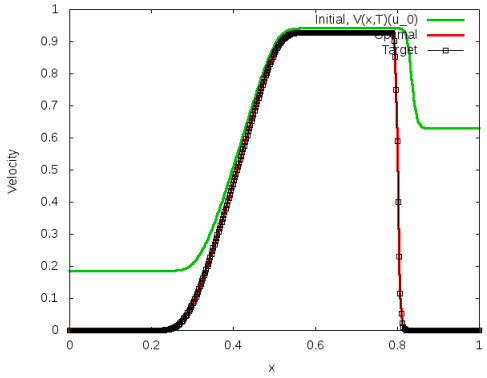

(c) First-order test

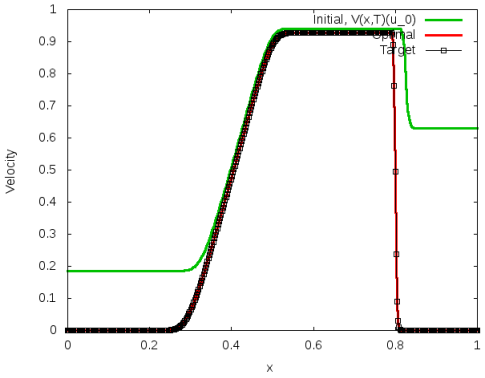

(d) Second-order test

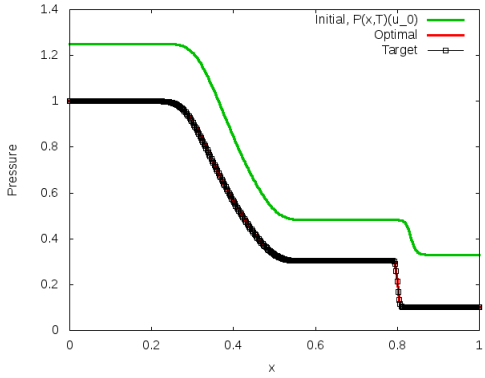

(e) First-order test

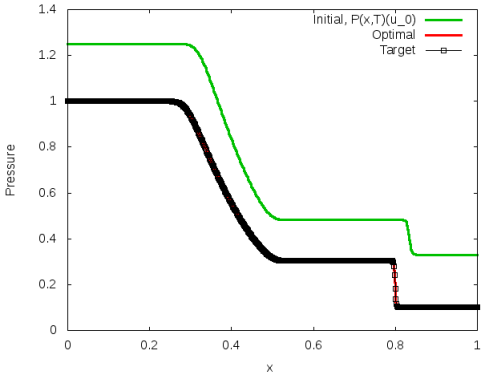

(f) Second-order test

Figure 4.19: First-order (Left) and second-order (Right) 1D Euler Equations optimal control results. Optimal (red solid line) and target (black solid line with squares at data points) solutions, for density, velocity and pressure profiles obtained with the discrete kinetic scheme. Same parameters as in Figure 4.18. The x-axis represents the space variable x and the y-axis represents density (top), velocity (middle) and pressure (bottom).

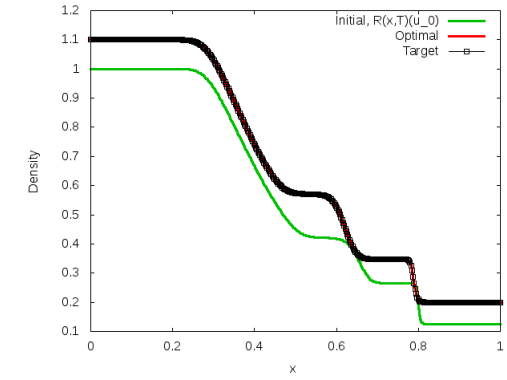

(a) First-order test

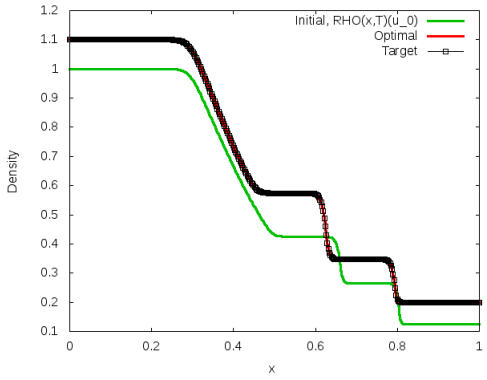

(b) Second-order test

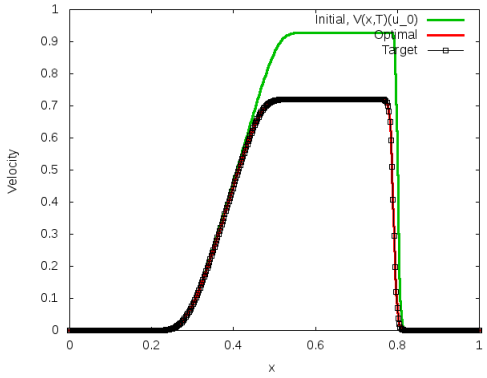

(c) First-order test

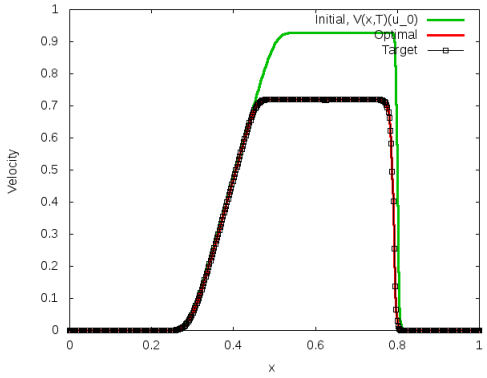

(d) Second-order test

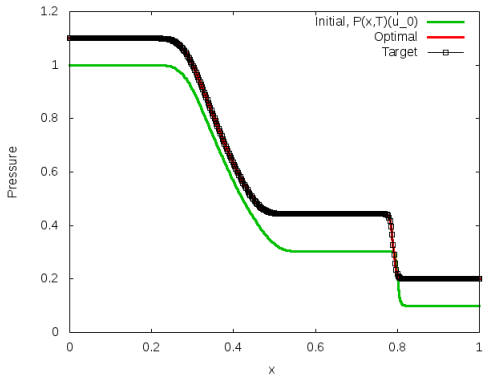

(e) First-order test

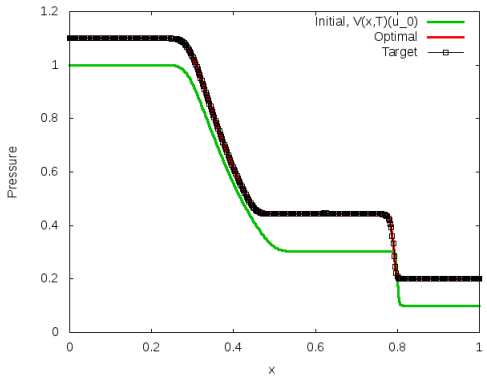

(f) Second-order test

Figure 4.20: First-order (Left) and second-order (Right) 1D Euler Equations optimal control results. Optimal (red solid line) and target (black solid line with squares at data points) solutions, for density, velocity and pressure profiles with JIN XIN scheme at time, $T = 0.17$, $u_L = (1.0,\ 0.0,\ 1.0)$, $u_R = (0.1,\ 0.0,\ 0.125)$ for optimal; and $u_L = (1.1,\ 0.0,\ 1.1)$, $u_R = (0.2,\ 0.0,\ 0.2)$ for target. $a_1 = 1.96,\ a_2 = 2.9,\ a_3 = 4.33$, $M = 400$ and $\epsilon = 10^{-8}$. The x-axis represents the space variable x and the y-axis represents density (top), velocity (middle) and pressure (bottom).

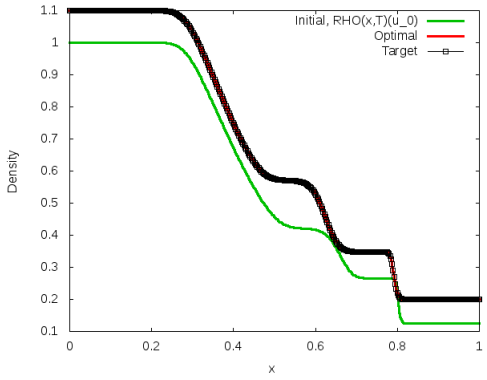

(a) First-order test

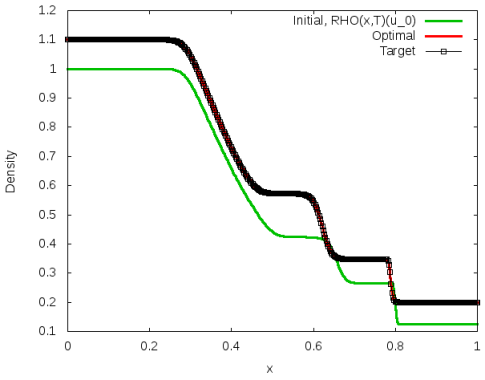

(b) Second-order test

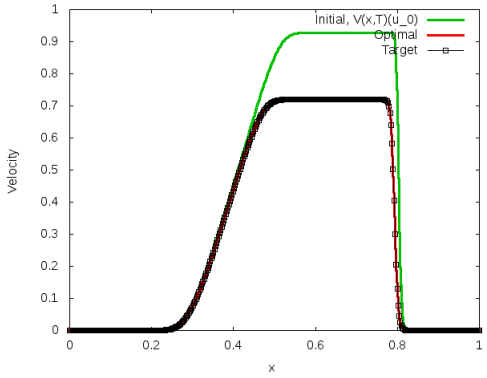

(c) First-order test

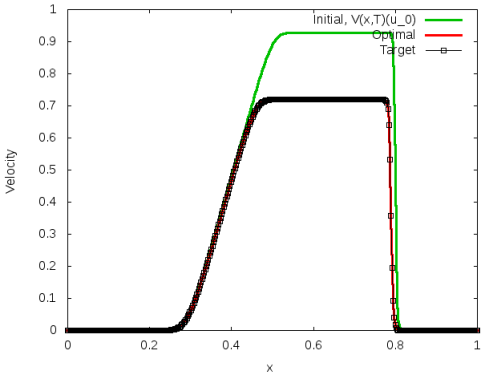

(d) Second-order test

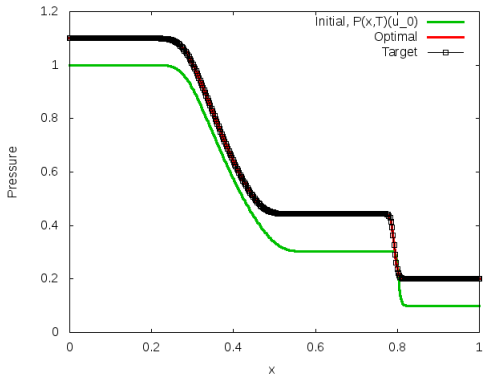

(e) First-order test

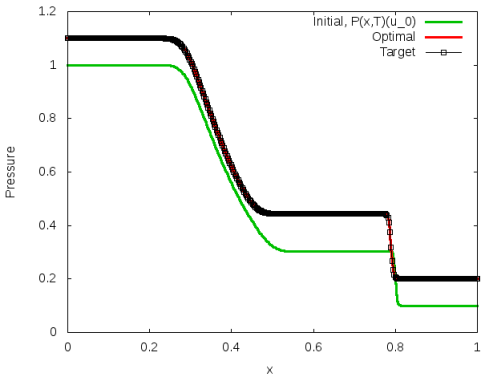

(f) Second-order test

Figure 4.21: First-order (Left) and second-order (Right) 1D Euler Equations optimal control results. Optimal (red solid line) and target (black solid line with squares at data points) solutions, for density, velocity and pressure profiles with discrete kinetic scheme at time, $T = 0.17$. Same parameters as in Figure 4.20. The x-axis represents the space variable x and the y-axis represents density (top), velocity (middle) and pressure (bottom).

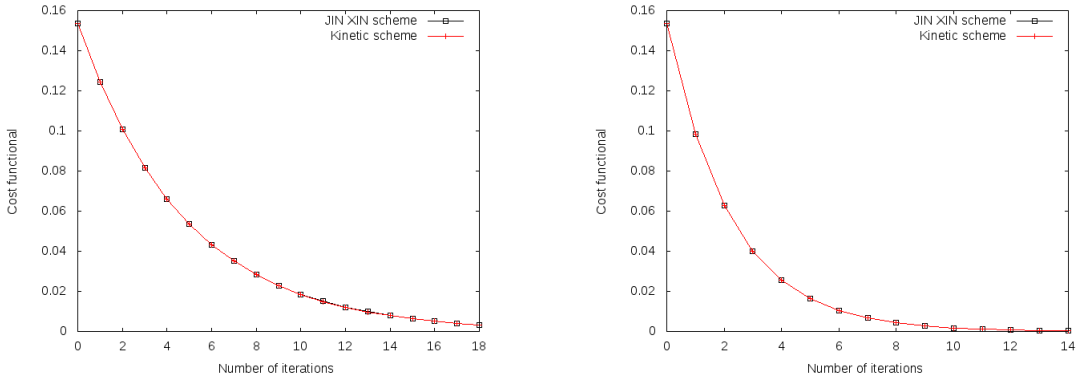

(a) Covergence history for first-order schemes (b) Convergence history for second-order schemes

Figure 4.22: Convergence history for the solution of the optimization problem computed with the first order (left) and second-order (right) relaxing schemes for both JIN XIN and discrete kinetic schemes. The x-axis represents the number of iterations and the y-axis represents the cost functional value.

Table 4.1: Computational time for first-order JIN XIN and discrete kinetic schemes

M	NI	JIN XIN	Discrete kinetic
200	22	$1.8245\times\ 10^{+2}$	$1.26 \times 10^{+2}$
400	22	$9.07168 \times 10^{+2}$	$4.9572 \times 10^{+2}$
800	22	$1.9837 \times 10^{+3}$	$1.2961 \times 10^{+3}$

Table 4.2: Computational time for second-order JIN XIN and discrete kinetic schemes

M	NI	JIN XIN	Discrete kinetic
200	15	$4.3234 \times 10^{+2}$	$2.97 \times 10^{+2}$
400	15	$1.7576 \times 10^{+3}$	$1.1453 \times 10^{+3}$
800	15	$3.2761 \times 10^{+3}$	$2.370 \times 10^{+3}$

5. Conclusions

This research has been a tour on a mixed survey of well-known results and the present contributions. A great deal of theoretical perspectives from previous works has been substantiated by the numerical results obtained, second-order adjoint-based optimization in this context. However, a review and development of effective numerical schemes has been central to our optimization approach.

Research has been focused on the adjoint approach to optimize problem constrained by nonlinear systems of HCLs. We started by deriving the optimality systems for the two relaxation approach discussed, we then developed their corresponding relaxing schemes: first and second order in time and space. These schemes were then tested for both the solutions and the adjoint-based optimal control of the scalar and systems of HCLs. Contrary to the existing numerical results in [10, 94, 128], we have managed to utilize the theoretical second-order adjoint scheme derived in [10], and obtained up to second-order optimal control numerical results. Although for the second-order optimal control, the descent is computed via a first-order gradient method, we are convinced that this is a reasonable estimate since all the coupling information that involve in calculation of gradient come from the second-order schemes. However, we reviewed the first-order optimal control numerical results discussed in [10, 94, 128], and through generalization we were able to develop new adjoint relaxing schemes, first-order and second-order in time and space for the discrete kinetic model. The coupling information obtained by solving flow and adjoint systems during optimization cycle, enabled us to complete the optimization process, the first and second order numerical results obtained are promising and comparable.

Talking from efficient point of view, computer runtimes for both schemes, of the flow equations and that of the adjoint equations are almost equal. But the discrete kinetic scheme takes shorter computer runtime compared to the she JIN XIN scheme. Results convince that storage requirements are solely equal since each scheme fundamentally handles and processes almost the same amount of data during computations. We can roughly draw that, a single optimization cycle is equivalent to solving two to three times the flow equation. If there are extra constraints added to the optimization algorithm in order to satisfy certain conditions, this may no longer be the case.

Care have been taken in solving the adjoint systems as discontinuities soon develop when solving backward in time. This realm is due to the fact that solutions for HCLs are not easily reversible and highly unstable even for scalar conservation laws. Characteristics interact immediately loosing the correct track of information propagation. We realized that, there must be a means to check that stability condition is satisfied at every optimization cycle. Therefore, information that pertains to insuring stability condition is subject to change at every step. Comparing the two schemes for flow and adjoint equations in term of stability, adjoint scheme is more prone

and suffers severely than the scheme for the flow equations.

This study has been motivated by the fact that, both the HCLs and the adjoint-based optimization considered have a lot of applications in the real life. For example, transport equation in modeling chemical processes and pollutants in a river, Burgers' Equation could be applied in modeling traffic flows. For systems of HCLs, we have considered the Euler Equations of gas dynamics, typically applied in modeling gas in pipelines and in aircraft configurations. It is our expectations that, this study could have contributions in these areas of applications and also brings challenges to researchers and scientists for further investigations.

It was never expected that, this study could explain all, and it has not done so far. We hope this study will be judged, not primarily by the degree to which it explains, but by the extent to which it lays down the foundation for further work. Options for further research in the context of this work are diverse. One may decide to extend this research to incorporate much higher-order schemes during optimization process. It is also possible to extend this work to deal with multi-dimensional problems, especially when bearing in mind that the approach is featured by a number of valuable characteristics which make it easily extendable. However, adjoint approach to optimization, as we have discussed, can be inter-twined with other numerical schemes for optimization purpose apart from relaxing. More importantly, is to consider high than first-order optimality conditions for adjoint-based optimization. Finally, our future work may involve one or more of the possible extensions we have mentioned, most likely, we intend to apply similar ideas to consider high order optimality conditions.

Bibliography

[1] D. A. ANDERSON, J. C. TANNEHILL, and R. H. PLETCHER. *Computational Fluid Mechanics and Heat Transfer*. McGraw-Hill, 1984.

[2] W. K. ANDERSON and D. L. BONHAUS. Airfoil design on unstructured grids for turbulent flows. *AIAA J.*, 37(2):185–191, 1999.

[3] W. K. ANDERSON and V. VENKATAKRISHNAN. Aerodynamic design optimization on unstructured grids with a continuous adjoint formulation. *AIAA Paper 97-0643*, 1997.

[4] R. ANSORGE. Towards numerical procedures for those technical phenomena whose mathematical models leads to non-standard conservation laws: A survey. *Mathematics and Computers in Simulation, ELSEVIER*, 61:449–463, 2003.

[5] D. AREGBA-DRIOLLET and V. MILISIC. Kinetic approximation of a boundary value problem for conservation laws. *J. Num. Math.*, 97:595–633, 2004.

[6] D. AREGBA-DRIOLLET and R. NATALINI. Convergence of relaxation schemes for conservation laws. *Applicable Analysis*, (61):163–193, 1996.

[7] D. AREGBA-DRIOLLET and R. NATALINI. Discrete kinetic schemes for multidimensional conservation laws. *SIAM J. Numer. Anal.*, 37(6):1973–2004, 2000.

[8] L. ARMIJO. Minimization of functions having Lipschitz continuous first partial derivatives. *Pacific J. Math*, 16(1):1–3, 1966.

[9] M. K. BANDA and M. HERTY. Multiscale modeling of gas flow in pipe networks. *Mathematical Methods in the Applied Sciences*, 31(8):915–936, 2008.

[10] M. K. BANDA and M. HERTY. Adjoint IMEX-based schemes for control problems governed by hyperbolic conservation laws. *Comput Optim Appl. DOI: 10.1007/s10589-010-9362-2*, pages 1–22, October 2010.

[11] M. K. BANDA, M. HERTY, and A. KLAR. Coupling conditions for gas network governed by the isothermal Euler Equations. *Networks and Heterogeneous media*, 1(2):295–314, June 2006.

[12] M. K. BANDA, M. HERTY, and A. KLAR. Gas flow in pipeline networks. *Networks and Heterogeneous media*, 1(1):41–56, March 2006.

[13] M. K. BANDA and M. SEAÏD. Higher-order relaxation schemes for hyperbolic systems of conservation laws. *J. Numer. Math.*, 13(3):171–196, May 2005.

[14] P. BHATNAGAR, E. GROSS, and M. KROOK. A model for collision processes in gases. I. small amplitude processes in charged and neutral one-component systems. *Phys. Rev.*, 94:511–525, 1954.

[15] S. BIANCHINI. On the shift differentiability of the flow generated by a hyperbolic system of conservation laws. *Discrete Contin. Dynam. Systems*, 6(2):329–350, 2000.

[16] J. P. BORIS and D. L. BOOK. Flux corrected transport I, SHASTA, a fluid transport algorithm that works. *J. Comp. Phys.*, 11:38–69, 1973.

[17] F. BOUCHUT and T. MORALES de LUNA. Semi-discerete entropy satisfying approximate Riemann solvers. The case of the Suliciu relaxation approximation. 2009,

[18] F. BOUCHUT and F. JAMES. Differentiability with respect to initial data for a scalar conservation law, International Series. Numer. Math. *Birkhäuser*, 129:113–118, 1999.

[19] A. BRESSAN and G. GUERRA. Shift-differentiability of the flow generated by a conservation law. volume 3, pages 35–58. Discrete Contin. Dynam. Systems, (1997).

[20] A. BRESSAN and M. LEWICKA. Shift differentials of maps in BV spaces, in Nonlinear Theory of Generalized Functions, Vienna, 1997. Chapman and Hall/CRC Res. Notes Math. *Chapman and Hall/CRC, Boca Raton, FL*, vol. 401:47–61, 1999.

[21] A. BRESSAN and A. MARSON. A maximum principle for optimally controlled systems of conservation laws. *Rend. Sem. Univ. Podova*, 94:79–94, 1995.

[22] A. BRESSAN and A. MARSON. A variational calculus for discontinuous solutions to conservation laws. *Commun. Partial Differ. Equ.*, 20:1491–1552, 1995.

[23] A. BRESSAN and W. SHEN. Optimality conditions for solutions to hyperbolic balance laws. Control methods in PDE-dynamical systems. *Contemp. Math.*, 426:129–152, 2007.

[24] H. CABUK, C.H SHUNG, and V. MODI. *Adjoint operator approach to shape design for internal incompressible flow.* In Pennyslvania State Univ., 3rd International Conference on Inverse Design Concepts and Optimization in Engineering Sciences. 1991.

[25] M. CARPENTER and C. KENNEDY. Fourth-order 2N-storage Runge-Kutta schemes, NASA TM 109112. *NASA Langley Research Center*, (MR 90k:65160), June 1994.

[26] J. CARRILLO, I. M. GAMBA, A. MAJORANA, and C.-W. SHU. A WENO-solver for the transients of Boltzmann-Poisson systems for semiconductor devices: performance and comparisons with Monte Carlo methods. *J. Comput. Phys.*, 184:498–525, 2003.

[27] G. Q. CHEN, D. LEVERMORE, and T. P. LIU. Hyperbolic conservation laws with stiff relaxation terms and entropy. *Comm. Pure Appl. Math.*, 47(1994):787–830.

[28] J. CHEN and Z. SHI. Application of a fourth-order relaxation scheme to hyperbolic systems of conservation laws. *Applicable Analysis*, (61):163–193, December (2005).

[29] V. CHERUVU, R.D. NAIR, and H. M. TUFO. A spectral finite volume transport scheme on the cubed sphere. *Appl. Numer. Math.*, 57:1021–1032, 2007.

[30] B. COCKBURN, F. LI, and C.-W. SHU. Locally divergence-free discontinuous Galerkin methods for the Maxwell Equations. *J. Comput. Phys.*, 194:588–610, 2004.

[31] B. COCKBURN and C.-W. SHU. TVB Runge-Kutta local projection discontinuous Galerkin finite element method for conservation laws II: General framework. *Math. Comp.*, 52(186):411–435, 1989.

[32] P. COLELLA. Glimm's method for gas dynamics. *SIAM J. Sci. Stat. Comput.*, (3):76–110, 1982.

[33] C. M. DAFERMOS. *Hyeperbolic Conservation Laws in Continuum Physics*, volume 325. Springer, 2010.

[34] I. DANAILA, P. JOLY, S. M. KABER, and M. POSTEL. *An Introduction to Scientific Computing. Twelve Computational Projects Solved with MATLAB.* Springer, 2006.

[35] R. DONAT and A. MARQUINA. Capturing shock reflections: an improved flux formula. *J. Comp. Phys.*, 125:42–58, 1996.

[36] B. EINFELDT. On Godunov-type methods for gas dynamics. *SIAM J. Num. Anal.*, 25:294–318, 1988.

[37] J. ELLIOTT. Aerodynamic optimization based on the Euler and Navier-Stokes equations using unstructured grids. *PhD Thesis, MIT, Department of Aeronautics and Astronomy*, 1998.

[38] J. ELLIOTT and J. PERAIRE. Practical 3D aerodynamic design and optimization using unstructured meshes. *AIAA J.*, 35(9):1479–1485, 1997.

[39] B. ENGQUIST and S. OSHER. One sided difference schemes and transonic flow. *Proc. Nat. Acad. Sci. U.S.A.*, 77:3071–3074, 1980.

[40] B. ENGQUIST and S. OSHER. Stable and entropy satisfying approximations for transonic flow calculations. *Math. Comp.*, 34:45–75, 1980.

[41] B. ENGQUIST and S. OSHER. One sided difference approximations for nonlinear conservation laws. *Math. Comp.*, 36:321–352, 1981.

[42] L. C. EVANS. *Partial Diffferential Equations*. Volume 19. American Mathematical Society, 1997.

[43] L.-L. FENG, C.-W. SHU, and M. ZHANG. A hybrid cosmological hydrodynamic/n-body code based on a weighted essentially nonoscillatory. 612:1–13, 2004.

[44] M. B. GILES and N. A. PIERCE. An introduction to the Adjoint Approach to design. *Flow, Turbul. Combust.*, 65(3-4):393–415, 2000.

[45] M. B. GILES and N. A. PIERCE. An Introduction to the Adjoint Approach to design. *Flow, Turbul. Combust.*, 65(3-4):393–415, 2000.

[46] E. GODLEWSKI and P.-A. RAVIART. *Numerical Approximation of Hyperbolic Systems of Conservation Laws*. Springer-Verlag, New York, 1996.

[47] S. K. GODUNOV. A finite-difference method for the numerical computation of discontinuous solutions of the equations of fluid dynamics. *Mat. Sb.*, (47):271–290, 1959.

[48] S. GOTILLIEB and C.-W. SHU. Total Variation Diminishing Runge-Kutta Schemes. *Mathematics of Computation*, 67(221):73–86, 1996.

[49] S. GOTTLIEB, D. I. KETCHESON, and C.-W. SHU. High-order Strong Stability Preserving Time Discretizations. *Journal of Scientific Computing*, 38(3), March 2009.

[50] S. GOTTLIEB, C.-W. SHU, and E. TADMOR. Strong stability-preserving high-order time discretization methods. *SIAM Rev.*, (43):89–112, 2001.

[51] M. D. GUNZBURGER. *Perspectives in Flow Control and Optimization, Advances in design and control*. SIAM, PA. USA, 2003.

[52] W. W HAGER. Runge-Kutta methods in optimal control and the transformed adjoint system. *Numerische Mathematik*, (87):247–282, 2000.

[53] A. HARTEN. In proceedings, International Conference on Hyperbolic Problems, Saint-Etienne.

[54] A. HARTEN. High resolution schemes for hyperbolic conservation laws. *J. Comput. Phys.*, 49:357–393, 1983.

[55] A. HARTEN, B. ENGQUIST, S. OSHER, and S. CHAKRAVARTHY. Uniformly high-order accurate essentially nonoscillatory schemes, III. *J. Comput. Phys.*, 71:231–303, August 1987.

[56] A. HARTEN and P. D. LAX. On a Class of High Resolution Total-Variation-Stable Finite-Difference Schemes. *SIAM J. Numer. Anal.*, 21(1):1–23, 1984.

[57] A. HARTEN, P. D. LAX, and B. VAN LEER. On upstream differencing and Gudunov-type schemes for hyperbolic conservation laws. *SIAM Review*, 25:35–61, 1983.

[58] A. HARTEN and S. OSHER. Unifromly high-order accurate nonoscillatory schemes, I. *SIAM J. Numer. Anal.*, 24:279–309, 1987.

[59] C. HIRSCH. *Numerical Computation of Internal and External Flows.* John Wiley and Sons, 1988.

[60] C. HOMESCU and I. M. NAVON. Optimal control of flow with discontinuities. *J. Comp. Phys.*, 187:660–682, 2003.

[61] J. M. HYMAN. On robust and accurate methods for the calculation of compressible fluid flows I. *to appear.*

[62] Z. JACKIEWICZA, R. RENAUT, and A. FELDSTEIN. Two-step Runge-Kutta methods. *SIAM J. Numer. Anal.*, 28:1165–1182, 1991.

[63] S. JIN. Runge-Kutta Methods for Hyperbolic Conservation Laws with Stiff Relaxation Terms. 122(1):51–67, 1995.

[64] S. JIN and Z. XIN. The relaxation schemes for systems of conservation laws in arbitrary space dimensions. *Comm. Pure Appl. Math*, (48):235–276, 1995.

[65] D. KRONER. *Numerical Schemes for Conservation Laws.* Wiley-Teubner series, 1997.

[66] E. J. KUBATKO, J. J. WESTERINK, and C. DAWSON. Semi discrete discontinuous Galerkin methods and stage-exceeding-order, strong-stability-preserving Runge-Kutta time discretizations. *J. Comput. Phys.*, 222:832–848, 2007.

[67] P. D. LAX. *Selected Papers.* Volume I. Springer-Verlag, Arizona, 1968.

[68] P. D. LAX. *Shock waves and entropy, in: E. M. Zarantello (Ed.), Contribututions to Non-linear Functional Analysis.* Academic Press, New York, 1971.

[69] P. D. LAX. *Hyperbolic Systems of Conservation Laws and the Mathematical Theory of Shock Waves, vol. II of Regional Conference Series in Applied Mathematics.* SIAM, 1973.

[70] P. D. LAX. *Hyperbolic Partial Differential Equations: Courant Lecture Notes in Mathemnatics.* AMS, New York, 2006.

[71] B. VAN LEER. Towards the ultimate conservative difference scheme I. the quest of monotonicty. 18:163–168, 1973.

[72] B. VAN LEER. Towards the ultimate conservative difference scheme IV. A new approach to numerical convection. 23:276–299, 1977.

[73] B. VAN LEER. Towards the ultimate conservative difference scheme V. A second-order sequel to Godunov's method. 32:101–136, 1979.

[74] B. VAN LEER. *Flux-vector splitting for the Euler equations. In E. Krause*, volume 170. Lecture Notes in Physics, Springer-Verlag, 1982.

[75] R. J. LEVEQUE. *Numerical Methods for Conservation Laws.* Birkhäuser-Verlag, 1990.

[76] R. J. LEVEQUE. *Numerical Methods for Conservation Laws.* 2nd Edition. Birkhäuser Verlag, Berlin, 1992.

[77] R. J. LEVEQUE. *Finite Volume Methods for Hyperbolic Problems. Cambridge Texts in Applied Mathematics.* Cambridge University Press, 2002.

[78] R. J. LEVEQUE, D. MIHALAS, E.A. DORFI, and E. MULLER. *Computational Methods for Astrophysical Fluid Flow: Swiss Society for Astrophysics and Astronomy, 27th Saas-Fee Advanced Course Lecture Notes.* Springer-Verlag, Berlin Heidelberg New York, 1997.

[79] M. J. LIGHTHILL and G. B. WHITHAM. A theory of traffic flow on long crowded roads. *Proc. R. Soc., London A*, 229:317–345, 1955.

[80] M.-S. LIOU. A sequel to ausm: Ausm+. to appear. *J. Comp. Phys.*

[81] M.-S LIOU. and C. J. STEFFEN Jr. A new flux splitting scheme. *J. Comp. Phys.*, 107:107, 1993.

[82] T. P. LIU. Hyperbolic conservation laws with relaxation. *Comm. Math. Phys.*, 108:153–175, 1987.

[83] X. LIU, S. OSHER, and T. CHAN. Weighted essentially non-oscillatory schemes. *J. Comput. Phys.*, 115:200–212, 1994.

[84] Z. LIU and A. SANDU. On the properties of discrete adjoints of numerical methods for the advection equation. *Int. J. for Num. Meth. in Fluids*, (56):769–803, 2008.

[85] R. MAcCORMACK. Proceedings of the Second International Conference on Numerical Methods in Fluid dynamics, Lecture Notes in Physics, (M. Holt, Ed.). 8, 1971.

[86] A. MARQUINA. Local piecewise hyperbolic reconstruction of numerical fluxes for non-linear scalar conservation laws. *SIAM J. Sci. Comput.*, 15:892, 1994.

[87] T. MATSUZAWA and M. HAFEZ. Optimum shape design using adjoint equations for compressible flows with shock waves. *International Journal for Computational Fluid Dynamics*, 7(3):343–365, 1998.

[88] V. MILISIC. Stability and convergence of discrete kinetic approximations to an initial-boundary value problem for conservation laws. *Proceeding of the Amer. Math. Soc., to appear*, 97:595–633, 2004.

[89] S. K. NADARAJAH and A. JAMESON. A Comparison of the Continuous and Discrete Adjoint Approach to Automatic Aerodynamic Optimization. *AIAA Paper 2000-0667*, 2000.

[90] M. NAKASHIMA. Embedded pseudo-Runge-Kutta methods. *SIAM J. Numer. Anal.*, 28:1790–1802, 1991.

[91] R. NATALINI. Convergence to equilibrium for the relaxation approximations of conseravtion laws. *Comm. Pure Appl. Math.*, (49):795–823, 1996.

[92] R. NATALINI. A discrete kinetic approximation of entropy solutions to multidimensional scalar conservation laws. *J. Differential Equations*, 148(2):292 – 317, 1998.

[93] R. NATALINI and A. TERRACINA. Convergence of a relaxation approximation to a boundary value problem for conseravtion laws. *Comm. Partial Differential Equations*, (26):1235–1252, 2001.

[94] J.-M. T. NGNOTCHOUYE, M. HERTY, and M. K. BANDA S. VEELKEN. Relaxation Approaches to the Optimal Control of the euler Equations. *Computational and Applied Mathematics (Accepted).*

[95] N. T. NGUYEN. Continuous Adjoint-Based Optimization of Hyperbolic Equations with Nonlinear Differential Equation Constraints on Periodic Boundary Conditions, Preprint.

[96] J. NOCEDAL and S. J. WRIGHT. *Numerical optimization.* Springer-Verlag, New York, NY, 1999.

[97] O. OLEINIK. On the uniqueness of the generalised solution of the Cauchy problem for a non-linear systems of equations occurring in mechanics (Russ.). *Usp. Mat. Nauk. (N.S.)*, 12:169–176, 1957.

[98] S. OSHER and S. CHAKRAVARTHY. High Resolution Schemes and the Entropy Condition. *SIAM J. Numer. Anal.*, 21(5):955–984, October 1984.

[99] S. OSHER and S. CHAKRAVARTHY. Very High Order Accurate TVD Schemes. *IMA Vol. Math. Appl.*, 2:229, 1986.

[100] S. OSHER and F. SOLOMON. Upwind difference schemes for hyperbolic systems of conservation laws. *Math. Comput.*, 38:339–374, 1982.

[101] L. PARESCHI, G. PUPPO, and G. RUSSO. Central Runge-Kutta schemes for hyperbolic conservation laws. *SIAM J. Sci. Comp.*, 26:979–999, 2005.

[102] L. PARESCHI and G. RUSSO. Implicit-Explicit Runge-Kutta schemes for stiff systems of differential equations. *Recent Trends in Numerical Analysis (Eds. Brugano, Trigiante)*, 3:269–284, 2000.

[103] L. PARESCHI and G. RUSSO. Asymptotically SSP schemes for hyperbolic systems with stiff relaxation. *Hyperbolic problems: Theory, Numerics, Applications: Proceedings of the Ninth International Conference on Hyperbolic Problems Held in CaItech, Pasadena*, pages 241–255, 2003.

[104] L. PARESCHI and G. RUSSO. Implici-Explicit Runge-Kutta schemes and applications to hyperbolic systems with relaxation. *J. Sci. Comput.*, 25(1-2):129–155, 2005.

[105] S. PATEL and D. DRIKAKIS. Effects of preconditioning on the accuracy and efficient of incompressible flows. *International Journal for Numerical Methods in Fluids*, 47:963–970, 2005.

[106] R. PEYRET. *Handbook of Computational Fluid Mechanics.* Academic Press, Nice, 1995.

[107] R. PEYRET and T. D. TAYLOR. *Computational Methods for Fluid Flow.* Springer, 1983.

[108] R. RICHTMYER. A Survey of Difference Methods for Non-Steady Fluid Dynamics, NCAR Technical Note 63-2, National Center for Atmospheric Research. 1962.

[109] R. RICHTMYER and K. MORTON. *Difference Methods for Initial-Value Problems.* 2nd ed. Interscience, New York, 1967.

[110] P. L. ROE. Approximate Riemann solvers, parameter vectors, and difference schemes. *J. Comput. Phys.*, 43:357–372, 1981.

[111] V. V. RUSANOV. *J. Comp. Math. Math. Phys. USSR*, (2), 1962.

[112] S. J. RUUTH and R. J. SPITERI. Two barriers on strong-stability-preserving time discretization methods. *Journal of Scientific Computation*, 17:211–220, 2002.

[113] S. J. RUUTH and R. J. SPITERI. Higher-order strong-stability-preserving Runge-Kutta methods with downwind-biased spatial discretizations. *SIAM J. Numer. Anal.*, 42:974–996, 2004.

[114] G. B. WHITHAM F. R. S. *LINEAR AND NONLINEAR WAVES*. JOHN WILEY and SONS, 1974.

[115] R. H. SANDERS and K. H. PRENDERGAST. The possible relation of the 3-kiloparsec arm to explosions in the galactic nucleus. *Astrophys. J.*, 188:489, 1974.

[116] H. J. SCHROLL. Relaxed High Resolution Schemes for Hyperbolic Conservation Laws. *Journal of Scientific Computing*, 21(2):1–11, October 2004.

[117] C. SHU. Total-variation diminishing time discretizations. *SIAM J. Sci. and Stat. Comput.*, 9:1073–1084, 1988.

[118] C.-W SHU. TVB uniform high-order schemes for conservation laws. *Math. Comp.*, 49:105–121, 1987.

[119] C.-W. SHU and S. OSHER. Efficient implementation of essentially non-oscillatory shock-capturing schemes. *J. Comput. Phys.*, 77:439–471, 1988.

[120] G. SOD. *Numerical Methods for Fluid Dynamics*. Cambridge University Press, 1985.

[121] G. A. SOD. A Survey of Several Finite Difference Methods for Systems of Nonlinear Hyperbolic Conservation Laws. *Journal of Computational Physics*, (27):1–31, 1978.

[122] J. L. STEGER and R. F. WARMING. Flux vector splitting of the inviscid gas dynamic equations with applications to finite-difference methods. *J. Comp. Phys.*, 40:263, 1981.

[123] Y. SUN, Z. J. WANG, and Y. LIU. Spectral (finite) volume method for conservation laws on unstructured grids VI: Extension to viscous flow. *J. Comput. Phys.*, 215:41–58, 2006.

[124] P. K. SWEBY. High resolution schemes using flux limiters for hyperbolic conservation laws. *SIAM J. Num. Anal.*, 21:995–1011, 1984.

[125] E. F. TORO. *Riemann Solvers and Numerical Methods for Fluid Dynamics, A Practical Introduction*. 3rd Edition. Springer-Verlag, Berlin, Heidelberg, 2009.

[126] J. A. TRANGENSTEIN. *NUMERICAL SOLUTION OF HYPERBOLIC PARTIAL DIFFERENTIAL EQUATIONS*. Cambridge University Press, 2007.

[127] S. ULBRICH. A sensitivity and adjoint calculus for discontinuous solutions of hyperbolic conservation laws with source terms. *SIAM J. Control Optim.*, 41(3):740, 2002.

[128] S. VEELKEN, M. HERTY, J.-M. T. NGNOTCHOUYE, and M. K. BANDA. Optimal Control of the Euler Equations via Relaxation Approaches. *PAMM*, 10(1):595–596, November 2010.

[129] W. C. WANG and Z. XIN. Asymptotic limit of initial boundary-value problems for conservation laws with relaxational extensions. *Comm. Pure Appl. Math.*, 51:505–535, May 1998.

[130] Z. J. WANG and Y. LIU. The spectral difference method for the 2D euler equations on unstructured grids. *In 17th AIAA Computational Fluid Dynamics Conference. AIAA*, 2005.

[131] Z. J. WANG, Y. LIU, G. MAY, and A. JAMESON. Spectral difference method for unstructured grids II: Extension to the euler equations. *J. Sci. Comp.*, 32(1):45–71, 2007.

[132] J.H. WILLIAMSON. Low-storage Runge-Kutta schemes. *J. Comput. Phys.*, 35(MR: 81a: 65070):48–56, 1980.

[133] L. DEL ZANNA and N. BUCCIANTINI. An efficient shock-capturing central-type scheme for multidimensional relativistic flows: I. hydrodynamics. *Astronomy and Astrophysics*, 390:1177–1186, 2002.

[134] L. DEL ZANNA, N. BUCCIANTINI, and P. LONDRILLO. An efficient shock-capturing central-type scheme for multidimensional relativistic flows: II. magnetohydrodynamics. *Astronomy and Astrophysics*, 400:397–414, 2003.